RESONANCE RAMAN STUDIES ON SOME METALLOPORPHYRINS

MAMATA SARKAR

DEPARTMENT OF PHYSICS
SCHOOL OF PHYSICAL SCIENCES
NEHU

A THESIS
SUBMITTED
IN
FULFILMENT OF THE REQUIREMENT OF THE DEGREE OF

DOCTOR OF PHILOSOPHY

To

THE NORTH-EASTERN HILL UNIVERSITY

SHILLONG

INDIA

DECEMBER, 1986

-Thesis

DS
544.64
SAR

DEDICATED
TO
MY PARENTS

Dr. A. L. VERMA
Professor
Department of Physics

North-Eastern Hill University
SHILLONG 793 003

I certify that the thesis entitled ***'Resonance Raman Studies On Some Metalloporphyrins'*** *submitted by Miss Mamata Sarkar for the degree of* **Doctor of Philosophy** *of the North-Eastern Hill University, Shillong, embodies the record of original investigation carried out by her under my supervision. She has been duly registered, and the thesis presented is worthy of being considered for the award of Ph.D. Degree. This work has not been submitted for any Degree of any other Universities.*

A. Verma
17.12.86

Date: **December 1986**
Place: SHILLONG

(Dr. **A. L. VERMA**)
Supervisor

North-Eastern Hill University
DEPARTMENT OF PHYSICS
Shillong 793 003

CERTIFICATE

This is certified that Miss Mamata Sarkar has cleared the following four Pre-Ph.D. courses obtaining on average 'A' grade (on Seven Point Scale).

Course	G.P.A.	Grade
1) Polymer Physics	4.70	A
2) Group Theory and Molecular Physics	5.30	A
3) Chemical Binding	5.40	A
4) Computer Programming	4.20	B

(C S SHASTRY)
Professor & Head

ACKNOWLEDGEMENTS

It is with great pleasure that I wish to express my deepest sense of gratitude to Dr. **A. L. Verma** for his supervision and guidance on this work. I am grateful for his constant encouragement, advice and help without which this work would have not been possible.

I take this opportunity to thank Prof. **C.S. Shastry** and Dr. **K. Kumar** for their help and encouragement during the course of this work. I am also extremely grateful to Dr. **J. Subramanian,** Department of Chemistry for his manifold help during this work.

This column remains incomplete if I forget to acknowledge all the members of my family for their keen interest and encouragement. I thank Dr.S.S. Khatri, Mr. T. Chakraborty, Mr. N.K. Choudhury, Mr. G.S.S. Saini and my other friends for their cooperation and encouragement throughout my course.

I acknowledge my sincere thanks to Mr. A.K. Rathore for helping me to record the Raman Spectra.

I also express my thanks to Mr. N.K. Paul Choudhury for his adept typing of this thesis.

Finally, I am grateful to the Department of Science & Technology, New Delhi for providing the financial assistance during the period of this work.

Mamata Sarkar

Miss **MAMATA SARKAR**

Date: **December 1986**

CONTENTS

*Page No.115 is typographically missing.

RESONANCE RAMAN STUDIES ON SOME METALLOPORPHYRINS

Porphyrins and their derivatives are of great biological importance and have received considerable attention during recent years.[1,2] They play a major role in the electron transfer reactions in many enzymes and form important chromophores in haeme proteins, chlorophylls, cytochrome oxidase etc. It is therefore important to study the physicochemical properties of metalloporphyrins and their aggregates in greater details which can provide useful insight into the mechanisms of their actions in various biological processes. Studies on these systems, however, do not stem exclusively because of their biological significance. This class of compounds offer ample opportunities to understand many fundamental problems of molecular physics, quite apart from their inherent interest in biology.

The advent of lasers and improved technical devices have stimulated considerable interest in the utility of resonance Raman (RR) spectroscopy as a probe to study the structure and dynamics of porphyrins and metalloporphyrins as well as their role in biological systems.[3-5] When the frequency of the exciting radiation is tuned through the electronic absorption region of the system, intensities of certain

vibrational modes show preferential enhancement due to their coupling with either a single excited electronic state or through vibronic coupling between two nearby electronic states. The selectivity and sensitivity offered by the resonance Raman technique provides valuable informations about several molecular properties such as electronic and geometrical structure, intra and intermolecular forces, nature of the bond etc. and play a key role in understanding many fundamental problems of biology.

Resonance Raman studies of metalloporphyrins and haeme proteins are of great interest.[3-5] The early resonance Raman studies on porphyrins and metalloporphyrins were reported by Verma **et al.**[6-8] and it was shown that even peripheral and saturated substituents exert a profound influence on the vibrational pattern and depolarization ratios. Copper porphin was found to have D_{4h} symmetry[8] and vibrational modes of A_{2g} symmetry showed almost infinite depolarization ratio. During resonance Raman study of Manganese(III) aetioporphyrin-I, Asher and Sauer[9] could interprete the complicated electronic spectrum of the system by selective excitation of Raman spectra within charge transfer and $\pi - \pi^*$ transitions which showed dramatic changes in the resonance Raman spectra. Numerous resonance Raman studies have provided a great deal of knowledge about the metalloporphyrins as well as on haeme proteins and cytochromes.[3-5, 10]

However, in spite of several studies on porphyrins and metalloporphyrins, the role of haemoglobin in the control of oxygen binding is not fully understood. The specific role of vinyl groups in the cooperative binding of oxygen is also not clear. It has been proposed that the protein-haeme interactions occur via vinyl side chains and the role of such interactions in controlling O_2 binding is an area of growing research activity.[11-13] Therefore if the role of vinyl groups in the RR spectra of haeme proteins could be properly understood, it may be of great help in monitoring their role in important biochemical processes. However, there are several factors which add complexity to the RR spectra of haeme proteins. It is thus esential to understand the RR spectra of basic chromophore before attempting to investigate the effects of protein and other axial ligands on the vibrational modes of the chromophore in haeme proteins.

There has also been considerable interest in the study of Manganese(III) porphyrin complexes during recent years.[9,14-16] The absorption spectra of these complexes are strikingly different from the absorption spectra of normal metalloporphyrin complexes. This has been attributed to strong metal-porphyrin interactions, which modify the normal spectra and induce many new distinct features to appear in the absorption. However, unambigous assignment for these bands is still lacking and consequently a more detailed study is desirable.

Mn(III)-porphyrins have biological importance owing to their possible role in Manganese dependent green plant photosynthesis.[17] A thorough understanding of Manganese porphyrin complexes would also be valuable in sorting out the closely related and biologically important Iron systems, as well as for the understanding of metalloporphyrin structure and spectra, in general.

The axially bridged dimeric metalloporphyrin complexes have also drawn much attention to probe the energy transduction mechanisms in various biological systems. However, despite the utility of RR spectroscopy as a subtle and sensitive probe of environmental and structural factors, RR studies on these systems have not been carried out to a great extent.[18-2] Therefore, further systematic Raman investigations are necessary to achieve a proper understanding of these systems. In the present thesis we have attempted to resolve some of the outstanding problems on metalloporphyrins by combining resonance Raman, infrared (IR) and electronic absorption techniques.

The thesis is divided into seven chapters. Chapter I reviews the existing interpretations and their shortcomings as reported in literature on metalloporphyrins and related systems and introduces the problems under consideration.

Chapter II presents detailed theoretical background relevant to the present study. It discusses two well known techniques, viz., electronic absorption spectroscopy and

resonance Raman spectroscopy and explains the types of informations which can be obtained by analyzing the resonance Raman data. Some pertinent aspects of IR technique are also given in this chapter.

Chapter III deals with the experimental techniques like sample preparation, instrumental set up which include various types of lasers, SPEX Raman spectrometer, photon counting arrangement etc. used in the present study.

Chapter IV describes the effect of vinyl groups on the RR spectra of protoporphyrin-IX. RR spectra of free base protoporphyrin-IX (PP), mesoporphyrin-IX (MP), and haematoporphyrin-IX (HP) having identical molecular symmetries, along with the copper and cobalt complexes of PP and MP have been compared to delineate the contributions of vinyl groups in the RR spectra of PP. The main conclusion of this work is that the vinyl groups in PP perturb the symmetry of the chromophore in the same way as the other substituents in the HP and MP, resulting in C_s symmetry for all the systems. This indicates either i) the conjugation of the vinyl groups with the porphyrin macrocycle in PP is decreased due to large steric interactions of the mesohydrogens with the vinyl group hydrogens in the coplanar configuration and/or ii) the vibrational modes of the vinyl groups are not effective in vibronic coupling of the excited electronic states of the macrocycle

and therefore do not get enhanced in the RR spectra.[22]

Chapter V presents the resonance Raman studies of tetraphenylporphinato Manganese(III) chloride (Mn(III)TPPCl). Three aspects of these systems have been discussed in detail: the electronic structure, the state of conjugation of the phenyl rings with the macroring and the symmetry of the molecular system. It has been seen that due to strong metal porphyrin interactions, bands due to charge transfer transitions and singlet-triplet (π, π^*) transitions arise, which are not observed in the absorption spectra of normal metalloporphyrins. No direct evidence is found for the conjugation of phenyl rings with the macrocycle. The symmetry of the system is reduced from C_{4v}, probably because of the non-symmetric disposition of the phenyl rings.[23]

Chapter VI reports the resonance Raman spectra of oxygen-bridged Manganese(III) tetraphenylporphin dimer (O-$(MnTPPH_2O)_2$). The data obtained serves as a measure to probe the intradimer coupling, which is found to be non significant in this case. No direct contributions of the phenyl groups is found in the RR spectra of the dimer indicating thereby that the phenyl groups are not conjugated with the porphyrin macrocycle.[24]

Chapter VII gives the summary of the present work and important conclusions drawn from the study.

REFERENCES

1. 'The Porphyrins' ed. D. Dolphin, Academic Press: New York, vols. **I-VII**, 1978.
2. 'Porphyrins and Metalloporphyrins' ed. K.M. Smith, Elsevier: Amsterdam, 1975.
3. T.G. Spiro, in 'Iron Porphyrins' eds. A.B.P. Lever and H.B. Gray, Addison-Wesley: Reading, MA, Part II, 89(1983).
4. D.L. Rousseau, J.M. Friedman and P.F. Williams, in 'Topics in Current Physics' vol. **11**, 203(1979).
5. T. Kitagawa, in 'Hemoglobin' eds. A.G. Schnek and C. Paul, Brussel Univ. Press: Brussel, 235(1984).
6. A.L. Verma and H.J. Bernstein, Biochem. Biophys. Res. Commun. **57**, 255(1974).
7. A.L. Verma, R. Mendelsohn and H.J. Bernstein, J. Chem. Phys. **61**, 383(1974).
8. A.L. Verma and H.J. Bernstein, J. Chem. Phys. **61**, 2560(1974).
9. S. Asher and K. Sauer, J. Chem. Phys. **64**, 4115(1976).
10. A. Warshel, Annu. Rev. Biophys. Bioeng. **6**, 273(1977).
11. T. Asakura and M. Sono, J. Biol. Chem. **249**, 7087(1974).
12. B. Gellin and M. Karplus, Proc. Natl. Acad. Sci. USA, **74**, 801(1977).
13. A. Warshel and R.M. Weiss, J. Am. Chem. Soc. **103**, 446(1981).
14. L.J. Boucher, Coord. Chem. Rev. **7**, 289(1972).
15. R.R. Gaughan, D.F. Shriver and L.J. Boucher, Proc. Natl. Acad. Sci. USA, **72**, 433(1975).
16. J.A. Shelnutt, D.C. O'shea, N.-T. Yu, L.D. Cheung and R.H. Felton, J. Chem. Phys. **64**, 1156(1976).
17. M. Calvin, Rev. Pure Appl. Chem. **15**, 1(1965).
18. J.M. Burke, J.R. Kincaid and T.G. Spiro, J. Am. Chem. Soc. **100**, 6077(1978).

19. G.A. Schick and D.F. Bocian, J. Am. Chem. Soc. **105**, 1830(1983).
20. J.A. Hofmann and D.F. Bocian, Inorg. Chem. **23**, 1177(1984).
21. J.A. Hofmann and D.F. Bocian, J. Phys. Chem. **88**, 1472(1984).
22. M. Sarkar and A.L. Verma, J. Raman Spectrosc. **17**, 407(1986).
23. M. Sarkar and A.L. Verma, Communicated.
24. M. Sarkar and A.L. Verma, Unpublished work.

INTRODUCTION

Porphyrins and their derivatives are important class of compounds from the point of view of physical studies as well as their importance in biophysical processes. The metal derivatives of porphyrins form chromophores in many biological systems like haemoglobin, myoglobin, chlorophylls, cytochromes and play major role, in the electron transfer processes in many enzymes, photosynthesis in the green plant etc. Iron complex of protoporphyrin-IX constitutes the prosthetic group of both haemoglobin and myoglobin and either this or a peripherally modified form is contained in the cytochromes[1] and the enzymes like peroxidases and catalases. Chlorophyll — the most important pigment active in photosynthesis – is a Magnesium complex of porphyrin with a phytol chain substituent. Manganese porphyrins have been discussed as participants in the photosynthetic system,[2] and also seem to occur in blood.[3] Changes or modifications in general porphyrin metabolism have been associated with cancer, drug metabolism and other specific diseases like porphyria.[4]

Apart from their significant role in different biological processes, the study of the physical and chemical properties

of these systems is very important as they provide ample opportunities for many fundamental studies in molecular physics, chemistry and spectroscopy. For these reasons, active research work on porphyrins and related systems is being persued by several groups all over the world for the last several years using various experimental techniques and theoretical models.[5-7] In more recent times, renewed interest on these systems has aroused because of their technological possibilities in various types of devices such as solid catalysts, photoconductors, organic semiconductors etc.[8] and also because they are used for photochemotherapy and diagnosis of malignant tumors.[9,10]

The structure of the simplest class of porphyrins without any side chain substituents, the free base porphin(H_2P) is shown in Fig. 1.1. The basic skeleton for all porphyrins and related systems consists of four pyrrole rings fused together by methine bridges and the two protons in the centre of H_2P can be exchanged by a metal to give a metal porphin(M_eP). Almost all the naturally occuring porphyrins and metalloporphyrins found in living systems are fully substituted at the pyrrole carbon atoms at positions 1 to 8 in Fig. 1.1 with substituents such as methyl, ethyl, vinyl, propionic acid and acetic acid groups. Iron protoporphyrin-IX having $4(CH_3)$, $2(CH{=}CH_2)$ and $2(CH_2\text{-}CH_2\text{-}COOH)$ groups as side chain substituents at specific positions is the most important metalloporphyrins occuring in nature. The porphyrin ring

can be regarded as an 16 atom aromatic system whose properties are governed by the electron donating and withdrawing characteristics of the substituents and the nature of the central metal ion.

Spectroscopically, the absorption spectra of all metalloporphyrin have some features in common. They all exhibit a very intense band between 380 nm and 420 nm, called Soret or γ band; a much weaker band between 500 and 600 nm, called Q(0,0) or α band alongwith an associated vibronic sideband called Q(1,0) or β on the higher energy side of the α band. In general, the electronic spectra of the nearly planar metalloporphyrins may be ascribed to the transitions of the delocalized π electrons which have their maximum density above and below the plane of the molecule. The σ electrons are considered to be strongly localized between the nuclei and as a first-order approximation, do not contribute to the absorption in the visible region of the spectrum. A typical absorption spectrum of Cu-porphin is shown in Fig. 1.2. In addition to the normal $\pi \longrightarrow \pi^*$ transitions, the absorption spectra of certain metalloporphins, for example involving Mn(III) ion, contain extra bands which may arise due to charge transfer, metal d $\longrightarrow$ d, different $\pi \longrightarrow \pi^*$ transitions etc. Detailed theoretical and experimental aspects of these spectral features shall be discussed in later chapters.

The role of these systems in various biophysical processes

is obviously associated with their intrinsic physical and chemical properties. The unique coordination chemistry of porphyrins have been the subject of many recent reviews.[11-14] The study of the absorption and luminescence have helped much for understanding the theory of vibronic coupling effects in aromatic hydrocarbons[15] as well as the theory of radiationless decay, in general.[16] The resonance Raman studies on these systems have helped to clarify several fundamental aspects of the scattering process itself.[17-20] They also provide ideal systems to study the relation between resonance Raman and resonance fluorescence.[21] The different experimental techniques such as electronic and luminescence spectroscopy[16,22,23] including fine structure quasiline spectra[24] (Shpolskiĭ effect), X-ray,[25,26] ESR,[27] NMR,[28] Mösbauer spectroscopy,[29] magnetic susceptibility measurements,[29,30] infrared(IR)[31] and Raman spectroscopy[17-21,32-39] etc. have been applied to elucidate their physical and chemical properties. At the same time, many theoretical approaches including quantum mechanical calculations, have been attempted by several workers[40,41] which have helped to rationalize many experimental results.

Historically, the study of electronic and luminescence characteristics of porphyrins and metalloporphyrins have provided much information about the electronic properties of the excited states, nature of bonding, structure of

chromophore etc. The absorption bands are quite sensitive to the structure and environment of the chromophore and have been frequently used for characterization of these systems. The structural properties of metalloporphyrins are intimately related to their important role in biological processes. It is therefore very necessary to know the configurational details, bonding state of the metal atom and the basic coordination chemistry of these systems. The best available technique for determining structural details and molecular conformation in the solid state is the X-ray crystallography. Many X-ray crystallographic studies on different metalloporphyrins have been performed to determine their structure.[25,26]

The spectacular development of molecular biology during the last decade has opened the prospect of understanding biological functions in terms of molecular structure. With the availability of basic structural information from X-ray diffraction methods, there arises a need for spectroscopic techniques to monitor structural features and detect changes due to accompanying biological function. A large variety of such techniques have been used, each with particular liabilities and advantages, depending on the kind of information needed. The study of molecular vibrational frequencies has great potential for understanding the function of biologically important materials as they are very sensitive to the geometric

and bonding arrangements of localized groups in a molecule and also reflect intermolecular interactions. The advent of the laser and pulse counting detection techniques have caused a renaissance in the use of Raman spectroscopy as a powerful tool in physics, chemistry and biophysics during the last decade or so.

Raman scattering arises as a result of interaction of electromagnetic radiation with matter resulting in inelastic scattering of light from different excitations in the medium. With the availability of strong, monochromatic and polarized light from lasers, it has become much easier to monitor the intensity, half-width, polarization properties and frequency shifts of Raman bands as a function of frequency of exciting light, temperature, pressure, concentration and other external parameters. Availability of continuously tunable dye lasers have made possible the systematic exploration of the resonance Raman(RR) effect which has emerged as a very selective and sensitive technique for probing structural details of biological chromophores at physiologically relevant concentrations. Resonance enhancement of certain vibrations occur when the system is excited by light whose wavelength lies within an electronic absorption region of the system. By tuning the excitation frequency through the optically allowed transitions of the system, selective enhancement of those vibrations occur

which involve mainly the motion of the atoms in that part of the chromophore where the electronic transition is localized.

The selectivity offered by the RR technique allows the study of different chromophores independently without the interference from others. Under resonance conditions, the intensity enhancement of the vibrations coupled to the electronic transition may be 10^3- 10^6 orders higher compared to normal Raman scattering; where the excitation wavelength is far from the absorption band. The enormous intensity enhancement helps to obtain RR spectra at very low concentrations of $\sim 10^{-4}$M or even lower. The peak positions of the vibrational bands in RR spectra are a property of the ground electronic state, while peak intensities are strongly dependent on the excited as well as ground electronic states. The information content in the RR spectra may be used to characterize the structural and electronic properties of the molecule in greater details.

Porphyrins and metalloporphyrins are amenable to RR studies because of their strong absorption in the visible region. The appearance of bands with enhanced intensity in the RR spectra depends upon the nature of the particular excited electronic state involved and thus can provide a direct monitor of the nature of the state involved in the scattering process. The selective and specific enhancement of vibrations in RR spectra due to excitation in different

spectral regions allow these bands to be classified according to their origin. One advantage of RR spectroscopy over electronic spectroscopy is that, although the same vibronic transitions are involved in both the processes, RR technique can provide more detailed information about the electronic as well as vibrational states of the molecule because Raman spectra can resolve those vibrations that are often not resolved in the absorption spectra in solution. Since the RR scattering depends upon the π electronic structure of the conjugated systems, responsible for the absorption in the visible region, this technique can also be used to explore the effect of conjugating substituents with the chromophore. If the delocalization of the π electron cloud extends over the side chain substituents also, the RR spectra should reflect changes in intensity of vibrational modes and in some cases, the frequencies of the vibrational modes related to the substituents may also be observed. The study of the effect of the substituent groups on the RR spectra of porphyrins sometimes can bring conceptual simplicity in the understanding of many biological systems and their functions. During the last few years, considerable amount of information regarding the electronic and vibrational states of these systems has been obtained using RR spectroscopy.

The vibrational modes are also very sensitive to the changes in central metal, variations in the spin and oxidation

state.[42] The planarity of the metal with respect to the porphyrin plane,[43] the external side chain substituents[44,45] or the axial ligands[43,46] etc. have been shown to cause pronounced changes in the RR spectra of metalloporphyrins and haeme proteins. The sensitivity of the RR technique to molecular conformations is menifested in the RR spectra of four isomers of CuETP[47] which differ only in the order of methyl and ethyl substituents in the Cu-porphin ring, and have markedly different RR spectra in the 650-850 cm^{-1} region. RR data can also be used to gain information about the structure of the molecule.[45,48,49] Although X-ray diffraction studies provide the most detailed crystal structure in the solid state, spectroscopic techniques are extremely useful for monitoring the structure in solution. The main advantage of spectroscopic methods over X-ray crystallographic technique is that it imposes no conditions of sample crystalizability, since spectra can be obtained in both solid and liquid phases. RR data coupled with IR data can provide informations about the symmetry of the system as well as to the understanding of intermolecular interactions in molecular aggregates.[50-53]

The dependence of Raman intensity and depolarization ratio on the exciting frequency has been used to account for many important aspects of these systems. The plot of intensity variation with the excitation frequency gives Raman excitation profiles (REP) and it thus resembles an absorption

spectrum for the mode being monitored. REP's are therefore the proper signals for the study of electronically excited states. Since each observable Raman mode produces a separate REP, an enormous resolution over ordinary absorption spectroscopy is achieved. On the other hand,dispersion of depolarization ratio with exciting frequency can give valuable structural information about the symmetry of the molecule. By studying the dispersion of depolarization ratio the symmetry of porphin in solution is confirmed to be C_{2h}[54] and that of Cu-porphin is D_{4h}.[48]

Thus significant progress has been made towards the investigation of porphyrin and metalloporphyrin complexes by means of resonance Raman technique. In addition, resonance Raman studies on these systems have clarified several fundamental aspects of the scattering process itself.[17-20] Resonance Raman studies of haeme proteins[55] and other metalloporphyrins[43] provide very good examples to illustrate the vibronic nature of the scattering. The observation of Raman bands with inverse polarization in haeme proteins and metalloporphyrins constitutes the first experimental confirmation of antisymmetric vibrational scattering, although the phenomenon was predicted theoretically by Placzek[56] in 1934.

One of the most serious technical difficulties which arises in studying the RR spectra of porphyrins and

metalloporphyrins is the separation of unrelaxed Raman emission from much more intense relaxed emission due to luminescence. Sometimes, impurities in the sample produce substantial background, which can be removed by further purification of the sample. Of course, if the luminescence is intrinsically associated with the chromophore then a change of excitation wavelength helps in the improvement of Raman signals compared to the luminescence signal. Sometimes addition of an external quenching agent helps for achieving better signal to noise ratio. Other experimental problems arise because of the photoreaction of the samples induced by laser irradiation and decomposition of samples due to strong absorption and local heating. These problems can be partly overcome by rotating the sample with respect to the laser beam so that a part of the sample is exposed to laser light for a very short time. Further advancements in analyzing the RR spectra of porphyrins have been offered by normal coordinate calculations,[57,58] which have helped to gain more detailed information about these systems.

In view of so many extensive studies by different techniques on these systems, several aspects have been clarified but still much remains in question. At the present time, the role of the active site of haemoglobin in the control of oxygen binding is not clear. The function of the vinyl groups in the cooperative binding of oxygen in haemoglobin

is also not fully understood and the mode of interactions of vinyl groups with the protein residues is of much current interest. Substitution studies have indicated that the cooperativity decreases when vinyl group is replaced by Br or CH_3 group and is reduced drastically when vinyl groups are replaced by hydrogen in haeme proteins.[59] Vinyl, being a conjugating group, can control the physical and chemical properties of the porphyrin ring via its ineractions with the amino acid residues of the protein.[60-63] Such interactions have been proposed for the vinyl groups of protohaeme, in haemoglobin[60-62] and cytochrome b[63] and for the formyl group of haeme a in cytochrome c oxidase.[64-66] Thus it will be of great help if the influence of the vinyl groups on the functioning of haeme proteins can be properly monitored.

As the resonance Raman spectroscopy is a very sensitive probe of the π electronic structure of the porphyrin and the effects of conjugating substituents, it can therefore reveal lot of relevant informations about the system. However, there are several complicating factors which affect the RR spectra of haeme proteins (for example non planarity of the iron ion, side chain substituents, haeme protein interactions etc.). It is therefore highly desirable to study the comparatively simpler chromophore protoporphyrin-IX and its metal chelates and to compare their RR spectra with those of similar systems having saturated substituents in place of the vinyl

groups. characterization of such system is necessary before the position specific and substituent specific porphyrin protein interactions can be sorted out.

The study of Mn(III)-porphyrin complexes has also been an area of growing research activity during recent years.[14,67-70] These complexes exhibit an atypical electronic absorption spectrum which is diagnostic of their unusual electronic structure. This arises because of strong metal ligand interactions, thereby inducing distinct new features in the absorption. However, despite many studies, the complex absorption spectra of these systems are not fully and properly understood and consequently a more detailed study is desirable.

The study of the structural and electronic properties of the aggregates of the metalloporphyrin molecules is also essential in elucidating the energy transduction mechanisms in various biological processes. Out of the many oligomeric metalloporphyrins known, axially bridged dimeric species are particularly important as model systems for monitoring the interchromophore induced perturbations as they are generally very stable and rigid. The characterization of the dimers is therefore essential to clarify several aspects of biological chemistry. However, uptil now only few RR studies on metalloporphyrin dimers have been carried out[50-53] and therefore it is necessary to extend these studies as a basis to understand porphyrin chemistry in general and their biological implications.

In this thesis, we have undertaken systematic resonance Raman studies on proto, meso and haematoporphyrin-IX as well as on Copper and Cobalt complexes of proto and mesoporphyrin-IX dimethyl esters, tetraphenylporphinato Manganese(III) chloride and its μ-oxo-bridged dimeric species with a view to understand some of the specific aspects mentioned above.

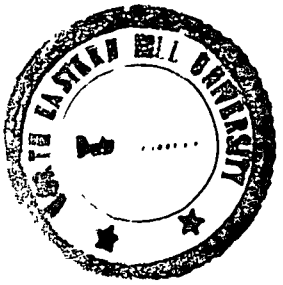

REFERENCES

1. R. Lemberg and J. Barrett, in 'Cytochromes' Academic Press: London, (1973).
2. M. Calvin, Rev. Pure Appl. Chem. **15**, 1(1965).
3. D.C. Borg and G.C. Cotzias, Nature **182**, 1677(1958).
4. A. Goldberg and C. Rimington, in 'Diseases of Porphyrin Metabolism' Thomas: Springfield, (1962).
5. J.E. Falk, in 'Porphyrins and Metalloporphyrins' Elsevier: Amsterdam, 1964.
6. 'The Porphyrins' ed. D. Dolphin, Academic Press: New York, vols. **I-VII**, 1978.
7. 'Porphyrins and Metalloporphyrins' ed. K.M. Smith, Elsevier: Amsterdam, 1975.
8. A.D. Adler, F.R. Longo and F.Kampas, in 'The Porphyrins' ed. D. Dolphin, Academic Press: New York, vol. **V**, 483(1978).
9. T.J. Dougherty, J. Natl. Cancer Inst. **52**, 1333(1974).
10. G. Jori, in 'The Molecular Biology of Photodynamic Action, in: Lasers in Photomedicine and Photobiology' eds. R. Pratesi and C.A. Sacchi, Springer: New York, 58(1980).
11. J.W. Buchler, in 'Porphyrins and Metalloporphyrins' ed. K.M. Smith, Elsevier: Amsterdam, 157(1975).
12. P.D. Smith, B.R. James and D. Dolphin, Coord. Chem. Rev. **39**, 31(1981).
13. M. Tsutsui and G.A. Taylor, in 'Porphyrins and Metalloporphyrins' ed. K.M. Smith, Elsevier: Amsterdam, 279(1975).
14. L.J. Boucher, Coord. Chem. Rev. **7**, 289(1972).
15. M.H. Perrin, M. Gouterman and C.L. Perrin, J. Chem. Phys. **50**, 4137(1969).
16. M. Gouterman, in 'The Porphyrins' ed. D. Dolphin, Academic Press: New York, vol. **III**, 1(1978).
17. B.B. Johnson and W.L. Peticolas, Annu. Rev. Phys. Chem. **27**, 465(1976).

18. T.G. Spiro and P. Stein, Annu. Rev. Phys. Chem. **28**, 501(1977).

19. J.A. Shelnutt, L.D. Cheung, R.C.C. Chang, N.-T. Yu and R.H. Felton, J. Chem. Phys. **66**, 3387(1977).

20. J.A. Shelnutt and D.C. O'shea, J. Chem. Phys. **69**, 5361(1978).

21. F. Adar, M. Gouterman and S. Aronowitz, J. Phys. Chem. **80**, 2184(1976).

22. M. Gouterman, J. Mol. Spectrosc. **6**, 138(1961).

23. R.S. Becker and J.B. Allison, J. Phys. Chem. **67**, 2662, 2669(1963).

24. G.W. Canters, J. van Egmond, T.J. Schaafsma and J.H. van der Waals, Mol. Phys. **24**, 1203(1972).

25. R.G. Little, K.R. Dymock and J.A. Ibers, J. Am. Chem. Soc. **97**, 4532(1975).

26. D.M. Collins, R. Countryman and J.L. Hoard, J. Am. Chem. Soc. **94**, 2066(1972).

27. J. Subramanian, in 'Porphyrins and Metalloporphyrins' ed. K.M. Smith, Elsevier: Amsterdam, 555(1975).

28. H. Scheer and J.J. Katz, in 'Porphyrins and Metalloporphyrins' ed. K.M. Smith, Elsevier: Amsterdam, 399(1975).

29. P. Hambright and A.J. Bearden, in 'Porphyrins and Metalloporphyrins' ed. K.M. Smith, Elsevier: Amsterdam, 539(1975).

30. E.B. Fleischer, J.M. Palmer, T.S. Srivastava and A. Chatterjee, J. Am. Chem. Soc. **93**, 3162(1971).

31. J.O. Alben, in 'The Porphyrins' ed. D. Dolphin, Academic Press: New York, vol. **III**, 323(1978).

32. A.L. Verma and H.J. Bernstein, Biochem. Biophys. Res. Commun. **57**, 255(1974).

33. T. Kitagawa, Y. Ozaki and Y. Kyogoku, in 'Adv. Biophys.' vol. **11**, 153(1978).

34. R.H. Felton and N. -T. Yu, in 'The Porphyrins' ed. D. Dolphin, Academic Press: New York, vol. **III**, 347(1978).

35. D.L. Rousseau, J.M. Friedman and P.F. Williams, in 'Topics in Current Physics', vol. **11**, 203(1979).

36. S. Asher, in 'Methods Enzymol', Academic Press: New York, vol. **76**, 371(1981).

37. A. Warshel, Annu. Rev. Biophys. Bioeng. **6**, 273(1977).

38. T.G. Spiro, in 'Iron Porphyrins' eds. A.B.P. Lever and H.B. Gray, Addison-Wesley: Reading, MA, part 2, 89(1983).

39. T. Kitagawa, in 'Hemoglobin' eds. A.G. Schnek and C. Paul, Brussel Univ. Press: Brussel, 235(1984).

40. S.J. Chantrell, C.A. McAuliffe, R.W. Munn and A.C. Pratt, Coord. Chem. Rev. **16**, 259(1975).

41. A. Antipas and M. Gouterman, J. Am. Chem. Soc. **105**, 4896(1983).

42 T.G. Spiro and T.C. Strekas, J. Am. Chem. Soc. **96**, 338(1974).

43. A.L. Verma and H.J. Bernstein, J. Raman Spectrosc. **2**, 163(1974).

44. R. Mendelsohn, S. Sunder, A.L. Verma and H.J. Bernstein, J. Chem. Phys. **62**, 37(1975).

45. A.L. Verma, R. Mendelsohn and H.J. Bernstein, J. Chem. Phys. **61**, 383(1974).

46. R.H. Felton, N.-T. Yu, D.C. O'shea and J.A. Shelnutt, J. Am. Chem. Soc. **96**, 3675(1974).

47. S. Sunder, R. Mendelsohn and H.J. Bernstein, Biochem. Biophys. Res. Commun. **62**, 12(1975).

48. A.L. Verma and H.J. Bernstein, J. Chem. Phys. **61**, 2560(1974).

49. A.L. Verma, M. Asselin, S. Sunder and H.J. Bernstein, J. Raman Spectrosc. **4**, 295(1976).

50. J.M. Burke, J.R. Kincaid and T.G. Spiro, J. Am. Chem. Soc. **100**, 6077(1978).

51. G.A. Schick and D.F. Bocian, J. Am. Chem. Soc. **105**, 1830(1983).

52. J.A. Hofmann and D.F. Bocian, Inorg. Chem. **23**, 1177(1984).

53. J.A. Hofmann and D.F. Bocian, J. Phys. Chem. **88**, 1472(1984).

54. M. Lutz, Spectry. Letts. **6**, 455(1973).

55. T.G. Spiro and T.C. Strekas, Proc. Natl. Acad. Sci. USA, **69**, 2622(1972).

56. G. Placzek, in 'Rayleigh and Raman Scattering', UCR L Transl. No. 526(L) for Handbuch der Radiologie ed. E. Marx, Akademische Verlagsgesellschaft VI: Leipzig, vol. 2, 209(1934).

57. S. Sunder and H.J. Bernstein, J. Raman Spectrosc. **5**, 351(1976).

58. M. Abe, T. Kitagawa and Y. Kyogoku, J. Chem. Phys. **69**, 4526(1978).

59. D.W. Seybert, K. Moffat and Q.H. Gibson, J. Biol. Chem. **251**, 45(1976).

60. T. Asakura and M. Sono, J. Biol. Chem. **249**, 7087(1974).

61. B. Gellin and M. Karplus, Proc. Natl. Acad. Sci. USA, **74**, 801(1977).

62. A. Warshel and R.M. Weiss, J. Am. Chem. Soc. **103**, 446(1981).

63. G.N. LaMar, P.D. Burns, J.T. Jackson, K. M. Smith, K.C. Langry and P. Strittmatter, J. Biol. Chem. **256**, 6075(1981).

64. J.T. Coin and P.C. Hinkel, in 'Membrane Bioenergetics' eds. C.P. Lee, G. Schutz and L. Ernster, Addison-Wesley: Reading, MA, 405(1979).

65. C.K. Chang, in 'Oxygen, Biochemical and Clinical Aspects' ed. W.S. Caughey, Academic Press: New York, 437(1979).

66. G.T. Babcock and I. Salmeen, Biochemistry **18**, 2493 (1979).

67. R.R. Gaughan, D.F. Shriver and L.J. Boucher, Proc. Natl. Acad. Sci. USA, **72**, 433(1975).

68. J.A. Shelnutt, D.C. O'shea, N.-T. Yu, L. D. Cheung and R.H. Felton, J. Chem. Phys. **64**, 1156(1976).

69. S. Asher and K. Sauer, J. Chem. Phys. **64**, 4115(1976).

70. L.O. Spreer, A.C. Maliyackel, S. Holbrook, J.W. Otvas and M. Calvin, J. Am. Chem. Soc. **108**, 1949(1986).

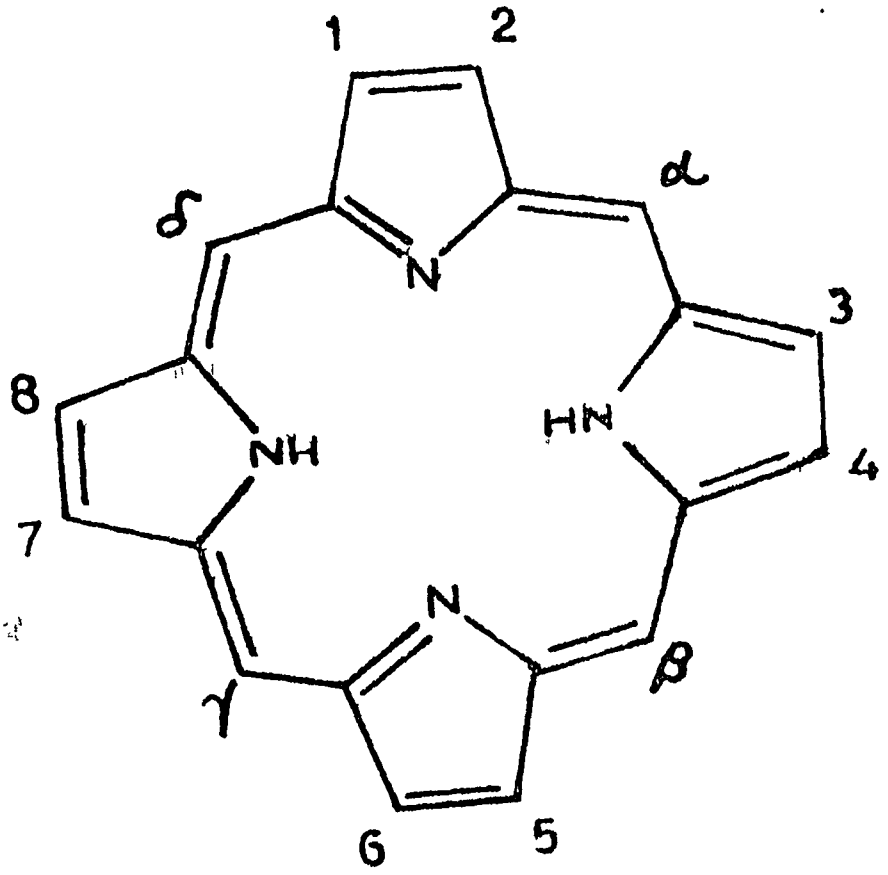

Fig.1.1 Structure of free base porphin.

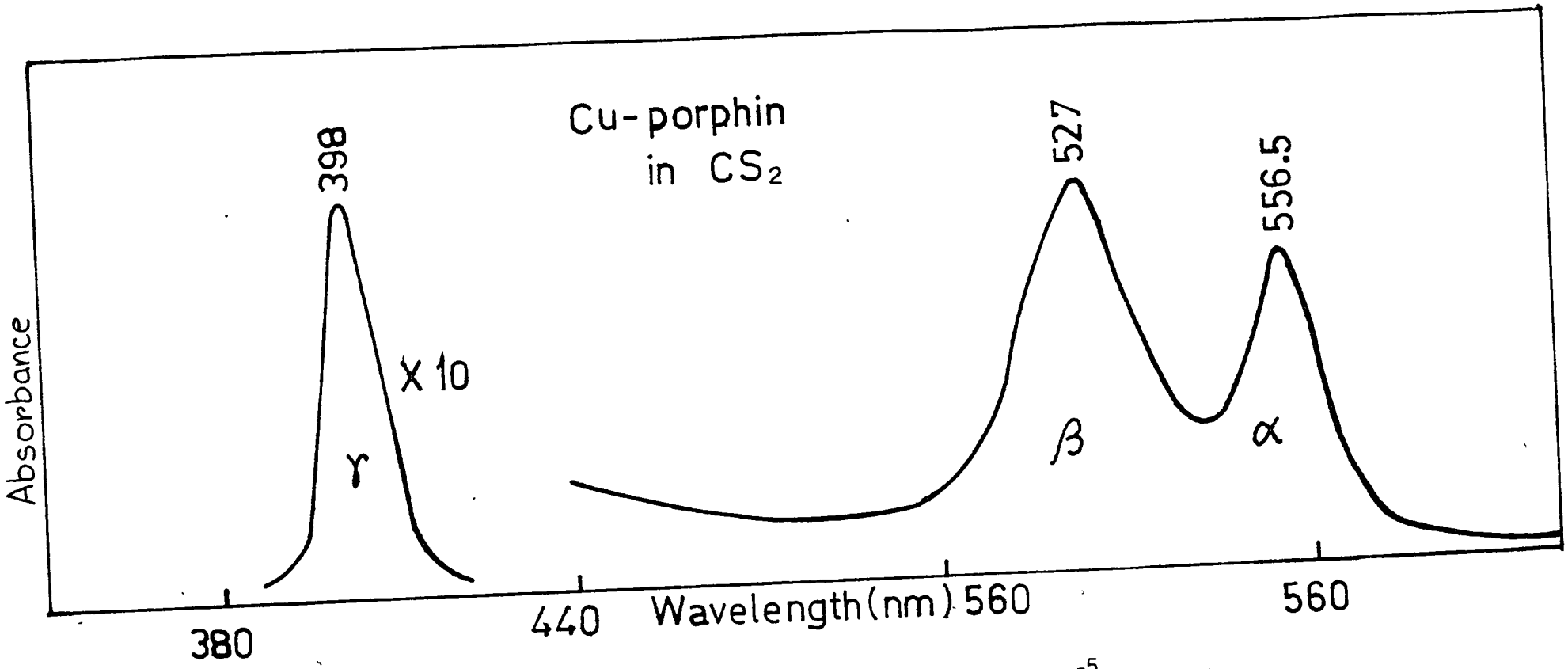

Fig.1.2 Absorption spectra of Cu-porphin in CS_2 solution ($\sim 10^{-5}$M concentration). Characteristic absorption bands are indicated by-α, β and γ.

THEORETICAL ASPECTS OF ELECTRONIC ABSORPTION AND RESONANCE RAMAN SPECTRA

In this chapter, we shall give a detailed theoretical background of the electronic absorption spectra of porphyrins and metalloporphyrins as well as the theory of resonance Raman spectra. Some aspects of IR spectroscopy have also been discussed in brief.

2.1 Structure and Nomenclature

The porphin molecules are derived from the basic skeleton of carbon and nitrogen atoms. Porphin structure consists of four pyrrole rings linked together by methine(=CH-) bridges as shown in Fig. 2.1. This cyclic tetrapyrrole structure was first suggested by Küster.[1] In general, the exo pyrrole positions are numbered from 1 to 8 and the interpyrrolic methine positions, usually termed meso positions, are designated as α, β, γ and δ. If at each positions 1 ... 8 and α ... δ, there is a single hydrogen atom and two hydrogen atoms in the centre, the compound is called "free base porphin'. The ring system may be substituted at any of the outer positions and are referred to as 'porphyrins'. If the central hydrogens are replaced by a metal, the system is known as 'metalloporphyrin'.

2.2 Absorption Spectra

The porphin molecule is highly coloured and possess a number of absorption bands in the optical region, a qualitative description of which is given below:

The free base porphyrins show a similar four-banded structure in the visible region numbered as I to IV and a strong band between 380 and 420 nm called Soret or B or γ band. In some cases a further small band is observed between the bands I and II. The normal metalloporphyrin absorption spectra contain a Soret band and two visible bands called α or Q(0,0) and β or Q(1,0) bands, where α appears to be related to the bands I and III and β with bands II and IV respectively of free base porphyrins. In addition to these, some metalloporphyrins show distinct additional features, which may arise due to charge transfer transitions, metal d→d transitions or some other type of transitions. These bands arise for those metals for which there is a strong interaction between the metal electrons and those of porphyrin ring. Fig. 2.2 gives the absorption spectra of free base TPP(tetraphenylporphin), CoTPP and MnTPPCl. The free base TPP spectrum consists of four banded visible spectrum along with a strong Soret band. On going to CoTPP, the four banded visible spectrum reduces to normal metalloporphyrin absorption spectrum. On the other hand, the absorption spectrum of Mn(III)TPPCl contains extra absorption features and the spectrum differs considerably

from the absorption spectrum of CoTPP.

The electronic absorption spectra of porphyrins and metalloporphyrins vary with the nature of chromophoric system and with various substituents, depending upon the chemical modifications to the basic structure. For example, electrophilic side chains such as vinyl, formyl groups etc. cause a shift to the longer wavelength of the absorption bands due to increase in the π electron density at the periphery of the porphyrin nucleus, i.e., with the decrease of porphyrin basicity. The correlation between the nature of the side chains and the optical absorption spectra were first described by Stern **et al,**[2] and later discussed by other workers.[3-5] The ratio of the intensities of the visible bands vary with the nature and distribution of the substituents and accordingly visible spectra can be classified as aetio, phyllo, rhodo and oxorhodo type.

2.3 Theoretical Aspects of Absorption Spectra

The earliest theory that provided a reasonable interpretation of porphyrin electronic structure was given by Simpson[6] on the basis of the 'free electron model'. The inner ring of the porphyrin is considered to be a 16 membered ring with 18 π electrons (16 from the C and N atoms of the inner ring and 2 from the central metal or hydrogens). Because of the

assumed cylindrical symmetry ($D_{\infty h}$), the Hamiltonian is invariant to rotations about the out of plane Z-axis and this causes the electronic angular momentum about the axis, I_Z, to be quantized. The molecular orbitals are eigenstates of I_Z and their angular part can be written as $\Psi \propto \exp(il\phi)$. Here l is the eigenvalue of I_Z; $l=0,\pm1,\cdots\cdots$ ($\hbar=1$) and ϕ denotes the angle about the Z-axis relative to a chosen reference In the ground state, orbitals with $l=0,\cdots\cdots\pm4$ are each occupied by two electrons (Pauli principle) resulting in a singlet ground state S_0 with the total angular momentum $L_Z=0$. Transitions from $l=\pm4 \longrightarrow l=\pm5$ states give rise to two pairs of excited states; one pair S_1 with total angular momentum $L_Z = \pm9$ and one pair S_2 with $L_Z= \pm1$. By analogy with Hund's rules, one expects the $L_Z= \pm9$ states to have a lower energy than those with $L_Z= \pm1$ because of electron-electron repulsion. Since the ground state is a closed shell with $L_Z=0$, the normal selection rule $\triangle L_Z= \pm1$ predicts that the higher energy singlet is allowed and the lower energy singlet is forbidden. Thus the Soret absorption band B is identified with the $L_Z= \pm1$ excited singlet state and the visible absorption band Q with the $L_Z= \pm9$ excited singlet state. Similar to the excited singlet states, excited triplet states are also formed. However, transitions from the ground state S=0, to a triplet state (S=1) are spin-forbidden and are not observed in the absorption spectra normally. However, in reality porphyrins do not have cylindrical symmetry; the nuclear conformation of a metallopor-

phyrin has approximately D_{4h} symmetry and a free base porphyrin has D_{2h} symmetry.

Although Simpson's model was able to explain some gross features of the absorption spectra, the quantitative predictions derived from this model proved to be rather poor. Many subsequent studies[7,8] were carried out by several workers to achieve a proper understanding of the porphyrin absorption spectra. The first model to take into account of the detailed porphyrin shape was the simple Hückel model. To describe the π electron system, the molecular orbitals are written as linear combinations of atomic orbitals and the orbital coefficients are determined by a variational procedure (LCAO-MO method). Longuet-Higgins **et al**[9] made the first Hückel calculations on porphyrins and obtained $3a_{2u}(\pi)$ and $1a_{1u}(\pi)$ as the top filled orbitals and the lowest empty degenerate orbitals as $4e_g(\pi^*)$. Their orbital coefficients are designated in Fig.2.3. According to them, the transition $3a_{2u} \longrightarrow 4e_g$ at lower energy was identified with the Q(0,0) band and the transition $1a_{1u} \longrightarrow 4e_g$ at higher energy as Soret band. However, this model predicts both transitions with equal absorption strengths, contrary to the observations that Q band is far weaker than the B band.

To relate all the observed phenomena in porphyrins, Gouterman[10,11] has developed the 'four-orbital model', combining

the free electron model[6] and LCAO-MO description.[9] Out of the LCAO-MO's, Gouterman considered only the two lowest empty orbitals and the two highest filled orbitals of the molecules in the ground state in D_{4h} symmetry. Because of the four fold symmetry, the two empty orbitals are degenerate. The top filled orbitals are of symmetry $a_{1u}(\pi)$ and $a_{2u}(\pi)$ which are not symmetry degenerate but Gouterman assumed that these orbitals are accidentally degenerate. The one-electron excitations a_{1u}, $a_{2u} \longrightarrow e_g$ give rise to two doubly degenerate excited configurations which transform like E_u under D_{4h} symmetry. These two transitions are nearly degenerate and hence suffer strong configuration interaction(CI) producing an intense Soret band in which the transition dipole moments add and a weak α band in which the transition dipole moments largely cancel. The problem of configuration interaction for the y-polarized states can be formulated mathematically in the following way:[5] (the x-polarized states will behave identically under D_{4h} symmetry). The excited states or configurations obtained by excitation of an electron from a_{2u} or a_{1u} to e_g orbitals are denoted as $(a_{2u}e_g)$ and $(a_{1u}e_g)$. Because they have the same symmetry, their overlap weighted by a Coulomb repulsion energy is finite and the states mix together. The results of the CI calculations are presented in Table 2.1. If H_{eff} is the Hamiltonian of the pure configurations and they interect via $H' = e^2/r_{ij}$, then the matrix

describing the mixed states can be calculated as shown in Table 2.1. The parameters are defined as follows:

$$A'_{1g} = 1/2[E(a_{1u}e_{gx}) + E(a_{2u}e_{gy})]$$

$$A_{1g} = 1/2[-E(a_{1u}e_{gx}) + E(a_{2u}e_{gy})]$$

$$A''_{1g} = \int(a_{2u}e_{gx})H(a_{1u}e_{gy})dv.$$

$$R_{1y} = \int(a_{1u}e_{gx})y\ \Psi_o dv.$$

$$R_{2y} = \int(a_{2u}e_{gx})y\ \Psi_o dv.$$

$$R = (1/\sqrt{2})(R_1 + R_2) \gg r = (1/\sqrt{2})(R_1 - R_2).$$

A'_{1g} is the centre of gravity of the two configurations (before their interaction), A_{1g} the splitting between them and A''_{1g} the configuration interaction. The R's are the transition dipole moments. The rows of the Table 2.1 represent (a) pure configurations, (a′) 50:50 mixtures, (b) exact mixtures as a function of configuration interaction, (c) approximate mixtures for the case in which the configuration interaction is much larger than the splitting between the pure states. In fact case (c) predicts weak α bands and a minimum in E(Soret)-E(α), which is what is observed in the specta of metalloporphyrins.

The lower energy transition α, borrows back about 10% of the intensity of the higher energy transition (Soret)

through vibronic mixing, with the formation of a vibronic sideband called β , on the higher energy side of the α band, such that

$$\nu_{\beta}^{max} = \nu_{\alpha}^{max} + \nu_{vib} \qquad \text{(see Fig.2.4)}$$

For most of the metalloporphyrins, the four-orbital model explains the absorption spectra nicely. Also, the frequencies of the Soret and Q bands vary only slightly for a wide variety of metal ions, indicating that the metal and porphyrin orbitals are weakly interacting. However, the absorption spectra of some metalloporphyrins, for example, Mn(III)-porphyrins, differ considerably from the normal absorption spectra, which implies that the metal and porphyrin orbitals are strongly interacting. Theoretical calculations predict[12] that the energies of metal d_{π} and porphyrin e_g orbitals match in this case. As a consequence the normal selection rules for absorption break down. The normal absorption spectra may be modified as well as additional bands which are otherwise forbidden may gain intensity and appear in the absorption. The extra features in the absorption spectra of Mn(III)-porphyrin complexes have been variously ascribed due to charge transfer transitions, metal d→d transitions, singlet-triplet (π, π^*) transitions which may be allowed because of large spin-orbin coupling, etc. However, the interpretation of the spectra of these complexes is rather difficult and much more extensive

work needs to be performed to achieve a full understanding of their spectra. Based on our resonance Raman(RR) studies on Mn(III)TPPCl, we have attempted to understand the origin of extra features in the absorption spectra of this system as discussed in Chapter V of the thesis.

2.4 Raman Scattering

When a matter particle, molecule or atom is subjected to the periodically varying electric field of an electromagnetic wave, the particle is polarized, i.e, a dipole is induced, usually one oscillating in phase with the incident wave. If the exciting frequency does not correspond to any dipole active frequencies of the system, the oscillating dipole instantaneously generates a secondary wave of the same frequency. In the wave model, it is the interaction or interference of this secondary emission with the incident radiation that is the basis for the phenomenon of refraction (transmission), reflection and scattering. In quantum theory the secondary emission of radiation is regarded as a process of excitation to some unstable and unobservable state followed by an immediate reemission (in about 10^{-14}sec). The incident light quantum is considered to be absorbed and reemitted. Usually the excited molecule drops back to the initial state. If the exciting frequency is in the visible or UV range, molecules sometimes fall to a different excited vibrational or rotational energy

level of the electronic ground state giving rise to secondary emission of different wavelength — a phenomenon called 'Raman effect'.

Whenever radiation passes from one dielectric medium to another dielectric medium, it is partially reflected and partially transmitted. In the new medium it retains its characteristic frequency but propagates with a different velocity and thus with a different wavelength. In general, radiation also changes direction abruptly at an interface, i.e., is refracted. If the interface is small in extent, such as when a small particle is suspended in some other material, the radiation is scattered rather than reflected. The division between reflection and scattering occurs when dimensions become of the order of a wavelength of the incident beam. Similar to reflection and refraction, scattering also has its origin in the induced secondary emission of particles that lie in the path of radiation.

Raman scattering is one member of a wide class of light scattering phenomena and has its origin in the fact that a collimated beam of light passed through a nonabsorbing medium is invariably found to be attenuated by the medium. When the scattered radiation is passed through a spectrometer, it is found that most of the radiation is scattered elastically, i.e., it is reradiated in all directions with no change in

energy (Rayleigh scattering). However, a small fraction of the radiation will be scattered inelastically giving rise to the Raman effect. In this process, the frequency of the incident light shifts from its original value by a quantum necessary for certain kind of excitation of the sample. The excitation may be translational, rotational, vibrational or electronic in nature, though in general, Raman spectra correspond to vibrational transitions.

Since only a small fraction of photons are scattered during the Raman process, the Raman lines are extremely weak ($I_{Rayleigh} \sim 10^{-3}$ of $I_{incident}$ and $I_{Raman} \sim 10^{-3}$ $I_{Rayleigh}$). This is why, only when intense monochromatic source like a laser is used, it is possible to obtain good quality Raman spectra. Two distinct events are possible: if the frequency of the scattered radiation is lower than the frequency of the incident radiation, it is called Stokes Raman scattering, whereas, if the frequency of the scattered radiation is higher than the frequency of the incident light, it is known as anti-Stokes Raman scattering.

In the limit of normal Raman scattering, i.e., when the exciting frequency is far removed from the stationary energy states of the system, the intermediate state cannot be associated with a particular molecular eigenstate and is a statistical superposition of large number of excited

electronic states of the system. When the incident light approaches an electronic absorption band, the intermediate state no longer remains a virtual state and appropriate electronic state dominates the sum. Thus by tuning the exciting frequency near and finally through an absorption band, one obtains pre-resonance and resonance Raman scattering respectively. In resonance Raman scattering, the intermediate state is dominated by a few (ro)-vibronic levels in the vicinity of the incident light frequency. Ultimately, the resonance fluorescence limit is reached when the incident light coincides with a single sharp level of the electronic manifold. This relationship between the various light scattering processes is illustrated symbolically in Fig. 2.5. Thus, for a given molecular system the Raman spectrum is classified on the basis of the range in which the frequency of the exciting light is chosen. However, it is important to distinguish the two limiting cases of resonance scattering, i.e., resonance Raman scattering and resonance fluorescence, as both involve excitation and emission within an absorption band system. It has been shown that the resonant scattering process depends not only on the energy difference between the molecular and photon states, but also on the lineshapes associated with them. In the limit of resonance fluorescence, the molecular state is much sharper than the photon state and is thus completely in resonance with the incident beam. The scattering

may then be described as a rapid population of the state followed by a slow decay characterized by the lifetime of this state. In the resonance Raman limit, the photon state is much sharper than the molecular state and is in resonance with only a small part of it. In this case two emission processes are observed, a fast one with the lifetime of the incident light and a slower one with the excited state lifetime. The later part represents the resonant contribution, while the former represents the non resonant part of the scattering. Thus the reemission lifetime is characteristic of either the excited state or of the incident radiation, whichever has the narrower linewidth. The term resonance fluorescence has been suggested to the former situation and resonance Raman scattering to the later.[13] However, it is to be noted that the distinction lies in the relative linewidths; the physical process involved is same in both the cases.

2.5 Theory of Resonance Raman Scattering

When a molecule is placed in an electromagnetic field, its charge-distribution is perturbed periodically by the electric and magnetic component of the field. The resultant induced alternating dipole moment acts as a source of radiation and gives rise to the light scattering phenomena. This treatment serves admirably well to demonstrate how polarizability fluctuations give rise to frequency shift in the scattered

light but offers no clues to the underlying nature of the interactions between the radiation and the vibrational modes of the medium, nor is it able to explain important effects like resonance and stimulated Raman scattering. A quantum theory of scattering should treat the radiation and molecule together as a complete system and explore how energy may be transferred between the radiation and the molecule as a result of their interaction. Such a quantum electrodynamical treatment for RR scattering was given by Jacon,[14] but essentially correct results for RR scattering may be obtained by a semi-classical treatment of interaction of radiation with the scattering system which relates the scattering tensor to the wavefunctions and energy levels of the system. The radiation, treated classically, is regarded as a source of perturbation of the energy levels of the scattering system and quantum mechanical techniques are used to investigate transitions between the energy levels of the perturbed system. This type of treatment of Raman scattering was first given by Kramers and Heisenberg[15] and later extended by different workers.[16-23]

If the molecule is considered at the origin of a space fixed coordinate system which interacts with an incident plane wave light beam with electric vector,

$$\bar{E}\sigma = \vec{E}_0^{\circ} \exp(i\bar{k}\cdot\bar{r} - i\omega t) \quad \text{-----(2.1)}$$

propagating along $\bar{k}$ with angular frequency ω, the oscillating electric dipole moment induced in the molecule is given by

$$(\bar{\mu})_{mn} = (\tilde{\alpha}_{\rho\sigma})_{mn} \bar{E}_{\sigma} \quad \ldots\ldots\ldots (2.2)$$

where $(\bar{\mu}_{\rho})_{mn} = \langle \Psi_m | e\bar{\rho} | \Psi_n \rangle$ is the amplitude of the transition moment and Ψ_m and Ψ_n are the time dependent wavefunctions of the initial and final states respectively, $(\tilde{\alpha}_{\rho\sigma})_{mn}$ is the polarizability tensor for the transitions m to n and $\bar{\rho}$ and $\bar{\sigma}$ are molecular cartesian axes of the scattering tensor element $(\alpha_{\rho\sigma})$.

Suppose a molecule, initially in a vibronic state m is perturbed by plane-polarized incident light of frequency ν_o and intensity I_o, in a manner causing it to pass into a vibronic state n while scattering light of frequency $\nu_o \pm \nu_{mn}$. The total intensity of scattered light I_{mn} in photons per molecule per second in 4π solid angle, after averaging over all orientations of the molecule is given by

$$I_{mn} = \left[\left(\frac{2^7 \pi^5}{9c^4} \right) \right] \left[(\nu_o \pm \nu_{mn})^4 \{ \Sigma_{\rho,\sigma} (\alpha_{\rho\sigma})_{mn} \}^2 \right] I_o \quad \ldots\ldots (2.3)$$

where c is the velocity of light and the sum goes over $\rho = x,y,z$ and $\sigma = x,y,z$.

It must be noted that the intensity of the scattered radiation depends upon the frequency of the incident radiation, but more interesting dependence lies on $(\alpha_{\rho\sigma})_{mn}$ when the exciting radiation approaches an electronic absorption. The main task for the theory of Raman scattering is to provide

a theoretical framework for calculating $(\alpha_{\rho\sigma})_{mn}$ based on molecular properties.

Since only the initial and final state wavefunctions contribute to the polarizability changes in the Placzek's theory,[24] the role of the intermediate excited electronic state is completely obscured. However, under resonance conditions, the incident light of a frequency approaching that of a real electronic transition is used and the role of low lying electronic state is greatly emphasized. The quantum mechanical framework involves sum over all the electronic states and appears to be most suitable for the discussion of RR scattering. We shall follow this approach in the ensuing discussion.

In a system with a time-varying field $\bar{E}$, the Hamiltonian is time-varying and there are no stationary states. To determine the polarizability, one must calculate the distortion of wavefunctions due to periodic perturbations by light wave and then evaluate the electric dipole transition moments with the new wavefunctions by using time-dependent perturbation theory. The molecular wavefunctions are obtained as solution of the time-dependent Schrodinger equation,

$$i\hbar \frac{\partial}{\partial t} | \Psi > = (H_o + V) | \Psi > \quad \ldots\ldots\ldots\ldots \quad (2.4)$$

here H_o is the unperturbed molecular Hamiltonian;

$$| \Psi > = \sum_k a_k(t) | \Psi_k^{\circ}(t) > \quad \ldots\ldots\ldots\ldots \quad (2.5)$$

and

$$| \Psi_k^{\circ}(t) > = | \Psi_k^{\circ} > e^{-iH_o t/\hbar} \quad \ldots\ldots\ldots \quad (2.6)$$

is the solution for V=0.

$$V = -\frac{1}{2}\bar{\mu}_\rho \left[\bar{E}_\rho^{\circ} \exp(-i\omega t) + \bar{E}_\rho^{*\circ} \exp(i\omega t)\right] \quad \ldots\ldots\ldots (2.7)$$

describes the major part of the interaction of the molecule with the light wave.

From the Kramers-Heisenberg-Dirac dispersion theory[15,16] the $(\rho\sigma)$ th component of the matrix element of the polarizability tensor for the transition from a vibronic state m to a vibronic state n is given by the second order perturbation theory as:

$$(\alpha_{\rho\sigma})_{mn} = \frac{1}{h}\sum_r \left[\frac{(\bar{M}_\rho)_{rn}\,(\bar{M}_\sigma)_{mr}}{\nu_{rm} - \nu_o + i\,\Gamma_r} + \frac{(\bar{M}_\rho)_{mr}\,(M_\sigma)_{rn}}{\nu_{rn} + \nu_o + i\,\Gamma_r} \right] \quad \ldots\ldots (2.8)$$

where sum goes over the vibronic states of the molecule, $(\bar{M}_\rho)_{rn}$, $(\bar{M}_\sigma)_{mr}$ etc. refer to the scalar amplitudes of the corresponding transition moments. Thus for examples $(\bar{M}_\rho)_{mr} =$

$$\int \Psi_r^* \bar{P}_\rho \Psi_m d\tau \quad \ldots\ldots\ldots (2.9).$$

Ψ_m, Ψ_r represent vibronic wavefunctions, $\bar{P}_\rho = (e\bar{\rho})$ is the ρth component of the electric moment operator. The finite lifetime of the states r have been taken into account by assuming that the excited states decay exponentially with time where Γ_r is inversely proportional to the lifetime of the states r and turns out to be the homogeneous broadening contributions (both radiative and non-radiative) to the half width of the m-r absorption band at half the maximum height.

The expression (2.8) is completely general and is expected

to treat the scattering process within the limits of perturbation theory. However, it is very difficult to make meaningful calculations or interpretations from it because the states $|r>$, $|m>$ and $|n>$ must be described by complete rovibronic wave functions which depend on both the nuclear and electronic coordinates. A variety of approximations and expansions are therefore made at this point. Here, we shall adopt the approach which treats the Raman intensity as a problem of vibronic interactions.

In order to make equation (2.8) more meaningful the Born-Openheimer adiabatic approximation will be introduced for all wavefunctions involved and then expand the electronic wavefunctions in a Taylor's series around the ground state equilibrium configuration of the nuclei. A given vibronic state must now be identified according to electronic and vibrational levels. Thus, let $|m> = |gi>$, where g and i represent electronic and vibrational states respectively, $|n> = |gj>$ and $|r> = |ev>$ etc. The vibronic state function ψ_m has the form, $\psi_m = \Phi_g(q, Q)\ \kappa_j^g(Q)$ where $\Phi_g(q, Q)$ is the electronic wavefunction for state g and $\kappa_j^g(Q)$ is the jth vibrational state function of the ground electronic state g. The symbols q and Q represent the complete set of internal coordinates locating the electrons and nuclei respectively. Thus, equation (2.8) becomes,

$$(\alpha_{\rho\sigma})_{gi,gj} \frac{1}{\hbar} \sum_{ev} \left[\frac{(M_\rho)_{ev,gj}(M_\sigma)_{gi,ev}}{\nu_{ev,gi} - \nu_{\ell} + i\Gamma_{ev}} + \frac{(M_\rho)_{gi,ev}(M_\sigma)_{ev,gj}}{\nu_{ev,gj} + \nu_{o} + i\Gamma_{ev}} \right] \quad \ldots . \quad (2.10)$$

and similarly $(M_\rho)_{mr}$ becomes, $(\bar{M}_\rho)_{gi,ev} = \int (\Phi_e \kappa_v^e)^* \bar{P}_\rho (\Phi_g \kappa_i^g)\, dq dQ \ldots (2.11)$

The sum in equation (2.10) may exclude the ground electronic state with negligible error. Integration over the electronic coordinates in equation (2.11) results,

$$(\bar{M}_\rho)_{gi,ev} = \int (\kappa_v^e)^* [\bar{m}_\rho (Q)]_{g,e} (\kappa_i^g) dQ \quad \ldots \ldots \ldots (2.12)$$

where $[\bar{m}_\rho(Q)]_{g,e} = \int \Phi_e^* \bar{P}_\rho \Phi_g dq \quad \ldots \ldots \ldots (2.13)$

This is because the electric dipole operators, $\bar{P}_\rho$, acts only on the electronic coordinates, the contribution to the transition moment from the nuclear coordinates being negligible. The resulting matrix elements $\bar{m}(Q)$ are still parametrically dependent on Q through the electronic states. This dependence is supposed to be a weak function of the internuclear coordinates. At this point, the Herzberg-Teller expansion is introduced and $[\bar{m}_\rho (Q)]_{g,e}$ is expanded in a Taylor's series in nuclear displacements. Therefore we get,

$$\bar{m}_{g,e} = \bar{m}^\circ_{g,e} + \sum_s \lambda_{es}(Q) \bar{m}^\circ_{g,s} \quad \ldots \ldots \ldots (2.14)$$

where, to first order in Q,

$$\lambda_{es}(Q) = \left(\sum_a h^a_{es} Q_a\right)(\Delta E_{es})^{-1} \quad \ldots \ldots \ldots (2.15)$$

is derived from first order perturbation theory. The sum in eqauation (2.14) extends over all excited electronic states except the state e, and $\bar{m}^\circ_{g,s}$ is the electronic transition moment to state s evaluated for the ground state equilibrium configuration. In equation (2.15) the sum is over all normal

modes where Q_a is the displacement of the ath normal mode, h^a_{es} is a perturbation energy per unit displacement of the ath normal mode due to mixing of ground state equilibrium configuration of electronic states Φ^0_s and Φ^0_e under vibrational perturbation, i.e., $h^a_{es} = \langle \Phi^0_e | (\frac{\partial H}{\partial Q_a})_o | \Phi^0_s \rangle$. (If H is the electronic Hamiltonian, $(\partial H/\partial Q_a)_o Q_a$ is the perturbing operator and $\Delta E^0_{es} = E^0_e - E^0_s$ appears as the resonance denominator. From, equation (2.15) and, the ρth component of equation (2.14), equation (2.12) becomes

$$(\bar{M}_\rho)_{gi,ev} = (\bar{m}_\rho)^o_{g,e} \langle ev|gi\rangle + \sum_{s,a} h^a_{es} (\Delta E^o_{es})^{-1} (\bar{m}_\rho)^o_{g,s} \langle ev|Q_a|gi\rangle \quad \ldots (2.16)$$

Similar expressions are obtained for the remaining transition moments. It is assumed that the wavefunctions are real, so that, for example, $(\bar{m}_\rho)^o_{e,g} = (\bar{m}_\rho)^o_{g,e}$ for all ρ.

It is to be noted that for resonance or near resonance conditions, i.e., when the incident radiation approaches, and becomes equal to that of a molecular transition, the first term of equation (2.10) gives rise to large increase in scattering, this increase being limited by the numerator and half width Γ_{ev} of the resonant state e. The second term is non resonant and produces a slowly varying background, which is negligible in the resonance region.

Writing $\Delta E^0_{es} = -h(\nu_s - \nu_e)$ and with appropriate substitution, equation (2.10) becomes,

$$(\alpha_{\rho\sigma})_{gi,gj} = A_{\rho\sigma} + B_{\rho\sigma} \quad \ldots\ldots (2.17)$$

where,

$$A_{\rho\sigma} = \frac{1}{h} \sum_{v} \left[\frac{(m_\rho)^\circ_{g,e} (m_\sigma)^\circ_{g,e} \langle gi|ev\rangle \langle ev|gj\rangle}{\nu_{ev,gi} - \nu_0 + i\Gamma_{ev}} \right] \quad \ldots\ldots (2.17a)$$

and $B_{\rho\sigma} =$

$$-\frac{1}{h^2} \sum_{v} \sum_{s} \sum_{a} h^a_{es} \left[\frac{(m_\rho)^\circ_{g,e} (m_\sigma)^\circ_{g,s} \langle gj|ev\rangle \langle ev|Q_a|gi\rangle + (m_\sigma)^\circ_{g,e} (m_\rho)^\circ_{g,s} \langle gi|ev\rangle \langle ev|Q_a|gj\rangle}{(\nu_{ev,gi} - \nu_0 + i\Gamma_{ev})(\nu_s - \nu_e)} \right] \ldots (2.17b)$$

Thus, we can summarize the findings as follows: When Raman spectra are excited in the region of an electronic absorption band, the vibrational modes which are expected to show enhancement are the ones which lend intensity to the electronic spectrum, i.e., they are vibronically active modes. These may be of two types (a) modes which connect the ground state to the excited state involved in resonance through the Franck-Condon(FC) overlap (A-type term); (b) modes which mix the resonant electronic state to another one of higher energy (B-type term). In FC effect, the potential energy curve of the excited electronic state is shifted so that the vibrational wavefunctions are not orthogonal. Raman scattering due to FC effect can arise only when the orthogonality is removed between a ground and excited state. A difference in vibrational frequency between the ground and excited state can also give rise to Raman modes; however in most

of the cases the change is too less to give rise to any appreciable FC effect. Totally symmetric modes can have their origin shifted in the excited state,* whereas by symmetry, shift of equilibrium position cannot take place along non-totally symmetric modes. Thus modes enhanced by type (a) mechanism are expected to be totally symmetric modes. The modes which will be enhanced by the type (b) mechanism involve mixing of two electronic states and thus transfer of electronic transition moment by means of vibrations of appropriate symmetry. The modes may have any symmetry which is contained in the direct product of the two electronic transition representations and thus allow scattering via non-totally symmetric modes also. In case of porphyrins the transitions giving rise to both the α and Soret bands are of E_u symmetry and hence vibronic coupling between these states occurs when $\Gamma_{vib} \subset E_u \times E_u = A_{1g}+A_{2g}+B_{1g}+B_{2g}$. The A_{1g} modes, however, do not participate in the vibronic coupling since there is no change of symmetry when products with A_{1g} are involved (although there is some evidence to the contrary[25]). The problem of FC effect and vibronic coupling mechanism is shown schematically in Fig. 2.6.

As can be seen from equation (2.17a) that this term relates to Raman scattering from totally symmetric modes for which both the transition dipole matrix elements $(m_\rho)^\circ_{g,e}$ and $(m_\sigma)^\circ_{g,e}$ must be non zero. The A-term scattering is particularly sensitive to the intensity of the resonant electronic

*Please see Appendix for clarification of this point.

absorption. The A-term contribution of the scattered intensity depends on the square of the electronic transition moment (extinction coefficient). As a result, upon excitation into an intense absorption band such as Soret band, strong enhancement of A_{1g} modes is expected in the RR spectra.

Equation (2.17b) gives rise to Raman scattering for the non-totally symmetric modes. For a fundamental Raman transition i=0, j=1. In this case, one finds two conditions of resonance. The frequency denominator reaches minimum values both at $\nu_0 = \nu_{e1,g0}$(i.e. ν_{0-1}) and at $\nu_0 = \nu_{e0,g0}$(i.e. ν_{0-0}). At the same time the first term in the numerator is at a maximum when v=1, while the second term is at a maximum when v=0. Consequently, this term will give rise to two maxima in the excitation profile when the excitation frequency corresponds to ν_{0-0} as well as ν_{0-1}. B-term scattering may become dominant in resonance with a weakly allowed transition that is vibronically coupled to a nearby strongly allowed transition and depends linearly on the extinction coefficient.

One of the important advantages of RR technique is its selectivity. The appearance of the resonance enhanced Raman features depend upon the nature of the particular electronic state(s) involved in the scattering process. This selectivity offered by the RR technique provides a direct monitor of the excited electronic state(s) from which the nature of the electronic transition can be elicited.

2.6 Resonance Raman Scattering From Manganese(III) Porphyrins

The absorption spectra of Mn(III)-porphyrin complexes are strikingly different from normal porphyrin spectra and show many additional features as compared to the absorption spectra of normal metalloporphyrins. RR scattering can be used to assign these bands. In order to see which vibrations may gain intensity due to excitation in different spectral regions, we shall elaborate on the contributions of porphyrin and metal orbitals in polarizability changes.

The ground state of Mn(III)-porphyrin can be written as follows:[26]

$$|g\rangle = \Psi_p \Psi_m$$

$$= NA \prod_i^m \Phi^2_{p_i} \Phi^{*0}_p \, d^1_{xy} d^1_{xz} d^1_{yz} d^1_{z^2} d^0_{x^2-y^2}$$

The different excited states of the system may be written as

$$|e\rangle = N_e A \prod_i^{m-1} \Phi^2_{p_i} \Phi^1_{p_m} \Phi^{*1}_p \, d^1_{xy} d^1_{xz} d^1_{yz} d^1_{z^2} d^0_{x^2-y^2},$$

$$|s\rangle = N_s A \prod_i^{m-2} \Phi^2_{p_i} \Phi^1_{p_{m-1}} \Phi^2_{p_m} \Phi^{*1}_p d^1_{xy} d^1_{xz} d^1_{yz} d^1_{z^2} d^0_{x^2-y^2},$$

$$|d\rangle = N_d A \prod_i^m \Phi^2_{p_i} \Phi^{*0}_p \, d^1_{xy} d^0_{xz} d^1_{yz} d^1_{z^2} d^1_{x^2-y^2},$$

and

$$|c\rangle = N_c A \prod_i^{m-1} \Phi^2_{p_i} \Phi^1_{p_m} \Phi^{*0}_p \, d^1_{xy} d^1_{xz} d^2_{yz} d^1_{z^2} d^0_{x^2-y^2},$$

Where Ψ_p and Ψ_m represent the wavefunctions of the porphyrin and metal, $|e\rangle$ and $|s\rangle$, $|d\rangle$, $|c\rangle$ represent excited states reached by $\pi \rightarrow \pi^*$ transition, metal d$\longrightarrow$ d transition and charge trnasfer transitions. N is the normalization factor,

A is the antisymmetrizer, Φ_{p_i} are the occupied molecular orbitals in the ground state configuration of the porphyrin, Φ_p^* is the lowest unoccupied porphyrin molecular orbital. The superscripts indicate the electron occupancy of the orbitals.

The enhancement of resonance Raman features by the A-term will depend upon the factors $\langle gi|ev\rangle\langle ev|gj\rangle$. Under Born-Openheimer approximation, the wavefunction of a molecule in a vibronic state $|e\rangle$ can be written as: $\Psi_e = \Phi(q,Q)\kappa(Q)$. To proceed further, we resolve $\kappa(Q)$ in terms of modes associated with macrocycle and the metal, so that $\kappa(Q) = \kappa_p(Q)\kappa_m(Q)$. Therefore we have,

$$|gi\rangle = \Phi_p \Phi_m \kappa_p^i \kappa_m^i,$$

$$|gj\rangle = \Phi_p \Phi_m \kappa_p^j \kappa_m^j,$$

and $$|ev\rangle = \Phi_p^e \Phi_m \kappa_p^{ev} \kappa_m^v,$$

$$|cu\rangle = \Phi_p^{*+} \Phi_m^{*-} \kappa_p^{u^{*+}} \kappa_m^{u^{*-}}$$

For resonance with a state $|e\rangle$ reached by $\pi \rightarrow \pi^*$ excitation the Franck-Condon factors will be,

$$\sum_v \langle \kappa_p^j \kappa_m^j | \kappa_p^{ev} \kappa_m^v \rangle \langle \kappa_p^{ev} \kappa_m^v | \kappa_p^i \kappa_m^i \rangle$$

$$= \sum_v [\langle \kappa_p^j | \kappa_p^{ev} \rangle \langle \kappa_p^{ev} | \kappa_p^i \rangle][\langle \kappa_m^j | \kappa_m^v \rangle \langle \kappa_m^v | \kappa_m^i \rangle] \quad \ldots\ldots (2.18)$$

Since the $\pi \rightarrow \pi^*$ transition involves charge redistribution in the porphyrin macrocycle the distortion of the excited electronic state occurs within the macrocycle and as a result the macrocyclic modes are enhanced. Similarly, it can be shown that the change of the excited state configuration occurs within both the macrocycle and metal, when the excitation

occurs within a charge transfer band and as a result both metal and macrocyclic modes will be enhanced.

The vibronic mixing between the excited electronic states $|e\rangle$ and $|s\rangle$ occurs via the factors $\langle e|(\frac{\partial H}{\partial Q_a})_o|s\rangle$. In order to see which type of vibrations would be enhanced by excitation in a particular absorption region, it is necessary to resolve the spatial properties of $\langle e|(\frac{\partial H}{\partial Q_a})_o|s\rangle$. The operator $(\partial H/\partial Q_a)_o$ which mixes the electronic states is a one-electron operator, since the only part of the electronic Hamiltonian that depends on the nuclear position is the Coulomb potential between electrons and nuclei. The change of the electronic Hamiltonian with respect to the normal coordinate is given by,

$$(\frac{\partial H}{\partial Q_a})_o = - e' \sum_j \sum_n \partial (Z_n/r_{jn})/\partial Q_a,$$

where the summation is over all the electrons j and nuclei n, e' is the electronic charge, Z_n is the charge on the nucleus n and r_{jn} is the distance between electron j and nucleus n. For any one electron operator, we can write,

$$O \equiv \int O(r)\, \Phi'(r) dr,$$

and therefore

$$\langle e|O|s\rangle = \int \langle e|\, \Phi'(r)|s\rangle\, O(r) dr \quad . . . . . (2.19)$$

where, O is equivalent to ($\partial H / \partial Q_a$) and $\langle e|\, \phi'(r)|s\rangle$ is known as transition density and represent spatial overlap of $|e\rangle$ and $|s\rangle$. As has been shown by Albrecht[17] that if two orbitals occupy different regions of the molecule, then

contribution to Raman intensity by vibrational perturbation from the pair of orbitals will be very small or non-existent.

Suppose now the two $\pi \rightarrow \pi^*$ excited states $|e>$ and $|s>$ are coupled by vibrational perturbation. Then we shall have

$$\langle e| \phi(r) |s> = -e' \int \phi^1_{p_{m-1}} \delta(r - r_j) \phi^1_{p_m} dr_j \quad \ldots\ldots \quad (2.20),$$

since the integral equals unity for electrons not involved in the transition. $\phi_{p_{m-1}}$ and ϕ_{p_m} are the highest occupied molecular orbitals. These orbitals are localized in the porphyrin macrocycle and occupy similar regions. Therefore the vibrations which will show intensity enhancement via this term are those of macrocycle. In a similar manner, it can be shown that,

(i) for coupling of a charge transfer band in which an electron goes to a d_{yz} or d_{xz} orbital of metal with an excited state reached by a $\pi \Rightarrow \pi^*$ transition from the same occupied molecular orbital, the vibrations around the central metals will show the greatest activity.

(ii) for coupling of two different charge transfer excited states which are obtained by excitation of electrons from the same porphyrin ground state molecular orbitals to different d orbitals of metal, the vibrations related to metal-axial ligand may be picked out (since the two different d orbitals occupy different regions of space, the contribution from this term will be small, unless axial ligand vibrations and the constraints imposed by the pyrrole nitrogens mix the d orbitals).

(iii) for coupling of two charge transfer states which are obtained by excitation from different porphyrin

π orbitals to the same metal d orbitals, vibrations related to the macrocycle should be enhanced.

Based on the enhancement of specific modes in the RR spectra due to excitation in different spectral regions, one can obtain deeper insight about the nature of electronic transitions responsible for the absorption in the region.

2.7 Depolarization Ratio

When electromagnetic radiation interacts with a system, there is often a change in its plane of polarization. These changes are important parameters in Raman and Rayleigh scattering as they may be correlated with the symmetry of the scattering species. Consider now the molecule fixed at a space-fixed coordinate shown in Fig. 2.7. The incident light is plane polarized with the electric vector $\bar{E}$ lying in the XZ plane and propagating along Y axis. Scattered intensity is observed in the direction $\bar{n}'$, i.e., along the Z axis and perpendicular to the direction of propagation of the incident beam. The intensity scattered in the direction $\bar{n}'$ is made up of contribution of x and y components of the induced dipole. $\bar{\mu}_z$ makes no contribution, since an oscillating dipole does not emit in the direction of its axis. From classical radiation theory the scattered intensity is

$$dI = \frac{4\pi^3 (\nu')^4}{c^3}(|\mu_x|^2 + |\mu_y|^2)d\Omega \qquad \ldots\ldots\ldots (2.21)$$

with $\nu' = \nu \pm \nu_{mn}$. Since $I_x \sim |\mu_x|^2$ and $I_y \sim |\mu_y|^2$, the total intensity dI scattered into a solid angle $d\Omega$ is made up of the two

contributions, I_x and I_y. The ratio of the two components

$$\rho = \frac{I_y}{I_x} = \ldots\ldots \quad (2.22)$$

is called the depolarization ratio. Usually the depolarization ratio is measured for $\theta = 90°$. In this instance the electric vector $\bar{E}$ is perpendicular to the scattering plane defined by $\bar{n}$ and $\bar{n}'$. It is then customary to denote. I_x as $I_{||}$, i.e., $I_{||}$ is parallel to $\bar{E}$, and I_y as $I_\perp$, therefore,

$$\rho_l\ (\theta = 90°) = \frac{I_\perp}{I_{||}} \quad \ldots\ldots\ldots\ldots (2.23)$$

The subscript on ρ_l indicates linearly polarized incident radiation.

In fluids, the orientations of the molecules will not be fixed, since the molecules will be moving randomly. In this case, the observed Raman scattering from a sample will correspond to the average over all molecular orientations. The depolarization ratio for randomly oriented molecules for linearly polarized incident radiation is given by

$$\rho_l = \frac{3\gamma^2}{45\,\bar{\alpha}^2 + 4\gamma^2} \quad \ldots\ldots\ldots (2.24)$$

where $\bar{\alpha}$ is the isotropic part of the molecular scattering tensor*:

$$\bar{\alpha} = \tfrac{1}{3}(\alpha_{xx} + \alpha_{yy} + \alpha_{zz}),$$

and γ represent the anistropy of the tensor:

$$\gamma^2 = \tfrac{1}{2}[(\alpha_{xx} - \alpha_{yy})^2 + (\alpha_{xx} - \alpha_{zz})^2 + (\alpha_{yy} - \alpha_{zz})^2] + 3(\alpha_{xy}^2 + \alpha_{yz}^2 + \alpha_{zx}^2)$$

---

* In principle, Raman scattering tensors are written as $(\alpha_{\rho\sigma})_{mn}$ for m = n. In the present discussion, the subscripts m and n are omitted for clarity and it is implicit that the scattering tensor refers to a specific transition of the molecule.

Equation (2.24) is valid only if the tensor is symmetric, i.e., $\alpha_{\rho\sigma} = \alpha_{\sigma\rho}$.

In normal Raman scattering, it is well known that the measurement of linear depolarization ratio may identify the symmetry of the vibrational mode responsible for a given Raman band. $\rho_l < 3/4$ ($\rho_l = 0$ in cubic or higher symmetries) for totally symmetric modes and $\rho_l = 3/4$ for non-totally symmetric modes. Under resonance Raman scattering conditions the value of ρ_l and its dependence on the exciting frequency, may be more informative. This is because the symmetries of particular electronic states, as well as symmetry aspects of their vibronic manifolds become significant under resonance. In normal vibrational Raman effect, it is generally assumed that the scattering tensor is symmetric ($\alpha_{\rho\sigma} = \alpha_{\sigma\rho}$). Theory predicts that the scattering tensor may become both unsymmetrical and complex under resonance condition.[24] However, in the absence of magnetic perturbations (external magnetic field or spin-orbit coupling) the tensor becomes real but remaining unsymmetric, i.e., $\alpha_{\rho\sigma} \neq \alpha_{\sigma\rho}$. Placzek[24] had pointed out that in this case, the depolarization ratio ρ_l should be described as,

$$\rho_l = \frac{3g^s + 5g^a}{10g^o + 4g^s} \qquad \ldots\ldots\ldots (2.25)$$

where

$$g^o = 3\bar{\alpha}^2,$$

$$g^s = \tfrac{1}{3}[(\alpha_{xx} - \alpha_{yy})^2 + (\alpha_{xx} - \alpha_{zz})^2 + (\alpha_{yy} - \alpha_{zz})^2] + \tfrac{1}{2}[(\alpha_{xy} + \alpha_{yx})^2 +$$

$(\alpha_{xz}+\alpha_{zx})^2+(\alpha_{yz}+\alpha_{zy})^2]$,

$g^a=\frac{1}{2}[(\alpha_{xy}-\alpha_{yx})^2+(\alpha_{xz}-\alpha_{zx})^2+(\alpha_{yz}-\alpha_{zy})^2]$.

These three quantities (g^o, g^s, g^a) are called respectively, the isotropic, the quadrapole and the magnetic dipole components of the scattering tensor. A direct connection with equation (2.24) can be more conveniently made if we redefine the quadrapole and magnetic dipole quantities slightly, as two anisotropy invariants of the tensor, a symmetric part:

$$\gamma_s^2 = 3/2g^s$$

and an asymmetric part:

$$\gamma_{as}^2 = 3/2g^a$$

Then $$\rho_l = \frac{3\gamma_s^2 + 5\gamma_{as}^2}{45\bar{\alpha}^2 + 4\gamma_s^2} \qquad \ldots\ldots\ldots (2.26)$$

When each of the invariants contributes alone, a characteristic value of ρ_l results:

(a) pure isotropic scattering: $\bar{\alpha}^2 \neq 0, \gamma^2_s=0, \gamma^2_{as}=0; \rho_l=0$ (independent of value of $\bar{\alpha}^2$).

(b) pure symmetric scattering: $\bar{\alpha}^2=0,\ \gamma_s^2 \neq 0,\ \gamma^2_{as}=0; \rho_l=3/4$ (independent of the value of γ_s).

(c) pure antisymmetric scattering: $\bar{\alpha}^2 = 0, \gamma_s^2=0, \gamma^2_{as}\neq 0; \rho_l = \infty$ (independent of the value of γ_{as}).

It must be noted, however, that in case (c) if $\gamma^2_{as}=0$ due to symmetry of the scattering tensor ($\alpha_{\rho\sigma} = \alpha_{\sigma\rho}$) then $I_\perp = I_{||} = 0$ and no scattering is observed. For each of these pure types of scattering the value of ρ_l is a constant, independent of the excitation frequency. Under resonance condition, each of these invariants may show a different wavelength

dependence and the value of ρ_l for a particular mode will depend on the position of the exciting wavelength with respect fo the electronic absorption spectrum.

The consequences of the contributions from antisymmetric tensor to scattered radiation and depolarization ratios are interesting. For Raman scattering from non-totally symmetric modes,

$\bar{\alpha}^2 = 0$ and $\rho_l = \frac{3}{4} + \frac{5}{4}\frac{\gamma_{as}^2}{\gamma_s^2}$

If $\gamma_{as}^2 = 0$, we have normal polarization with $\rho_l = 3/4$. If $\gamma_{as}^2 \neq 0$, we have anomalous polarization with $\rho_l > 3/4$ provided $\gamma_s^2 \neq 0$; but inverse polarization with $\rho_l = \infty$ if $\gamma_s^2 = 0$.

For totally symmetric modes where $\bar{\alpha}^2 \neq 0$ and $\gamma_{as}^2 = 0$,

$$\rho_l = \frac{3}{(45\bar{\alpha}^2/\gamma_s^2 + 4)} \quad \text{and so} \quad 0 \leqslant \rho_l < 3/4$$

according as $\infty \gtrless \frac{45\,\bar{\alpha}^2}{\gamma_s^2} > 0$

Group theoretical considerations can provide information about the invariants which are non zero for particular vibrational modes in molecules of a given symmetry, and thus about the symmetry properties of the general polarizability tensor. The symmetries of the scattering tensor in different molecular point groups have been given by McClain.[27] This helps in evaluating the contributions from any of the invariants for a Raman process transforming under any irreducible representation .

'Dispersion of ρ_l with excitation frequency requires

mixed contribution from the invariants. This occurs when the scattering species belongs to a point group in which two or all three of the invariants transform under the same irreducible representation. The type of the tensor pattern alongwith the value of depolarization ratios for the point groups D_{4h}, C_{4v}, D_{2d}, D_4 and lower ones is given in Table 2.2. The dispersion of ρ_l with excitation frequency often provides valuable structural information about the symmetry of the molecule.

Under resonance conditions where $\alpha_{\rho\sigma} \neq \alpha_{\sigma\rho}$ in general, one can distinguish five distinct classes depending upon contributions from three parts as shown in Table 2.3. Experimentally the evaluation of all three tensor invariants requires three independent intensity measurements. The measurement of the total scattering at 90°, $(I_{||} + I_{\perp})$, and the depolarization ratio ρ_l, may be supplemented by a measurement involving circularly polarized light. It is usual to measure the reversal coefficient I_{contra}/I_{co}, which is the ratio of the intensity of contra-rotating to that of co-rotating light for the back scattering of pure circularly polarized incident radiation. This information is however, not sufficient to determine the point group symmetry of the molecule having modes which show a dispersion of ρ_l, i.e., vibrations belonging to classes I and III of the Table 2.3. In addition to the measurement at a particular exciting frequency, one requires measurements at various values of ν_0 such that if $I_{\perp}$ and $I_{||}$ are measured

at various exciting frequencies, one can determine unambiguously the classes in Table 2.3 to which the mode belongs. However, no separate evaluation of each of the $\bar{\alpha}^2$, γ_s^2 and γ_{as}^2 components is possible.

2.8 Antisymmetric Tensor Contributions

The resonance Raman spectra of porphyrins[28] and haeme proteins[29] provided the first example of inverse polarization. The modes which are responsible for this effect are of A_{2g} symmetry. The A_{2g} modes are inactive in normal Raman scattering since they are associated with antisymmetric scattering tensor, i.e. $\alpha_{\rho\sigma} = -\alpha_{\sigma\rho}$. An explicit demonstration of the antisymmetry of the scattering tensor for an A_{2g} mode in D_{4h} symmetry, was given by Warshel.[30] It has been shown, that, such situation exists in the presence of a doubly degenerate electronic level and a rotational type vibrational mode which leads to equal rotations of the two orthogonal transition moments. The A_{2g} vibrations have rotational symmetry around the four-fold axis. From the form of porphyrin molecular orbitals, shown in Fig. 2.3 and form of A_{2g} vibration shown in Fig. 2.8, it is clear that the A_{2g} mode will be effective in mixing the two electronic transitions and its intensity will be correspondingly enhanced. Thus, with proper exciting line, inverse polarization may be observed, i.e., the plane of polarization of the incident light is rotated through 90° on scattering and $\rho_\perp = \infty$. However, only in the case of a

weak electronic transition will the A_{2g} modes (whose intensities are dominated by the B-term contribution) have a significant RR intensity relative to that of the A-type contributions of the totally symmetric modes. Some of the bands in different systems have been observed for which $\rho_l \neq \infty$ but $\rho_l > 3/4$, are called anomalously polarized bands. There are two possible explanations for a significant parallel component of anomalously polarized modes. The effective symmetry of the molecule may be less than D_{4h} in which case the formerly A_{2g} modes may acquire symmetric as well as antisymmetric components of the scattering tensor. Alternatively, there may be accidental degeneracies between A_{2g} modes and modes of other symmetries, which are polarized (A_{1g}) or depolarized (B_{1g} or B_{2g}), giving an overall depolarization ratio which is anomalous.

2.9 Interference Effects In Raman Scattering

The expression for the Raman scattering tensor may contain a sum over all excited states of the scattering system. Under resonant condition only few excited states need to be taken into account. If these states are in any way related, such as via vibronic coupling, characteristic interference pattern will occur in the excitation and polarization dispersion spectra. The Raman intensity being proportional to the Raman tensor times its complex conjugate, does contain a cross-term that modify the excitation profile from that expected

for a totally isolated resonance.

Interference may be of two types (i) vibrational interference (ii) electronic interference. In case (i) two or more states belonging to the same adiabatic electronic manifold interfere, whereas in (ii) interference between different electronic states takes place. There can also be interference between resonant and non resonant contributions.

If the scattering tensor contains contribution from two terms $\dot{x}$ and $\dot{y}$, then the intensity will contain a cross-product 2xy. Since $I \propto |\alpha_{\rho\sigma}|^2 \Rightarrow x^2 + y^2 + 2xy$. The Raman intensity is thus not the simple sum of the individual contributions but there is an additional term 2xy. In off resonance region, x and y have the same sign. However, xy can assume positive or negative values depending on the relative signs of x and y. In the former case the Raman intensity shows monotonous increase as resonance is approached, while in the later case there is a chance that deenhancement of the Raman intensity may occur in a specific wavelength region due to destructive interference between the scattering terms.

In case of metalloporphyrins, under resonance excitation in the visible region, the incident light frequency is so close to the allowed electronic transitions that only the purely electronic state (the 0-0 state) and the first vibrationally excited state (the 0-1 state) need to be taken into

account. There is a possibility of intereference between the contributions from the 0-0 band and that from the 0-1 band.

By writing $\alpha_{\rho\sigma} = \alpha_{\rho\sigma}^{0-0} + \alpha_{\rho\sigma}^{0-1}$ and $\alpha_{\sigma\rho} = \alpha_{\sigma\rho}^{0-0} + \alpha_{\sigma\rho}^{0-1}$

and forming the symmetric and antisymmetric tensor components, the interference is constructive for the ($\alpha_{\rho\sigma} + \alpha_{\sigma\rho}$) components but destructive for the antisymmetric component($\alpha_{\rho\sigma} - \alpha_{\sigma\rho}$), when one is far from resonance. This explains nicely the fact that the antisymmetric tensor component vanishes for ordinary, non resonance Raman scattering. For excitation in the region between the 0-0 and 0-1 bands the interference is constructive for the antisymmetric component but destructive for the symmetric component explaining directly the depolarization ratio rises to a maximum between the 0-0 and 0-1 bands.[31]

2.10 Infrared Absorption

The infrared(IR) absorption is a phenomenon involving interaction between electromagnetic radiation and matter. To a first order approximation, it arises due to change in electric dipole moment of the molecular unit during its excitation to a higher energy state. It may, however, also arise due to change in electric moments of higher order, magnetic moments, etc., but the absorption induced by such interactions is negligibly weak. The frequencies of molecular vibrations fall in the IR range of the electromagnetic spectrum and

the intensity of an IR absorption band is proportional to the square of the change in dipole moment caused by molecular vibration.

Raman scattering and IR absorption are governed by different selection rules. Some transitions may be observed only through Raman scattering, some only in direct absorption and some both in direct absorption and through Raman scattering, depending upon the symmetry of the molecular system. Thus for a complete understanding of molecular dynamics a study of both Raman scattering and IR absorption is necessary.

Appendix to page No.40

From the theoretical development given in this chapter, it has been shown that the A-type term of the scattering tensor can give rise to the enhancement of totally symmetric modes only, while B-type term can contribute to the enhancement of modes of any symmetry which is contained in the direct product of the two electronic transition representations. The reason for the symmetry restrictions for the non-totally symmetric modes can be given as follows: Consider a molecule at the vibrational equilibrium in the ground electronic state so that there are no vibrational forces acting on it. If, upon undergoing an electronic transition, the nuclei are subjected to a force, tending to establish some new equilibrium geometry along a particular normal coordinate, then the potential minima of the excited state will be shifted along that normal coordinate. Since the potential energy of nuclear vibration is equal to the total electronic energy in the ABO approximation, it is possible to write the force along a coordinate Q, experienced in the electronic excited state $|e\rangle$, as the diagonal vibronic-coupling matrix element: $\langle e | (\partial H/\partial Q)_0 | e \rangle$. If $|e\rangle$ is non-degenarate, the matrix element of the force will vanish unless Q transforms under the totally symmetric irreducible representation of the point group. Hence, shifts of equilibrium positions in the excited electronic states take place only along the totally symmetric coordinates.

REFERENCES

1. W. Küster, Hoppe-Seyler's Z. Physiol. Chem. **82**, 463(1912).

2. (a) A. Stern and H. Wenderlein, Z. Physik. Chem. **A177**, 165(1936).
   (b) A. Stern and H. Molvig, Z. Physik. Chem. **A177**, 365(1936).
   (c) A. Stern and H. Molvig, Z. Physik. Chem. **A178**, 161(1937).
   (d) A. Stern and F. Pruckner, Z. Physik. Chem. **A178**, 420(1937).
   (e) A. Stern and M. Dezelic, Z. Physik. Chem. **A179**, 275(1937).
   (f) A.Stern and F. Pruckner, Z. Physik. Chem. **A180**, 321(1937).

3. J.E. Falk, in 'Porphyrins and Metalloporphyrins' Elsevier: Amsterdam, 1964.

4. J.R. Platt, in 'Radiation Biology' ed. A. Hollaender, McGraw-Hill: New York, vol. III, Ch.2(1956).

5. M. Gouterman, J. Chem. Phys. **30**, 1139(1959).

6. W.T. Simpson, J. Chem. Phys. **17**, 1218(1949).

7. W. Moffitt, J. Chem. Phys. **22**, 320(1954).

8. W. Moffitt, J. Chem. Phys. **22**, 1820(1954).

9. H.C. Longuet-Hi,gins, C.W. Rector and J.R. Platt, J. Chem. Phys. **18**, 1174(1950).

10. M. Gouterman, J. Mol. Spectrosc. **6**, 138(1961).

11. M. Gouterman, in 'Excited States of Matter' ed. C.W. Shoppee, Grad. Stud. Texas Tech Univ.: Lubbock, TX, vol.**2**, 63(1973).

12. M. Zerner and M. Gouterman, Theoret. Chim. Acta **4**, 44(1966).

13. J.M. Friedman and R.M. Hochstrasser, Chem. Phys. **6**, 155(1974).

14. M. Jacon, in 'Advances in Raman Spectroscopy' ed. J.P. Mathieu, vol. **1**, (1973).

15. H.A. Kramers and W. Heisenberg, Z. Physik **31**, 681(1925).

16. P.A.M. Dirac, Proc. Roy. Soc. London, **114**, 710(1927).

17. A.C. Albrecht, J. Chem. Phys. **34**, 1476(1961).

18. L.L. Krushinskii and P.P. Shorygin, Opt. Spectrosc. USSR, **19**, 312(1965).

19. F.A. Savin, Opt. Spectrosc. USSR, **19**, 308(1965).

20. E.M. Verlan, Opt. Spectrosc. USSR, **20**, 341(1966).

21. E.M. Verlan, Opt. Spectrosc. USSR, **20**, 447(1966).

22. J. Tang and A.C. Albrecht, in 'Raman Spectroscopy: Theory and Practice' ed. H.A. Szymanski, Plenum Press: New York, Vol. **2**, 33(1970).

23. A.L. Verma, Indian J. Phys. **54B**, 54(1980).

24. G. Placzek, in 'Rayleigh and Raman Scattering' UCR L Transl. No. 526(L) for 'Handbuch der Radiologie' ed. E. Marx, Akademische Verlagsgesellschaft VI: Leipzig, vol. **2**, 209(1934).

25. J.A. Shelnutt, D.C. O'shea, N.-T. Yu, L.D. Cheung and R.H. Felton, J. Chem. Phys. **64**, 1156(1976).

26. S. Asher and K. Sauer, J. Chem. Phys. **64**, 4115(1976).

17. W.M. McClain, J. Chem. Phys. **55**, 2789(1971).

28. A.L. Verma and H.J. Bernstein, J. Raman Spectrosc. **2**, 163(1974).

29. T.G. Spiro and T.C. Strekas, Proc. Natl. Acad. Sci. USA, **69**, 2622(1972).

30. A. Warshel, Chem. Phys. Lett. **43**, 273(1976).

31. A.L.Verma, R. Mendelsohn and H.J. Bernstein, J. Chem. Phys. **61**, 383(1974).

TABLE 2.1 Hamiltonians for y Polarized States*

	$(a_{2u}e_{gy})$	$(a_{1u}e_{gx})$	Dipole strength (q^2)
(a)			
$(a_{2u}e_{gy})$	$A'_{1g} + A_{1g}$	A''_{1g}	R_2^2
$(a_{1u}e_{gx})$	A''_{1g}	$A'_{1g}-A_{1g}$	R_1^2
	B_y°	Q_y°	
(a')			
$B_y^\circ \equiv (2)^{-1/2}[(a_{2u}e_{gy})+(a_{1u}e_{gx})]$	$A'_{1g}+A''_{1g}$	A_{1g}	$R^2 \equiv \frac{1}{2}(R_1+R_2)^2$
$Q_y^\circ \equiv (2)^{-1/2}[(a_{2u}e_{gy})-(a_{1u}e_{gx})]$	A_{1g}	$A'_{1g}-A''_{1g}$	$r^2 \equiv \frac{1}{2}(R_2-R_1)^2$
	B_y	Q_y	
(b) $[\tan 2\nu \equiv A_{1g}/A_{1g}]$			
$B_y \equiv \cos\nu B_y^\circ + \sin\nu Q_y^\circ$	$A'_{1g}+A''_{1g}/\cos 2\nu$	0	$\frac{1}{2}(1+\cos 2\nu)R^2+Rr\sin 2\nu+\frac{1}{2}(1-\cos 2\nu)r^2$
$Q_y \equiv -\sin\nu B_y^\circ + \cos\nu Q_y^\circ$	0	$A'_{1g}-A''_{1g}/\cos 2\nu$	$\frac{1}{2}(1-\cos 2\nu)R^2-Rr\sin 2\nu+\frac{1}{2}(1+\cos 2\nu)r^2$
(c) $[2\nu = A_{1g}/A''_{1g} < 1]$			
$B_y = B_y^\circ + \nu Q_y^\circ$	$A'_{1g}+A''_{1g}(1+2\nu^2)$	0	$R^2 - \nu^2R^2+2\nu Rr$
$Q_y = Q_y^\circ - \nu B_y^\circ$	0	$A'_{1g}-A''_{1g}(1+2\nu^2)$	$(\nu R - r)^2$

*Table reproduced from Gouterman.[5]

TABLE 2.2 **Irreducible Representations of the Raman Scattering Tensors and Expected Range of Depolarization Ratios (ρ_l) for Point Groups Relevant in this Study.**

Scattering Tensors	Range of ρ_l Values
$\begin{pmatrix} s_1 & s_2 & s_3 \\ s_4 & s_5 & s_6 \\ s_7 & s_8 & s_9 \end{pmatrix}$	A in C_1 and C_i $0 \leq \rho_l \leq \infty$
$\begin{pmatrix} s_1 & s_4 & 0 \\ s_5 & s_2 & 0 \\ 0 & 0 & s_3 \end{pmatrix}$	A in C_2, C_s and C_{2h} $0 \leq \rho_l \leq \infty$
$\begin{pmatrix} 0 & 0 & s_1 \\ 0 & 0 & s_2 \\ s_3 & s_4 & 0 \end{pmatrix}$	B in C_2, C_s, and C_{2h} $\frac{3}{4} \leq \rho_l \leq \infty$
$\begin{pmatrix} s_1 & 0 & 0 \\ 0 & s_2 & 0 \\ 0 & 0 & s_3 \end{pmatrix}$	A(A_1) in C_{2v}, D_2, D_{2h} $0 \leq \rho_l \leq \frac{3}{4}$
$\begin{pmatrix} 0 & s_1 & 0 \\ s_2 & 0 & 0 \\ 0 & 0 & 0 \end{pmatrix}$	A_2, B_1, B_2, B_3 (with cyclic permutations xy → yz → zx) in C_{2v}, D_2, D_{2h} $\frac{3}{4} \leq \rho_l \leq \infty$
$\begin{pmatrix} s_1 & 0 & 0 \\ 0 & s_1 & 0 \\ 0 & 0 & s_2 \end{pmatrix}$	A(A_1, Σ^+) in C_{nv}, D_n, D_{nh} (n=3,4.....,∞) D_{2d}, D_{3d} $\quad 0 \leq \rho_l \leq \frac{3}{4}$
$\begin{pmatrix} 0 & s_1 & 0 \\ -s_1 & 0 & 0 \\ 0 & 0 & 0 \end{pmatrix}$	A_2 in C_{nv}, D_n, D_{nh} (n=3,4.....∞) D_{2d}, D_{3d} $\rho_l = \infty$

Contd...

Table 2.2 contd..

Scattering Tensors	Range of ρ_l Values
$\begin{pmatrix} s_1 & s_3 & 0 \\ -s_3 & s_1 & 0 \\ 0 & 0 & s_2 \end{pmatrix}$	A in $C_n, C_{nh}(n=3,4,\ldots\ldots,\infty), S_4, S_6$ $0 \leq \rho_l \leq \infty$
$\begin{pmatrix} s_1 & 0 & 0 \\ 0 & -s_1 & 0 \\ 0 & 0 & 0 \end{pmatrix}$	B_1 in $C_{4v}, D_4, D_{2d}, D_{4h}$ $\rho_l = \frac{3}{4}$
$\begin{pmatrix} 0 & s_1 & 0 \\ s_1 & 0 & 0 \\ 0 & 0 & 0 \end{pmatrix}$	B_2 in $C_{4v}, D_4, D_{2d}, D_{4h}$ $\rho_l = \frac{3}{4}$
$\begin{pmatrix} 0 & 0 & s_1 \\ 0 & 0 & -is_1 \\ s_2 & -is_2 & 0 \end{pmatrix}$ +c.c.	$E(E_1, \Pi)$ in $C_{nv}, D_n, D_{nh}(n=3,4,\ldots\ldots\infty) D_{2d}$? D_{3d} $\frac{3}{4} \leq \rho_l \leq \infty$

c.c. complex conjugate.

TABLE 2.3 Distinct Classes Depending Upon Contributions from $\bar{\alpha}^2, \gamma_s^2$ and γ_{as}^2 to the Polarizability of the System and Expected Variation of ρ_l Values for Each Case.

	$\bar{\alpha}^2$	γ_s^2	γ_{as}^2	ρ_l
Class I	+	+	+	0-∞
Class II	+	+	0	0-3/4
Class III	0	+	+	3/4-∞
Class IV	0	+	0	3/4
Class V	0	0	+	∞

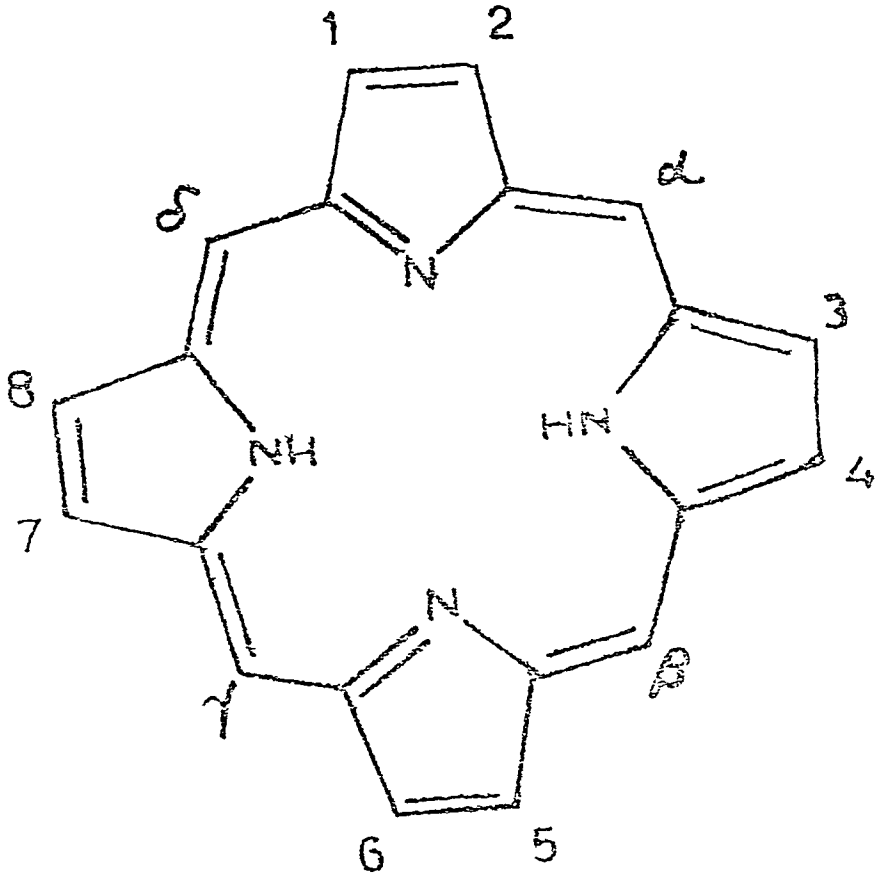

Fig.2.1 *Structure of free base porphyrin. Different porphyrins* are obtained by specific substitution at the α to δ or 1 to 8 positions.

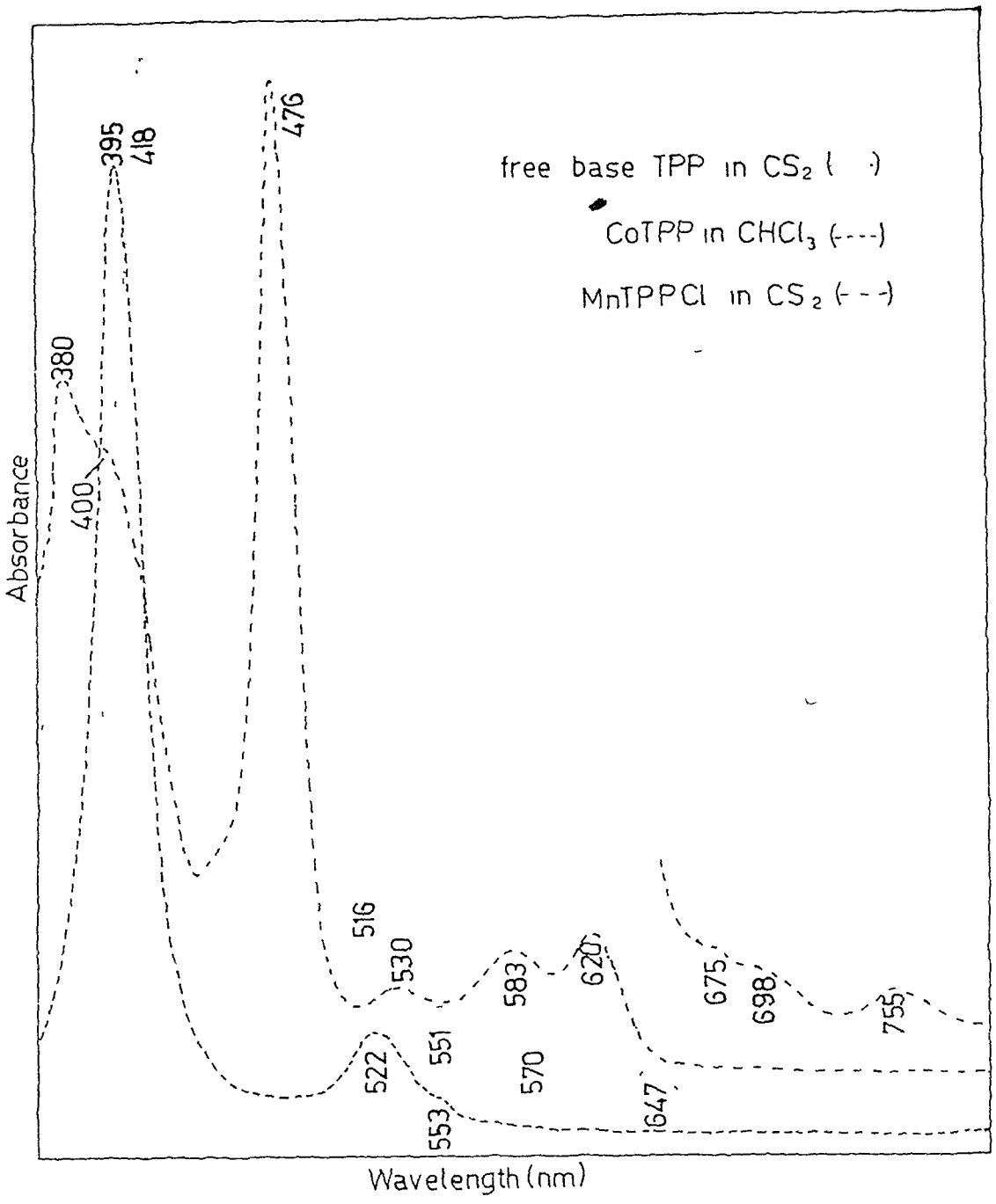

Fig.2.2 Absorption spectra of: free base TPP in CS_2; CoTPP in $CHCl_3$ and MnTPPCl in CS_2 solutions ($\sim 10^{-5}$ M conc).

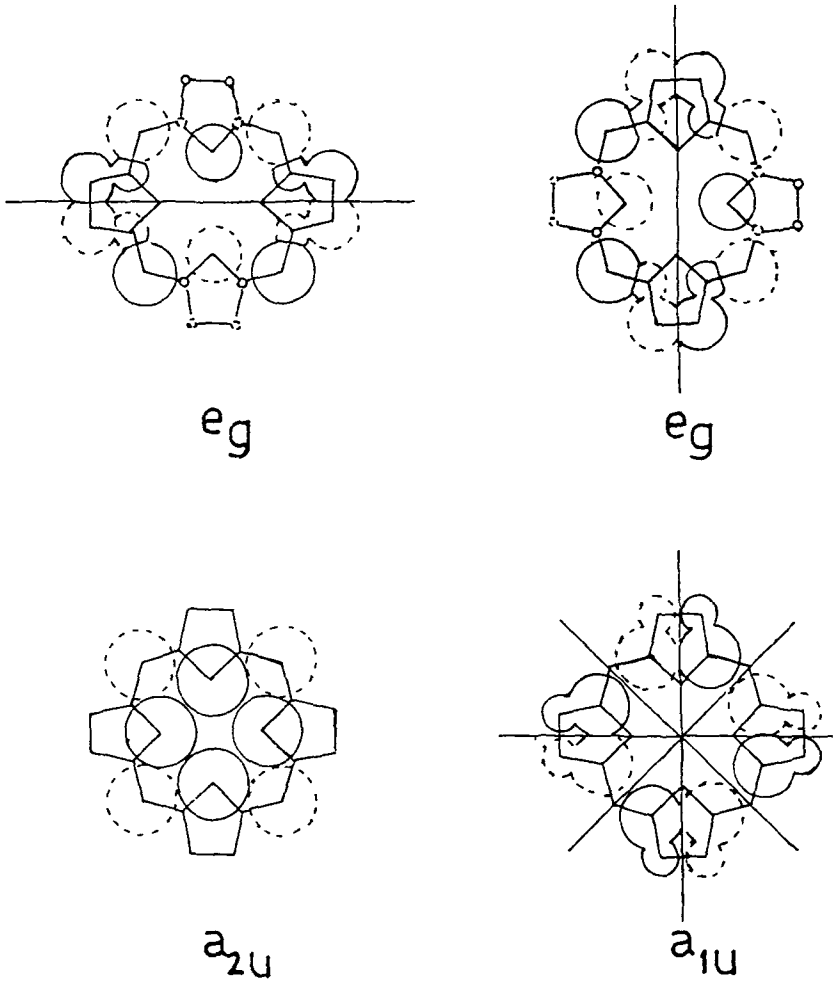

Fig. 2.3 Porphyrin top filled molecular orbitals e_g and lowest empty molecular orbitals a_{2u} and a_{1u}. The orbital coefficients are proportional to the size of the circles. Solid or dashed circles indicate sign of the orbitals. Lines indicate the symmetry nodes.

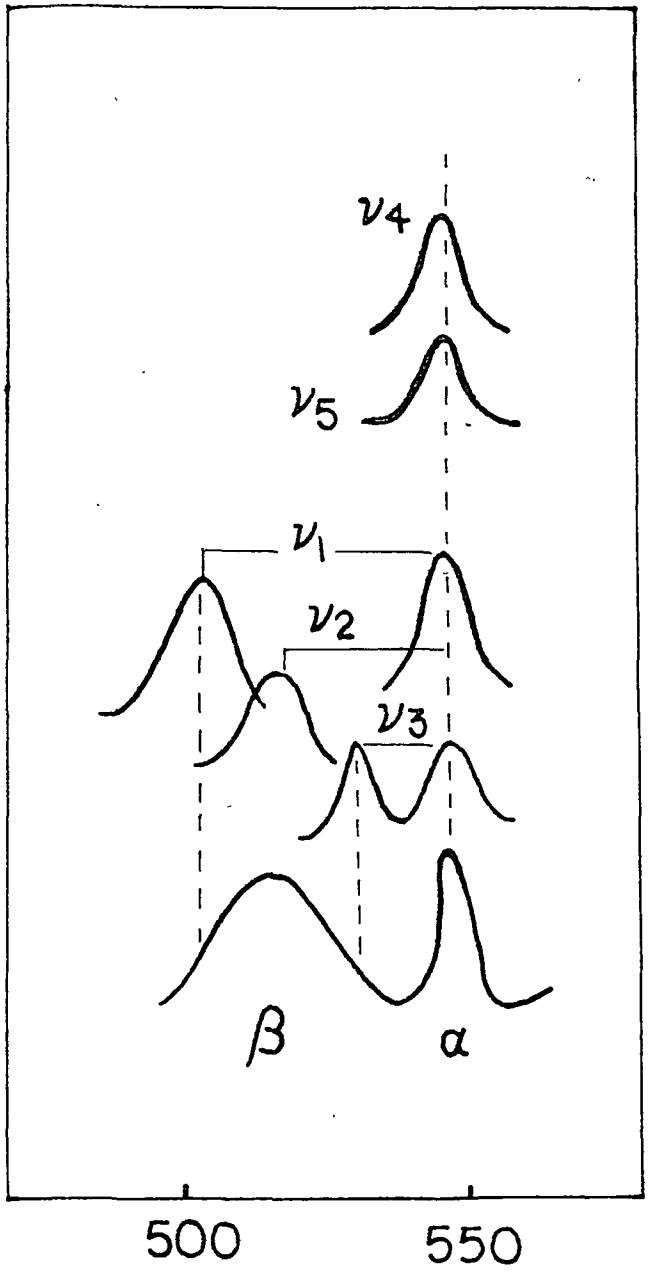

Fig. 2.4 Diagram showing that β absorption band is related to the α absorption band by $\nu_{\beta}^{max} = \nu_{\alpha}^{max} + \nu_{vib.}$

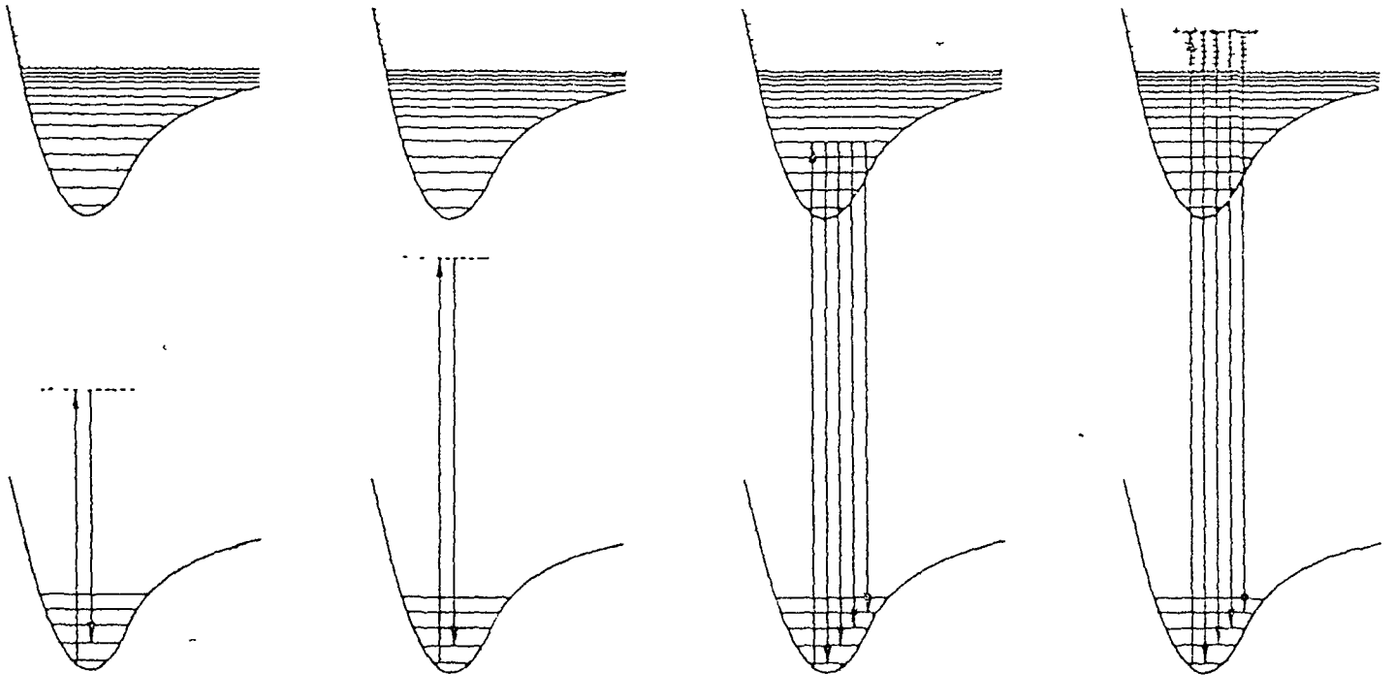

Fig. 2.5 Illustration of various light scattering processes.

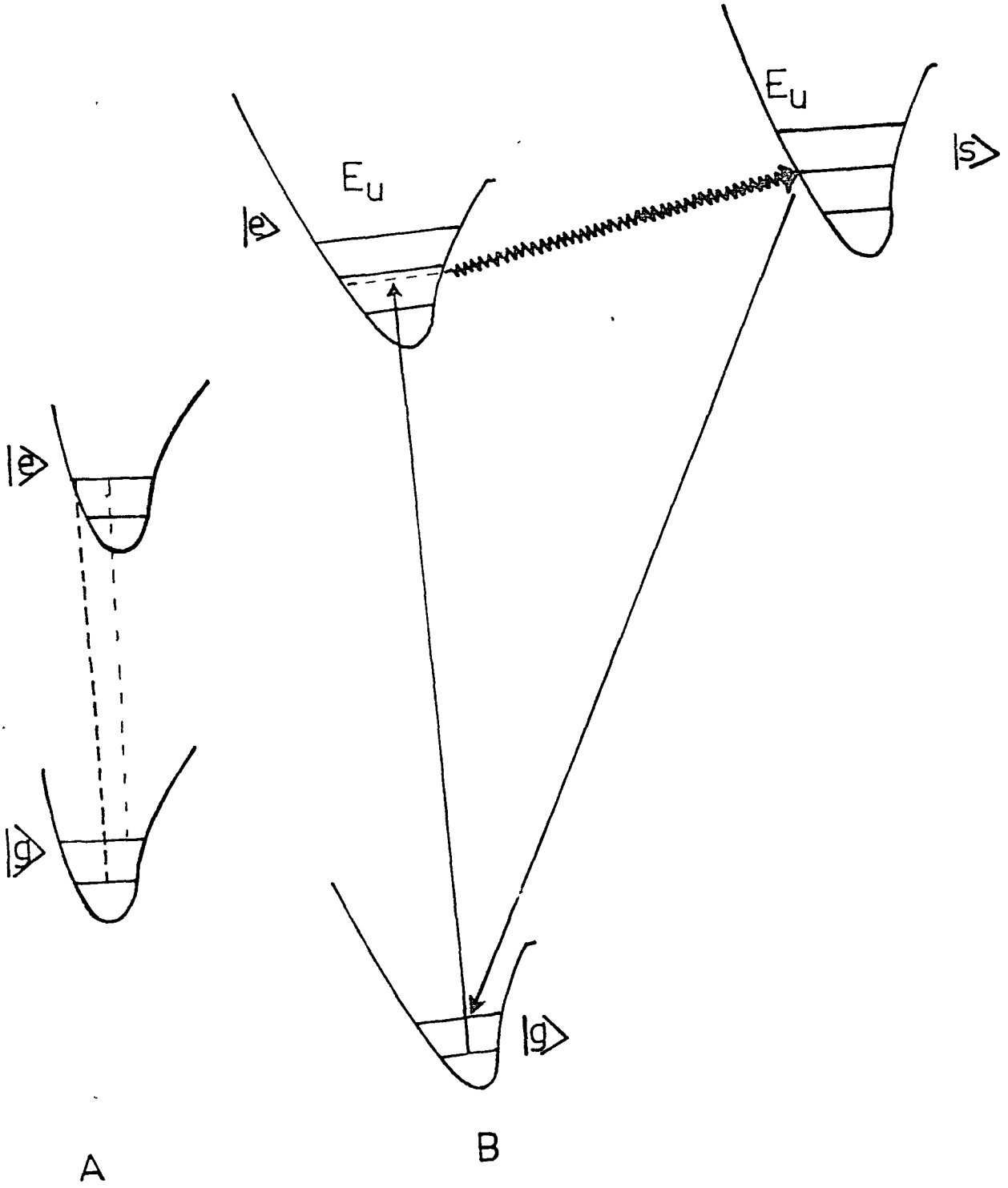

Fig. 2.6 Diagram illustrating the mechanism of (A) Frank-Condon (B) vibronic coupling processes for resonance Raman scattering.

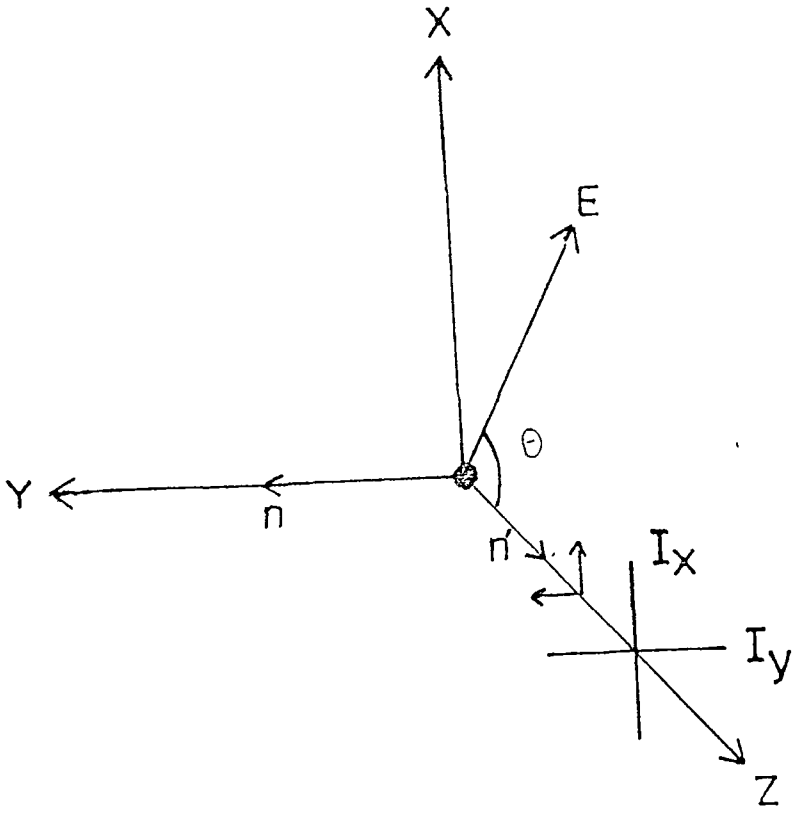

$$\rho_l = \frac{I_y}{I_x}$$

Fig.2.7 Raman scattering geometry. Light propagating along the Y direction is characterized by an electric vector E lying in the XZ plane. Scattered radiation is detected along the Z-direction. Conventional scattering experiment has $\theta = 90°$.

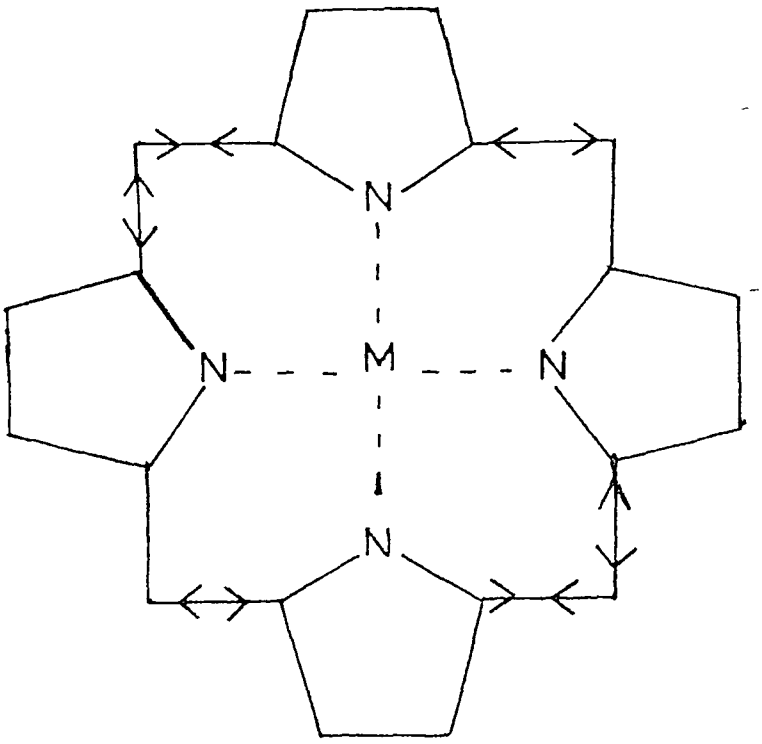

A_{2g} vibrations of porphyrins

$C_a - C_m$ bonds

Fig.2.8 Schemetic illustration of an antisymmetric vibrational mode of A_{2g} symmetry for a metalloporphyrin of D_{4h} point group. ^2A_g mode of this symmetry is formally equivalent to a rotation about the central Z axis, perpendicular to the molecular plane.

EXPERIMENTAL TECHNIQUES

In this chapter we shall present a brief discussion of the methods of sample preparations, the experimental techniques and the instruments used to obtain the vibrational spectra and electronic absorption spectra presented in this thesis.

3.1 Preparation of Samples

The derivatives of Cu- and Co- porphyrins (protoporphyrin-IX and mesoporphyrin-IX) were prepared by a method similar to that of Dorough **et al.**[1] A 2.0-5.0 ml aliquot ($\sim 10^{-4}$M) of the free base porphyrin purchased from Sigma Chemical Company, USA, was boiled gently in glacial acetic acid with about 50 mg of the metal acetate. After the conversion to the metalloporphyrin is complete which is indicated by the absence of free base absorption bands, the solution was transferred to a separating funnel. Benzene was added to the solution and the resulting benzene layer was washed with water several times to remove the reaction solvent and inorganic salts.The benzene layer was dried over anhydrous sodium sulphate and was evaporated to dryness under vacuam to yield metalloporphyrins. The purity of the samples was

checked by comparing their absorption and infrared spectra and with available information in the literature.

Free base meso-tetraphenylporphin(TPP) was synthesized by the following procedure:[2,3] Benzaldehyde(26 ml) and pyrrole (18 ml) were added simultaneously to refluxing propionic acid(1l) and the mixture was refluxed for 30 mins before being allowed to cool and kept at room temperature overnight. The product was filtered off and washed with water and methanol to give purple crystals of crude TPP(~5.6g). The crude TPP was dissolved in refluxing dichloromethane(700 ml) and then treated with a solution of 2,3-dichloro-5,6-dicyanobenzoquinone (DDQ)(1.44g) in dry benzene(60 ml). After refluxing for about 2 hours, the hot yellow tinged solution was filtered through a sintered glass funnel under suction containing alumina(~ 88g). The alumina was washed with water and dichloromethane(~ 60ml). The combined filtrate was evaporated to dryness and the residue was chromatographed on neutral alumina on hot chloroform. The TPP elute was evaporated to a bulk of ~ 300 ml and then equal volume of methanol was added for crystallization of TPP. Pure TPP was then obtained by filtration under suction.

The synthesis of tetraphenylporphinato Manganese(III) chloride(Mn(III)TPPCl) was done in the following way.[4] Free base TPP(5g) was added to refluxing dimethylformamide. After

few minutes when homogeneous solution was formed, stoichiometric amount of Manganous chloride (1g) was added. The reaction was then allowed to proceed for about ~ 1 1/2 hours. The completion of the reaction was checked by recording the electronic absorption spectra which did not show any band corresponding to free base TPP. The reaction vessel was cooled in a cold water bath. Chloroform was added to the reaction mixture and the resulting solution was washed with water several times to remove unreacted $MnCl_2$. The chloroform layer was dried over anhydrous sodium sulphate. The solution was then filtered; the filtrate was concentrated and was further purified by column chromatography over silica gel. The resulting solution was dried under vacuam which yielded green polycrystalline material of MnTPPCl. The formation of the correct compound was verified by recording absorption spectra, which was similar to the one reported in literature.[5]

The oxygen-bridged dimer of Manganese(III) tetraphenylporphin ($O-(H_2OMnTPP)_2$) was prepared by the following procedure.[6] MnTPPCl (0.5g) was dissolved in (100 ml) of Pyridine. Saturated solution of potassium hydroxide was added to it. The mixture was stirred thoroughly on a magnetic stirrer and then was evaporated to dryness on a steam bath. The solid was washed with water several times to remove excess alkali. The final dried solid was dissolved in benzene and filtered.

The filtrate was concentrated in a conical flask on a steam bath and placed aside for crystallization. The crystals were collected and dried in a vaquam desiccator over anhydrous $CaCl_2$.

3.2 Recording of Raman Spectra

Raman spectra of different porphyrins were recorded in 90° scattering geometry with a SPEX Ramalog 1403 tripple monochromator equipped with a cooled RCA 31034 photomultiplier and photon counting arrangement. The spectrometer control and data processing were achieved with the help of a micro-processor based 'SPEX' Datamate. Excitation wavelengths were provided by Spectra-Physics Model 165-09 Argon ion lasor, Spectra-Physics Model 375 jet stream dye laser, Liconix Model 4240 He-Cd laser and Coherent Model Innova 90K Krypton ion lasers.

3.3 Spectra-Physics Model 165-09 Argon Ion Laser

This laser consists of two parts, one the CW Model 165 laser head and the other Model 265 exciter. The laser head consists of a rugged troublefree berilium oxide plasma tube closed at both the ends by Brewster angle windows, a solenoid and an optical resonator formed by a spherical reflector at the output and a prism assisted by a flat mirror (to select wavelengths) at the back end. The plasma tube is

placed on a kinematically adjustable mount so that it can be positioned exactly on the mirror centre line. The external thumb wheel controls are provided for wavelength selection and for changing the intra-cavity aperture. The laser gives polarized light and by using the polarizer the plane of polarization can be changed to the desired plane for recording the polarized Raman spectra.

The exciter consists of the necessary electronic circuits to create, sustain and monitor the ion discharge in the plasma tube. An arrangement is provided to have a desired constant optical power when operated in the 'light control' mode. The necessary chilling for the exciter and the laser head is provided by a Neslab Model HX-500 air cooled water chiller plant, which circulates deionized distilled water at constant temperature (15°C) and at a pressure of 40 PSIG.

3.4 Spectra-Physics Model 375 Jet Stream Dye Laser

This model consists of a Model 375 dye laser along with a Model 376 dye circulator. The dye laser system is pumped by an Spectra-Physics Argon ion laser source to provide continuously tunable coherent light. The laser gain medium is a liquid solution of organic dye (Rhodamine 6G, in this case) which absorbs pump laser light focussed on it by an input mirror (with a radius of curvature of 5 cm), with a

coating to provide maximum reflection of the Argon ion laser wavelength. The dye emits light at a longer wavelength through fluorescence.The emitted light is reflected from the end mirror through the dye stream to the collimating mirror, to the output mirror back to the collimating mirror, through the dye stream and to the end mirror again. The emitted light is passed many times through the dye stream as it is reflected back and forth between the mirrors and as the light passes through the dye stream, dye molecules previously excited by the pump light are stimulated to emit light at fluorescence wavelengths providing laser action. A tuning wedge which is a Fabry-Perot etalon with a large free spectral range, tunes the resonant cavity to any point within the broad fluorescence bandwidth. Tuning is accomplished by sliding the tuning wedge laterally in the dye laser beam and the lateral position of the tuning wedge is controlled by the wedge position knob. Finer control of the output wavelength is achieved by a fine tuning etalon, which is a thin uncoated piece of glass approximately 0.11 mm thick. It is mounted in a holder for handling convenience. It acts as a transmission filter, allowing the laser to operate only at those frequencies for which the etalon is tuned, and provides continuous wavelength as it is tilted with respect to the dye laser beam. When the fine tuning etalon knob is rotated, the angle between the optical beam and the etalon is changed, resulting in a slightly

different wavelength being put out by the laser. An optical diagram of a dye laser is shown in Fig. 3.1.

The major components of a Model 376 dye circulator are the combination pump/motor, the reservoir bottle and the filter. The pump and motor are a single unit. The motor is magnetically coupled to the pump.The pump provides a minimum pressure of 4.2 N/cm^2($60lb/in^2$) and dye flow rate is about 15 cm^3/sec. The dye is preserved in a reservoir bottle. The filter housing contains a stainless steel filter screen and a 10 μm teflon Millipore filter through which all dye flowing to the nozzle must pass.

3.5 Coherent Model Innova 90K Krypton Ion Laser

This consists of mainly four major functional units; the laser head, the plasma tube within the laser head, the power supply and the control electronics. The laser head houses the plasma tube, the axial field magnet, the resonator structure, various electrical components and all optical controls and adjustment devices used to operate the laser. A combination cooling water/power cable umbilical extends from the laser head to the power supply. The plasma tube generates the gain for the laser light. The control electronics provide all of the electronic controls used to operate the laser and fault indicators. The power supply performs three functions; it provides all operating power required by the

laser head and control electronics, it interfaces the laser head with the cooling water sources and it interfaces the control electronics with the laser head.

3.6 Liconix Model 4240 Helium-Cadmium Laser

This laser comprises of two components, a laser head and a power supply. The head and supply are connected by three cables; one for control functions and two for high voltage power to the laser tube. The laser head is a self-cooled structure. The laser beam is extracted from a small opening at the end opposite to the cables. This end is equipped with a finger operated safety beam block. A small removable panel is provided in the top half of the body shell for maintenance access to the control electronics. The output available is ~40mW at 4416Å.

3.7 SPEX Model Ramalog 1403 Laser Raman Spectrophotometer

The Raman spectra were measured with the help of a SPEX Ramalog 1403 double monochromator coupled with a third monochromator and equipped with a cooled photomultiplier RCA 31034. Fig. 3.2 shows the optical diagram of the instrument.

The SPEX 1403 double monochromator is a f/7.8 instrument with a spectral coverage from 31000 to 11000 cm^{-1}. An accuracy of ±1 cm^{-1} in the 10000 cm^{-1} range, a spectral repeatability of ±0.2 cm^{-1} and a resolution of 0.15 cm^{-1} can be achieved

by this instrument. The 1800 grooves/mm holographic gratings blazed at 5000Å are used in this instrument. The gratings are mounted on a modified Czerny-Turner mount using the fundamental grating equation

$$m\lambda = d(\sin\alpha + \sin\beta) \quad \ldots\ldots\ldots \quad (3.1)$$

where, m = spectral order, λ = wavelength, d = grating spacing, α = angle of incidence and β = angle of diffraction. Putting $\alpha = \theta + \Phi$ and $\beta = \theta - \Phi$, where θ is the angle of grating rotation measured from zero as illustrated in Fig. 3.3 and Φ is the angle dependent constant on the instrument design. Equation 3.1 can be rewritten as

$$m\lambda = 2d \sin\theta \cos\Phi \quad \ldots\ldots\ldots \quad (3.2)$$

Since, in the Ramalog 1403 machine, the Raman peaks are observed in terms of frequency shift in cm^{-1} on a larger scale, it utilizes a cosecant drive for the grating rotation with $\Phi = 10°$ and $\cos\Phi = 0.984$ (manufacturer supplied values).

To record the Raman spectra, the laser beam is passed through the SPEX 1459 UVISIR illuminator after being diffracted from the 'lasermate', a small grating monochromator to isolate the background plasma lines. The filtered laser beam from the lasermate is deflected upwards by a mirror and focussed onto the sample to a spot of diameter ~ 10 µm by the fused silica condensing lens. Scattered radiation from the sample passes through a polarization analyzer, a device based on

birefringence and total reflection or on dichroism. The polarization analyser transmits light of a particular polarization depending on the orientation of the analyser. Use of polarization analyzer therefore gives direct information about the state of polarization of the observed Raman bands. For powdered sample or for samples in KBr matrix (pellet), the use of polarization analyzer becomes redundant becuase of the random orientation of the constituent molecules or microcrystals of the sample. The scattered radiation is collected by an elliptical mirror (f/1.4) and focussed onto the entrance slit of the spectrometer after passing through a polarization scrambler. The polarization scrambler consists of a wedge of birefringent material. The two components of polarized light is thrown out of phase. However, in contrast to the halfwave plate, the retardation varies from place to place and as a whole the emerging radiation is depolarized. To ensure a correct scrambling, it is obvious that this device has to be placed in a defocussed beam. Therefore by using the scrambler it is possible to get a constant spectrometer response as far as the polarization dependent efficiencies of the optical components and gratings of the spectrometer are concerned. The polychromatic scattered radiation focussed onto the entrance slit gets dispersed by the 1800 grooves/mm holographic gratings. Nearly monochromatic radiation of frequency ν for a particular tuning of the spectrometer reaches the exit slit of the double monochromator by the grating-mirror

combinations. The optical ray diagram is illustrated in Fig. 3.2. The exit slit of 1403 double monochromator is coupled with the SPEX model 1442V third monochromator.

3.8 The Third Monochromator

This is a device for reducing stray light where weak spectral features are not clearly visible in the vicinity of an intense line. This device functions as a variable band-pass, variable frequency filter. The third monochromator is a modified Czerny-Turner spectrograph attached to the exit slit of the double monochromator. In this configuration the light entering the third monochromator is nearly monochromatic at the particular tuning frequency of the double monochromator. This light is further dispersed and finally made to fall onto the exit slit of the third monochromator to which the photomultiplier tube is connected. This final dispersion and the adjustment of the exit slit is such that only the desired components of the incoming nearly monochromatic light pass between the slit blades of the exit slit of the third monochromator and the stray radiation at other frequencies is suppressed by the slit blades. The third monochromator can operate, in the fixed mirror mode, in the scanning grating mode or in the stationary grating mode.

3.9 Spectrometer Control And Data Processing

The spectrometer control (frequency scanning) and

data processing were carried out through a 8-bit dedicated microcomputer SPEX 'Datamate'. With the help of the inbuilt software, it was possible to manipulate the spectral data by background subtraction, integration, addition, division, frequency range and intensity range expansion/reduction, differentiation etc. whenever necessary. The incoming spectral data as well as the manipulated data array could be stored in the 4K data point storage in any of its eight variable length files. The stored data could be plotted in a stripchart recorder or transferred to external peripherals, example, floppy discs or to a general computer through the standard IEEE interface for further data manipulation. The unavoidable wavelength dependent distortions to the spectral data from the spectrometer optics could be erased by applying the radiometric corrections from the inbuilt 1K EAROM. Using the progrm-gramming option, all operations from data collection to output could be completely automated. It is also possible to bypass the data storing option and record the spectra directly on the stripchart recorder.

The raw data was obtained from the output of the preamplifier after photomultiplier. The anode of the photomultiplier tube was the input of the PC Dam. The preamplifier gain was 400. The high voltage required for operating the photomultiplier tube was also supplied by the Datamate with a stability of ±0.002% after half an hour warm-up time. An

RCA 31034 photomultiplier tube, cooled to -30°C by a thermo-electric cooling device was used for obtaining the spectral data. The RCA 31034 is a 2" diameter, head-on, 11-stage QUANTACON photomultiplier having a gallium arsenide chip as its photocathode, an ultraviolet transmitting glass window and an in-line copper beryllium dynode structure. The tube having an almost linear absolute responsivity in the 300.0 nm to 850.0 nm wavelength range was operated for a current gain of 10^6 with a maximum dark pulse summation of 12 CPS.

3.10 Scanning Of The Raman Spectra

There are a number of difficulties associated with recording Raman spectra of coloured samples under resonance conditions. These include (a) the optimization of the concentration of the scattering species in solution to minimize the reabsorption of the scattered light by the sample at the same time allowing the scattering to be maximum, (b) the local overheating of the sample due to absorption of exciting laser light which may give rise to thermal lens effect (in case of solution studies) and also decomposition of the sample (c) the strong background due to luminescence and photolysis of the samples.

Point (a) was best optimized by using samples of different concentrations until we obtained good quality spectra. To avoid local heating effect (point(b)), Keifer and Bernstein[7,8]

have devised a technique which involves a continuous rotation of the sample with respect to the laser beam. As the sample rotates continuously exposing fresh sample, the small area from which scattered Raman radiation is collected remains in laser focus for only a very short period of time that is insufficient for localized heating of the sample. In this way both the thermal lens effect and thermal decomposition can be minimized. For the suppression of fluorescence (point(c)) Raman spectra were obtained in solid form in KBr pellet. As the molecules come close to each other in solid phase, they quench the luminiscence to a large extent due to strong interactions.

To record the powdered spectra, the sample was pressed into a 13-mm diameter KBr pellet with the help of an evacuable stainless steel die and mounted in the sample rotator. This also helped to reduce fluorescence. For liquids, Raman sample (2-3 ml) was taken in a cylindrical quartz cell supported by 'O' rings in the liquid cell mount rotating at speed from 3500 rpm to 4500 rpm. The laser beam was made to strike the bottom of the cell very near to its perimeter, because in this way the self absorption of the scattered light was minimized. The spectra were calibrated with CCl_4, helium and krypton lamp lines and reported band positions are accurate to better than ± 2 cm^{-1}. Other spectral conditions such as laser power, integrating time, wavenumber increment, slit

width etc. were varied according to sample and different excitation wavelengths to optimize signal to noise ratio. To record the weak features, 3-4 spectra were averaged with the help of Datamate.

3.11 Infrared Spectra

The infrared spectra at room temperature were recorded on the Perkin Elmer Model 983 spectrophotometer. This is a dual beam f/4.2 monochromator with four gratings and nine filters and uses a coated cesium iodide lens thermocouple as the detector. This spectrometer covers the 5000 cm^{-1} to 180 cm^{-1} frequency range. The spectra were recorded with a resolution of ~ 2 cm^{-1}. The recorded spectra were calibrated with the standard spectrum of polystyrene film. The pellet technique was used in the present investigation. Fine powder of the sample was mixed with KBr. The mixture was pressed in an evacuable die and a transparent disc of 13 mm diameter was obtained. The spectra of the disc were obtained.

3.12 Electronic Absorption Spectra

The electronic absorption spectra were recorded on a Beckman UV VISIBLE 26 spectrometer. This spectrometer covers the 900 nm to 190 nm range (VIS: 900 nm - 350 nm; UV: 350nm - 190 nm).

REFERENCES

1. G.D. Dorough, J.R. Miller and F.M. Huennekens, J. Am. Chem. Soc. **73**, 4315(1951).
2. J.-H. Fuhrhop and K.M. Smith, in 'Porphyrins and Metalloporphyrins' ed. K.M. Smith, Elsevier: Amsterdam, 757(1975).
3. G.H. Barnett, M.F. Hudson and K.M. Smith, Tetrahedron Lett. No. 30, 2887(1973).
4. A.D. Adler, F.R. Longo, F. Kampas and J. Kim, J. Inorg. Nucl. Chem. **32**, 2443(1970).
5. L.J. Boucher, Coord. Chem. Rev. **7**, 289(1972).
6. E.B. Fleischer, J.M. Palmer, T.S. Srivastava and A. Chatterjee, J. Am. Chem. Soc. **93**, 3162(1971).
7. W. Kiefer and H.J. Bernstein, J. Appl. Spectrosc. **25**, 500(1971).
8. W. Kiefer and H.J. Bernstein, J. Appl. Spectrosc. **25**, 609(1971).

TABLE 3.1 Wavelength and Output Power Specifications for the Different Types of Lasers Used in the Present Study.

Type of Lasers	Output Wavelength(in Å)	Power Available
1. Spectra-Physics Model 165-09 Argon Ion Laser. Total power in all lines ≈ 5 Watts	5145	2.00 W
	5017	0.40 W
	4965	0.70 W
	4880	1.50 W
	4765	0.75 W
	4727	0.30 W
	4658	0.20 W
	4579	0.35 W
	4545	0.12 W
2. Spectra-Physics Model 375 Dye laser. Output with Rhodamine 6G dye ~ 500 mW	~ 5600Å - 6500Å continuously tunable	varying from ~ 500 mW to 100 mW
3. Coherent Model Innova 90K Krypton Ion Laser. Total power in all lines is 800 mW.	6471	500 mW
	5682	150 mW
	5309	200 mW
	4825	30 mW
	4762	50 mW
4. Liconix Model 4240 He-Cd Laser. Total power available is 40 mW.	4416	40 mW

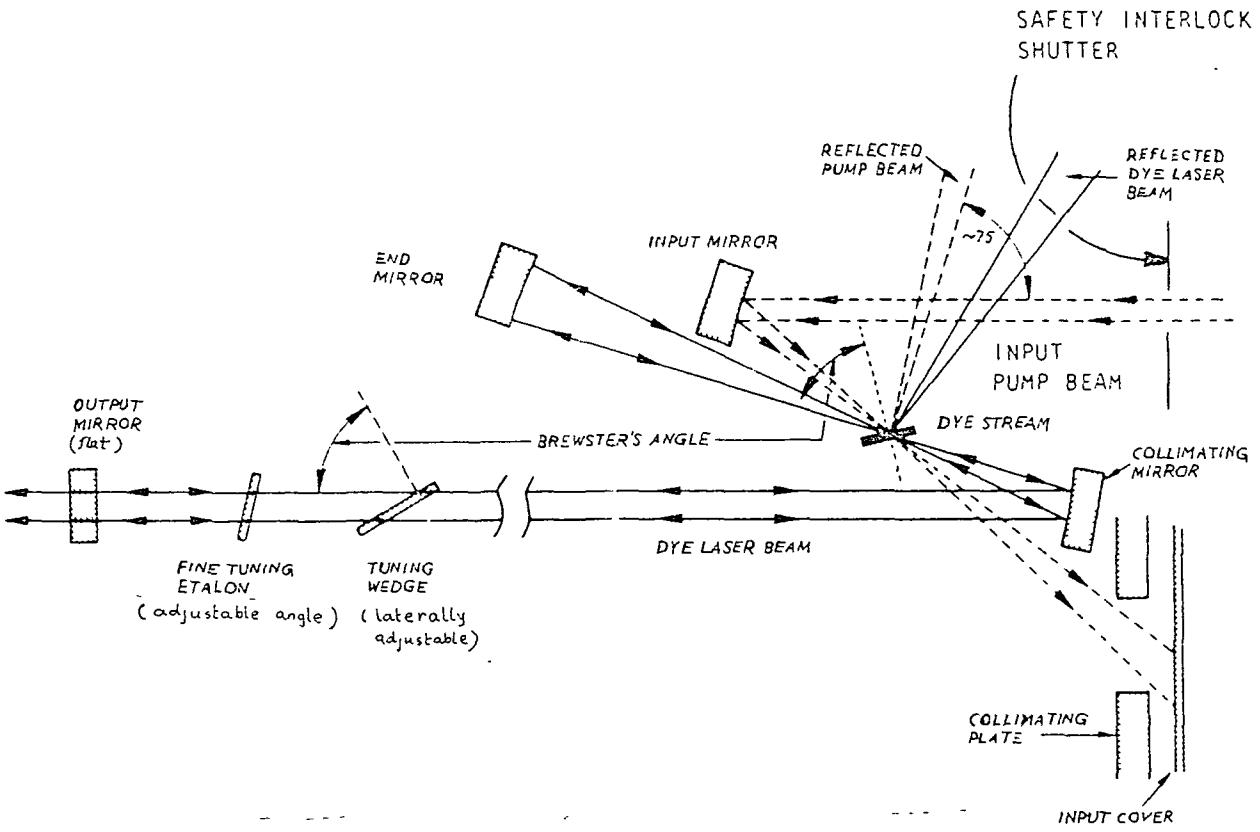

Fig.3.1 Optical diagram of a Spectra-physics Model 375 dye laser system.

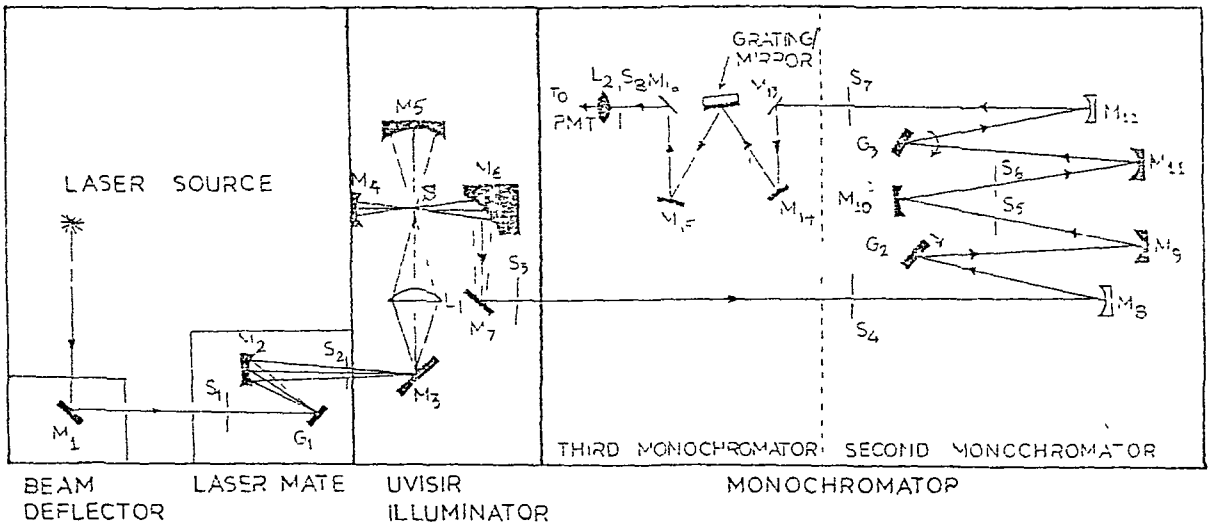

M_1 M_3 M_7 M_{13}-M_{16} PLANE MIRRORS · M_2 M_4 M_5 M_8 M_9 M_{10} M_{11} M_{12} CONCAVE MIRRORS : M_6 ELIPTCAL MIRROR · S_1-S_8 SLITS : L_1 FUSED SILICA CONDENSER LENS : L_2: FIELD LENS : S SAMPLE : G_1 G_2 G_3 GRATING . PMT PHOTOMULTIPLIER TUBE

Fig.3.2 Optical diagram of a SPEX Model Ramalog 1403 laser Raman spectrophotometer including lasermate, illuminator and the third monochromator.

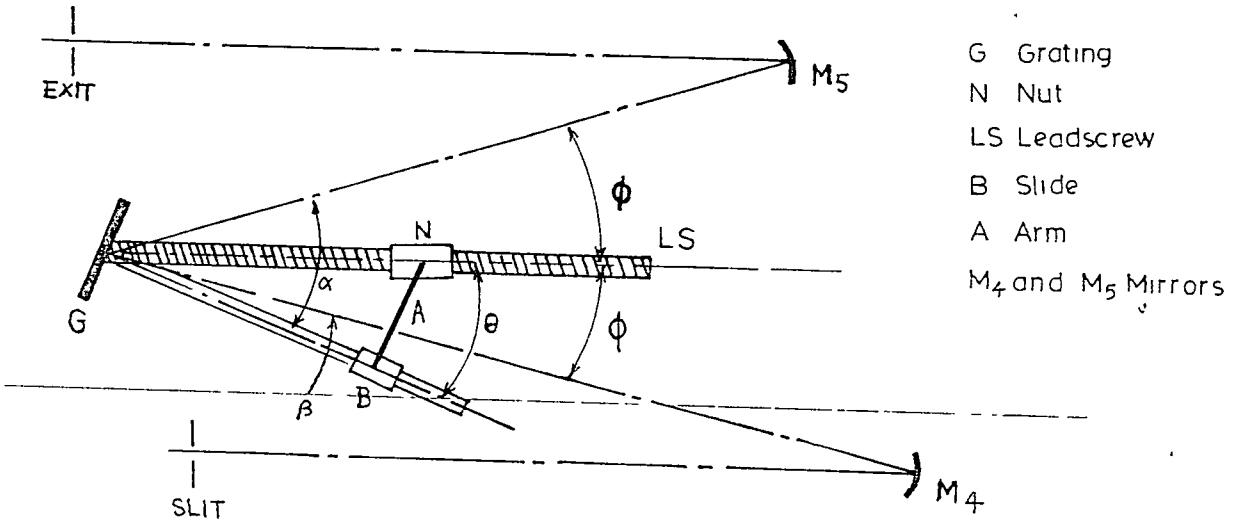

Fig.3.3 Mechanical cosecant drive mechanism for the Czerny-Turner mount of gratings for the SPEX Model 1403 Ramalog. The nut N moves along lead screw LS while the slide B moves along a bar held at right angles to the grating G. The grating rotates as the arm A moves along the bar.

EFFECT OF VINYL GROUPS ON RESONANCE RAMAN SPECTRA OF PROTOPORPHYRIN-IX*

ABSTRACT

Resonance Raman(RR) spectra obtained with several excitation wavelengths are compared for the following porphyrin compounds; free base protoporphyrin-IX, mesoporphyrin-IX and haematoporphyrin-IX; and Copper protoporphyrin-IX and Copper mesoporphyrin-IX dimethyl esters. Certain bands in the RR spectra of all the free base porphyrins or Copper complexes are unaffected with respect to frequency, whereas there is a shift in the frequencies of some vibrational modes in some systems. From a comparative study of the systems which have identical geometrical arrangements, no extra features were found in the RR spectra of protoporphyrin which can be attributed directly to the vinyl group modes. This suggests that the vibrational modes of vinyl groups do not distort the excited electronic state substantially, and are not effective in vibronic coupling with the electronic states of the porphyrin macrocycle and therefore do not gain intensity under resonance excitation. Most of the vibrational modes are strongly coupled and there are no extra distinct features in the RR spectra of PP which may be associated with selective vibrational coupling of the vinyl groups with the porphyrin skeletal modes.

---

*Based on these studies, a paper has been published. M.Sarkar and A.L. Verma, J.Raman Spectrosc, **17**, 407(1986).

4.1 Introduction

There has been considerable progress in the study of haeme proteins and metalloporphyrins by resonance Raman(RR) technique in recent years.[1-3] If this technique is to be exploited to understand the mechanism and dynamics of haeme proteins, the nature of the observed vibrational modes and their origin need to be properly understood. The role of vinyl groups in the cooperative binding of oxygen in haeme proteins is still not clear. It has been suggested that interaction of the vinyl groups with the amino acid residues of the protein control the physical and chemical properties of the porphyrin ring via conjugation which in turn can control the O_2 binding and cooperativity.[4-6] Similar interactions have been proposed for the vinyl groups of protohaeme in cytochrome b,[7] and for the formyl groups of haeme a in cytochrome c oxidase.[8-10]

Resonance Raman spectroscopy is a particularly sensitive probe of the π electronic structure of porphyrins[3,11] and the effects of conjugating substituents.[12-14] If the influence of vinyl groups in the RR spectra of haeme proteins could be properly monitored, it would be of great help in elucidating their role in important biochemical processes in these systems. However, there are several factors which complicate the RR spectra of haeme proteins. A major problem for spectral interpretation then becomes to disentangle the

different contributions which can manifest themselves in the spectra and the problem still remains unresolved. If the protein-haeme interactions through the peripheral substituents play an important role in determining biochemical activity of a haeme protein, characterization of vinyl bands in the RR spectra is essential to probe such activity in haeme proteins by RR spectroscopy. It is therefore necessary to elucidate the influence of vinyl groups on the RR spectra of isolated protoporphyrin systems before the haeme protein interactions can be sorted out.

Considerable progress has been made in this direction by several groups[12-17] after the first study on the RR spectra of free base porphyrins by Verma and Bernstein.[18] An important step was taken by Choi **et al** who have reported RR studies of Ni-protoporphyrin-IX(NiPP) with deuteriated vinyl groups and compared their results with the RR spectra of Ni-octaethylporphyrin(NiOEP),[19,20] They claim to have identified most of the vinyl group modes in the RR spectra of NiPP and protohaeme complexes.

The early RR studies of several metalloporphyrins[18,21] made it clear that the substituents at the porphyrin periphery influence the RR spectra of the chromophore substantially. By studying the dispersion of the depolarization ratios of some isolated bands as a function of excitation wavelength,

the rigorous symmetries of the Cu- and Co-mesoporphyrin-IX dimethyl esters(CuMP and CoMP),[21] having all saturated substituents were found to be C_s due to asymmetric placement of the substituents. However, the Cu- and Ni-porphin were shown to have D_{4h} symmetry.[22,23]

The extent of the influence of vinyl groups on the RR spectra of haeme proteins and their protoporphyrin-IX complexes is still a matter of great activity.[19,20,24-26] Previous studies[16] of the RR spectra of Cu- and Co-protoporphyrin-IX(CuPP and CoPP) and of CuMP and CoMP in a limited higher frequency region did not show any extra features which could be directly attributed to the vinyl groups in CuPP or CoPP. However, Choi **et al**[19] recently reported a comparative study of the NiPP and NiOEP systems which have rigorous molecular symmetries of C_s and D_{4h} respectively. It is likely that the extra weak features attributed to vinyl groups in the RR spectra of NiPP compared with the NiOEP may arise from a lowering in symmetry of the former system. Moreover, it is well known from normal coordinate analysis[27,28] and deuterium shifts in Cu-porphin-d_4[22,23] and other deuteriated systems that most of the vibrational modes in such a complicated molecule interact strongly with each other. Even the deuteriation of just four meso-hydrogens in Cu-porphin shifts the frequencies of several modes drastically.[22,23] Therefore, the deuteriation shifts of some modes cannot be taken as a confirmatory evidence for correlating those affected bands

directly with vinyl groups.

Some studies on haeme proteins[24,25] and metalloporphyrins[26,29] have been carried out recently to elucidate the influence of side chain substituents and selective interactions of these groups with the amino acid residues of the protein, on the RR spectra of porphyrin chromophores. For example, many structural and spectroscopic differences in haemoglobin and Cobalt substituted haemoglobins have been detected upon replacement of the protohaeme by a mesohaeme.[30-33] These differences could originate from a decrease in the π conjugation due to saturation of the vinyl groups in the mesohaemes or from stereochemical changes resulting from the different structural interactions between the protein and the vinyl groups, compared to that between the protein and the ethyl groups. On the other hand, it has been revealed that RR frequencies of some porphyrin skeletal modes are affected differently in different haeme protteins,[24,25] mainly owing to specific protein induced differences in the conformations of the side chains. However, inferences in many of these studies have been based on the assignment of the RR spectra of NiPP by Choi and coworkers.[19,20]

Because of these conflicting and unclear reports, we have undertaken a systematic and comparative study of the RR spectra of the free base protoporphyrin-IX(PP), mesoporphyrin-IX(MP) and haematoporphyrin-IX(HP) systems together

with the Cu- and Co- chelates of protoporphyrin-IX dimethyl esters(CuPP, CoPP) and mesoporphyrin-IX dimethyl esters (CuMP and CoMP) to probe the state of conjugation of the vinyl groups in PP and haeme proteins.

As can be seen from Fig. 4.1, all the free base porphyrins have the same side chain substituents except for two positions where there are vinyl groups in PP, ethyl groups in MP and $CH_3\dot{C}HOH$ groups in HP. Since both ethyl and $CH_3\dot{C}HOH$ groups are saturated and therefore do not form part of the conjugation of the macrocycle, a comparative study of the RR spectra of all these systems having similar molecular symmetries should yield direct information about the state of conjugation of the vinyl groups and their influence on the RR spectra of PP and other protohaemes. This work was aimed at clarifying these aspects, which may be of considerable help in understanding the complex spectra of various metalloporphyrins and haeme related proteins.

4.2 Experimental Results

The molecular structure of PP together with the side chain substituents in HP and MP is given in Fig. 4.1. Typical RR spectra for all the free base porphyrins using excitations near their corresponding absorption maxima are shown in Figs. 4.2 (4.2a, 4.2b), 4.3 and 4.4 respectively. The exact excitation wavelengths are given in figure legends. Fig. 4.5 shows

the RR spectra of CuPP and CuMP with excitations at their α band absorption maxima. Table 4.1 lists the Raman frequencies with their relative intensities, which were obtained using different exciting lines for all the free base porphyrins. Similarly, the Raman frequencies and depolarization ratios for the CuPP and CuMP at the indicated wavelengths are given in Table 4.2 together with the data on Cu-aetioporphyrin-IV. Correlations among various groups frequencies in the corresponding porphyrins or metal porphyrins are also given in the respective tables. Table 4.3 summarizes the Raman$_{\lambda}^{data}$ obtained with different$_{\lambda}^{f}$ excitation wavelengths. It also includes the observed IR data for all the systems. Also listed in Table 4.3 are the expected vinyl group frequencies as suggested by Choi **et al.**[19] The general experimental details and methods of preparation of samples, have been given in Chapter III.

4.3 Discussion

The free base planar porphyrins having eight side chain substituents (assumed to be point masses) have approximate D_{2h} molecular symmetry with four characteristic absorption bands in the visible region and a split Soret absorption band in the UV region. As has been stated earlier, these bands originate from the configuration interaction and vibronic mixing of the $\pi \longrightarrow \pi^*$ electronic transitions between the highest filled molecular orbitals of $a_{1u}(\pi)$ and $a_{2u}(\pi)$ symmetry and the lowest unoccupied orbitals of $e_g(\pi^*)$ symmetry.[34,35]

The lowering in symmetry to D_{2h} for free base porphyrins leads to a splitting of the x and y polarized components of the otherwise degenerate electronic transitions. The e_g orbital in D_{4h} symmetry splits into b_{2g} and b_{3g} components under D_{2h} symmetry. Although the side chain substituents in the free base porphyrins under consideration (PP, MP and HP) provide identical skeletal geometry for all these porphyrins, their rigorous symmetries are only C_s owing to the asymmetric placement of the side chain substituents. The 38 atom free base porphyrins (assuming side chains to be point masses) will have 108 normal modes of vibrations. Group theoretical analysis of metalloporphyrins under D_{4h} point group symmetry classifies the 105 vibrations as follows:

$$\Gamma_{\text{in plane}} = 9A_{1g}+8A_{2g}+9B_{1g}+9B_{2g}+18E_u.$$

$$\Gamma_{\text{out of plane}}=3A_{1u}+6A_{2u}+5B_{1u}+4B_{2u}+8E_g.$$

Replacing the metal ion by two protons leads to the lowering of symmetry to D_{2h}, while the asymmetric substituents further lowers it to C_s. Accordingly, we have

$$\Gamma_{\text{in plane}} = 19A_g+18B_{1g}+18B_{2u}+18B_{3u}$$

$\Gamma_{\text{out of plane}} = 8A_u+10B_{1u}+8B_{2g}+9B_{3g}$, vibrations for D_{2h} symmetry, and similarly,

$$\Gamma_{\text{in plane}} = 73A'$$

$\Gamma_{\text{out of plane}} = 35A''$, vibrations under C_s symmetry.

The nature and the electronic properties of the side chain substituents which differentiate these free base porphyrins determine the perturbation and shift in the electronic energy levels of the chromophore. This will also affect the vibrational frequencies and vibrational interactions between different modes. All the peripheral substituents in MP and HP are electronically and vibrationally similar and saturated and do not affecct the electronic structure of the chromophore much. However, the vinyl groups in PP are expected to be conjugated with the porphyrin aromatic system and therefore may perturb the π electronic system of the macrocycle significantly. As a result, the vinyl groups are expected to influence significantly the RR spectra of PP compared with those of other porphyrins.

The intensity enhancement of specific vibrational modes under RR excitation can take place[36] either through a mechanism involving an Albrecht's A-type term due to distortion of particular excited electronic state by those vibrations or through a B-type term involving vibronic coupling between two nearby electronic states through certain vibrations which show enhancement during RR conditions. Peripheral vinyl groups can influence the RR spectra of protoporphyrins in the following ways: i) because of the asymmetric disposition (Fig. 4.1) the centre of symmetry of the molecule is lost and consequently there can be Raman activity of the IR modes and vice versa.

The degeneracy of the E_u modes can also be lifted. (ii) the characteristic local modes of the vinyl groups, possibly perturbed by interactions with the skeletal modes, can contribute directly to the IR and Raman spectra, since RR intensity depends on the extent of vinyl mode involvement in the electronic excited state distortions and on the vibrational coupling with active skeletal modes.

The vinyl group ($CH=CH_2$) has 10 internal vibrational modes. Three of these are C-H stretches in the $\sim 3000\ cm^{-1}$ region, which are not expected to show RR enhancement and have not been included in the study. The remaining seven are shown schematically in Fig. 4.6, with typical values of their frequencies.[37] They consist of the double bond stretch, ν (C=C); three in plane deformations, δ ($=CH_2$) (CH_2 symmetric deformation), δ(CH=) (CH deformation), δ_{as}($=CH_2$) (CH_2 asymmetric deformation); and three out of plane deformations, γ (CH=) (CH wag), γ_s($=CH_2$)(CH_2 symmetric wag), γ_{as}($=CH_2$)(CH_2 asymmetric wag).

To observe the vibrational modes of vinyl groups in the RR spectra of PP, the conjugation of vinyl groups with the chromophore is a necessary but not sufficient condition to induce RR features from the side chains. In addition, the internal vibrations of the vinyl groups must be vibronically coupled to the electronic transitions of the whole macrocycle. Conjugation in the ground state may also affect the position

of Raman bands due to perturbation in vibrational coupling within the normal modes of molecules and can greatly affect the positions of Raman features associated with the side chains. Because of the asymmetric disposition of the vinyl groups in PP, they lower the D_{2h} symmetry of the porphyrin to C_s. Therefore, in principle, all the modes should be observable in the infrared absorption and Raman scattering and there are no degenerate modes. The characteristic local internal modes of the vinyl groups are expected to contribute directly and give extra features in the IR and Raman spectra of PP compared with the MP and HP systems. The intensity of the vinyl modes in the RR spectra is expected to depend on the extent of the involvement of the vinyl modes in the perturbation of the excited electronic states and their vibrational coupling with other skeletal modes of the porphyrin macrocycle.

Choi **et al**[19] recently made a detailed study of the RR spectra of NiPP, NiPP-d_{α} and NiPP-$d_{2\beta}$ deuteriated species and compared their spectra with that of NiOEP. The effective symmetry of the NiPP system is only C_s whereas the NiOEP has D_{4h} symmetry. In principle, the RR spectrum of NiPP is expected to show many more bands due to lowered symmetry even without participation of vinyl group modes as compared with the NiOEP.

Willems and Bocian[29] made a comparative study of Ni(II)-acetyl and -formyl deuterioporphyrins and identified some bands in the RR spectra due to the internal modes of

formyl and acetyl groups. They based their assignments on deuterium shifts and comparison of the RR spectra of these systems having only C_s symmetry, with that of NiOEP, which has D_{4h} symmetry. Desbois **et al.**[26] studied the RR spectra of 2-methylimidazole complexes of ferroprotoporphyrin-IX, ferrodeuterioporphyrin-IX, ferrohaematoporphyrin-IX and ferro-aetioporphyrin-I and found that the frequencies of some porphyrin skeletal modes are influenced by inductive effects from peripheral substituents. Rousseau **et al.**[24] suggested that the degree of π conjugation of vinyl groups with the porphyrin skeleton in the HbA(CO) and leghaemoglobin(CO) protein varies owing to different vinyl group conformations arising from different interactions of these groups with the amino acid residues of the proteins in the two systems. They also draw conclusions regarding the activity of the vinyl group internal modes by comparing the RR spectra of these systems, having virtually no symmetry with those obtained by Choi **et al** for the NiPP and NiOEP. Similar studies by Desbois **et al**[25] on some haemeproteins and peroxidases give clear indications that the protein induced differences in the conformations of the side chains do affect some Raman bands related to porphyrin skeletal modes.

To monitor the contribution of vinyl groups to the RR spectra of PP without other complicating factors, we undertook a systematic RR study of identical systems having the

same geometrical configuration where only vinyl groups in PP were replaced by saturated substituents in MP and HP, leaving all other substituents unaffected. The two vinyl groups in PP are well separated from each other spatially, and their modes will therefore occur in pairs having similar frequencies in a first approximation. These pairs will have in phase and out of phase combinations of the local vinyl group modes which may interact preferentially with the nearby porphyrin skeletal modes of appropriate symmetries. In addition to the internal modes of vinyl groups, one would expect a ring-vinyl stretch (C_b-C_α) and two deformation modes involving the vinyl group as a whole; one is centered at the vinyl C_α atom, $\delta(C_bC_\alpha C_\beta)$ and the other is centered at the pyrrole C_b atom, $\delta(C_bC_bC_\alpha)$ (see Fig. 4.6). Choi **et al**[19] associated several weak bands in the RR and IR spectra of NiPP with the vinyl groups based on either the non-coincidence of the RR and IR frequencies for a given vinyl mode or doubling of some bands in the Raman spectra. Some of the band pairs assigned to the same type of vinyl group modes in NiPP are at 1634(R) and 1620(IR), 1434(R) and 1343(R), 1167(R) and 1118(IR), 420(R) and 329(R) cm^{-1}. Except for the last two bands observed by Choi **et al.** with 4131Å excitation, we have observed bands corresponding to the rest of the bands in the RR and IR spectra of PP, MP and HP as shown in Table 4.3, where the expected vinyl group frequencies are also indicated. A comparison of the RR spectra in Figs. 4.2, 4.3 and 4.4

and the IR spectra shows that some of the RR bands and IR bands do differ in these systems but the most important aspect is that there are bands at corresponding positions in all three porphyrins studied here. It is therefore not justifiable to correlate some of the bands with the vinyl group modes as there are no extra features in the spectra of PP compared with those of MP and HP in the spectral regions of expected internal vinyl group modes. We have not attempted to analyze and assign the complicated spectral features observed for these systems.

Similarly, a comparison of the RR spectra of CuPP with that of CuMP (Fig. 4.5) and Cu-aetioporphyrin-IV shows that there are no extra and distinct features in the RR spectra of CuPP which can be attributed directly to the internal modes of the vinyl groups (Table 4.2). Of course, the positions and relative intensities of some of the bands differ in different systems for several reasons, for example, kinematic effects involving changes in the masses of the peripheral substituents, changes in the potential energy function from rearrangement of electronic change in the porphyrin macrocycle resulting from the electron withdrawing or donating nature of the substituents and alterations in the vibrational coupling with the skeletal modes and lowering in symmetry due to asymmetric placement of the substituents.

We have not been able to confirm the presence of extra features in NiPP at 420 and 329 cm^{-1} reported by Choi **et al.**[19] using 4067 and 4138Å excitations in the measured RR specrea of CuPP and CuMP and at this stage it is not clear whether the corresponding bands would be present in CuMP also. It is also likely that these bands in NiPP might be enhanced owing to the pre-resonance Raman effect as 4067Å excitation may satisfy a pre-resonance condition with absorption by the vinyl groups.

4.4 Conclusions

The findings on these system can be summarized as follows: the vinyl group in PP perturb the symmetry of the chromophore in the same way as the other saturated substituents in MP and HP, resulting in C_s effective symmetry for all the systems. The vibrational modes of the vinyl groups are not effective in vibronic coupling of the excited electronic states of the macromolecule and therefore are not enhanced in the RR scattering by this mechanism. The reduced symmetry and vibrational coupling with skeletal modes induce extra features in the RR spectra of all these systems compared with the systems having same side chain substituents with D_{2h} or D_{4h} symmetry. It is difficult to identify bands arising from selective coupling of vinyl group modes with skeletal modes. It is also plausible that the vinyl groups in PP are twisted slightly out of the porphyrin plane owing to steric

interaction of meso-hydrogens with the vinyl group hydrogens in the coplanar configuration. This may result in decreased conjugation of the vinyl groups with the macrocycle. This suggestion is also supported by crystal structure studies[38] of ferrihaemochrome(1-methylimidazole)-(protoporphyrin-IX)Iron-methanol-water system which shows that the two vinyl groups in this system are twisted by 24° and 41° with respect to the planes of the pyrroles. RR study on Lb(CO) and HbA(CO) clearly indicates that the vinyl group orientations are different in the two systems. From other studies[24,25] it also appears that the degree of π conjugation of the vinyl groups in different haemeproteins is dependent on the protein induced differences in the conformations of the vinyl groups. It is probable that the specific protein-vinyl group interactions in some haeme proteins may lead to a coplanar configuration of the vinyl groups with the macrocycle. This may induce some features in the RR spectra due to internal modes of the vinyl groups in these haemeproteins. On the other hand, in free base protoporphyrin, due to the absence of similar interactions, the vinyl groups orient themselves in a manner causing them unfavourable for conjugation.

Our conclusions are substantially different from those of Choi **et al.** The main reason appears that Choi **et al**[19] compared the RR spectra of NiPP and NiOEP, which have entirely different effective symmetrics, whereas we have made a comparative study of systems having similar molecular symmetries.

REFERENCES

1. A. Warshel, Annu. Rev. Biophys. Bioeng. **6**, 273(1977).

2. A.L. Verma, Indian J. Phys. **54B**, 54(1980).

3. T.G. Spiro, in 'Iron Porphyrins' eds. A.B.P. Lever and H.B. Gray, Addison-Wesley: Reading, MA, part II, 89(1983).

4. T. Asakura and M. Sono, J. Biol. Chem. **249**, 7087(1974).

5. B. Gellin and M. Karplus, Proc. Natl. Acad. Sci. USA, **74** 801(1977).

6. A. Warshel and R.M. Weiss, J. Am. Chem. Soc. **103**, 446(1981).

7. G.N. LaMar, P.D. Burns, J.T. Jackson, K.M. Smith, K.C. Langry. and P. Strittmatter, J. Biol. Chem. **256**, 6075(1981).

8. J.T. Coin and P.C. Hinkel, in 'Membrance Bioenergetics', eds. C.P. Lee, G. Schutz and L. Ernster, Addison-Wesley: Reading, MA, 405(1979).

9. C.K. Chang, in 'Oxygen, Biochemical and Clinical Aspects' ed. W.S. Caughey, Academic Press: New York, 437(1979).

10. G.T. Babcock and I. Salmeen, Biochemistry **18**, 2493(1979).

11. R. H. Felton and N.-T. Yu, in 'The Porphyrins' ed. D. Dolphin, Academic Press: New York, Vol. III, 347(1978).

12. T.G. Spiro and T.C. Strekas, J. Am. Chem. Soc. **96**, 338(1974).

13. F. Adar, Arch. Biochem. Biophys. **170**, 644(1975).

14. F. Adar and M. Erecinska, Arch. Biochem. Biophys. **165**, 570(1974).

15. M. Lutz, J. Raman Spectrose. **2**, 497(1974).

16. A.L. Verma, in 'Proceedings of the Fifth International Conference on Raman spectroscopy' eds. E.D. Schmid, J. Brandmuller, W. Kiefer, B. Schrader and H.W. Schrötter, Hans Ferdinand Schulz Verlag: Freiburg/Br., 198(1976).

17. A.L. Verma and H.J. Bernstein, J. Raman Spectrosc. **2**, 163(1974).

18. A.L.Verma and H.J. Bernstein, Biochem. Biophys. Res. Commun. **57**, 255(1974).

19. S. Choi, T.G. Spiro, K.C. Langry and K.M.Smith, J. Am. Chem. Soc. **104**, 4337(1982).

20. S. Choi, T.G. Spiro, K.C. Langry, K.M. Smith, D.L. Budd and G.N. LaMar, J. Am. Chem. Soc. **104**, 4345(1982).

21. A.L. Verma, R. Mendelsohn and H.J. Bernstein, J. Chem. Phys. **61**, 383(1974).

22. A.L. Verma and H.J. Bernstein, J. Chem. Phys. **61**, 2560(1974).

23. A.L. Verma, M. Asselin, S. Sunder and H.J. Bernstein, J. Raman Spectrosc. **4**, 295(1976).

24. D.L. Rousseau, M.R. Ondrias, G.N. LaMar, S.B. Kong and K.M. Smith, J. Biol. Chem. **258**, 1740(1983).

25. A. Desbois, G. Mazza, F. Stetzkowski and M. Lutz, Biochim. Biophys.. Acta **785**, 161(1984).

26. A. Desbois, Y. Henry and M. Lutz, Biochim. Biophys. Acta **785**, 148(1984).

27. H.J. Bernstein and S. Sunder, in 'Proceedings of the Fifth International Conference on Raman Spectroscopy' eds., E.D. Schmid, J. Brandmüller, W. Kiefer, B. Schrader and H.W. Schrötter, Hans Ferdinand Schulz Verlag: Freiburg/Br, 153(1976).

28. S. Sunder and H. J. Bernstein, J. Raman Spectrose, **5**, 351(1976).

29. D.L. Willems and D.F. Bocian, J. Am. Chem. Soc. **106**, 880(1984).

30. M. Sono and T. Asakura, J. Biol. Chem. **250**, 5227(1975).

31. M. Sono and T. Asakura, J. Biol. Chem. **251**, 2664(1976).

32. M. Tsubaki, K. Nagai and T. Kitagawa, Biochemistry **19**, 379(1980).

33. H. Hori, M. Ikeda-Saito and T. Yonetani, J. Biol. Chem. **257**, 3636(1982).

34. M. Gouterman, J. Mol. Spectrosc. **6**, 138(1961).

35. M. Gouterman, in 'Excited States of Matter' ed. C.W. Shoppee, Grad. Stud. Texas Tech Univ: Lubbock, TX, **2**, 63(1973).

36. A.C. Albrecht, J. Chem. Phys. **34**, 1476(1961).

37. N.B. Collhup, in 'Introduction to IR and Raman Spectroscopy' ed. L.H. Daly and S.E. Wiberly, Academic Press: New York, 246(1975).

38. R.G. Little, K.R. Dymock and J.A. Ibers, J. Am. Chem. Soc. **97**, 4532(1975).

TABLE 4.1 Resonance Raman Frequency Shifts (cm^{-1}) of HP, MP and PP

λ_{exc}=4416Å			λ_{exc}=5145Å			λ_{exc}=4965Å		
HP	MP	PP	HP	MP	PP	HP	MP	PP
1	2	3	1	2	3	1	2	3
318 w			502 w	502 w	502 w			
514 w			606 wm	606 w	605 w 658 w			
670 wm	670 m	670m	670 m	670 w				
741 ms	741 wm	741 m	741 vs	741 s	741 s			
771 m	771 sh	771 m	771 w	771 w				
843 w	843 wm		929 w	924 w	933 w		924 w 954 w	
			964 sh	964 sh	964 w	964w,br		970 w
964 vw							983 m	
	983 vw		982 m	983 m 996 sh	986 sh 996 m	996w,br		996 m
996 w		996 vw	1004 vw 1027 vw 1046 vw					
	1044 vw			1057 w 1084 w	1078 vw		1057 w 1096 w	1078 w 1103 w
			1103 w	1102 w				
					1113 w	1113 w	1113 wm	1128wm
1113 m	1113 w	1113 m	1128 ms	1128 s	1128 m	1128 wm	1128 m	1158sh
1128 sh	1128 w	1128 m	1167 m	1167 m	1158 sh	1167w,br	1167 ms	1170wm
1167 w	1167 w	1158 m	1181 sh	1181 sh	1170 m		1181 w	1209sh
							1214 sh	1228 m
1229 m	1129 wm		1229 m	1229 wm	1228 ms	1229w,br	1229 m	

Table cont..

Table 4.1 contd..

λ_{exc}=4416Å			λ_{exc}=5145Å			λ_{exc}=4965Å		
HP	MP	PP	HP	MP	PP	HP	MP	PP
1	2	3	1	2	3	1	2	3
			1264 w		1260vw			
				1273vw			1273w,br	
			1307sh	1295w	1307sh			
						1315sh	1316sh	1321sh
1328sh	1327w	1332w	1328s	1327vs	1332s	1328m	1327m	1332m
							1353sh	
			1356s	1356s	1356s	1356sh		1356sh
			1366s	1366s	1367s	1366m	1366m	1367m
1366s	1366s	1367vs	1387sh	1387m	1386sh	1387w	1387m	1386w
1387sh	1387sh							
	1401w		1424w		1424w	1424w	1419w	1424w
				1438w			1438w	
				1464w			1464w	1472sh
					1481m	1479m	1480m	1481m
1479m	1480m	1481wm	1479m	1480m		1516w		1514w
					1541s		1553s	1541m
1542m	1553m	1541m		1553m		1545m		
1545m	1570m	1563m	1545m					
1588m	1589ms	1586m	1588vs	1589s	1586vs	1588ms	1589vs	1586s
1599m			1599sh	1600sh				
		1605sh			1605sh	1605sh		1605sh
1617s	1617s	1612s	1617vs	1617s	1612vs	1617s	1617vs	1612vs
		1662w		1660w			1660w	
	1682w		1680w				1682w	

Abbreviations: br=broad; s=strong; m=medium; w=weak; v=very; sh=shoulder.

TABLE 4.2 Raman Shifts (cm^{-1}) for the Metal Complexes

λ_{exc}=5690Å		λ_{exc}=5640Å	λ_{exc}=5562Å	λ_{exc}=5145Å	
CuPP	CuMP	CoPP	CoMP	CuETP-IV in CS_2	CuETP-IV in KBr
				179±5vw	
233					
266	256		264vw,p	265w,br	
346	341		342w,p	346m	
372	371		378sh,p		
487	489		493vw,p		518w
	554			678m	679m
754s	756s	756s	750s	754vw	752m
					757w,sh
				789m	788m
				820w	819w
889vw	879			883vw	
920vw	928			928w,br	
945w		936	940w		
970w	968sh	975mw	969mw		
	991mw		986w	991sh	985w,sh
995w				998m	996m
	1000	1003	1002sh		
		1015sh			
1042vw	1057			1060vw	
1089w	1085	1094mw		1096vw	1087m
1123sh		1124sh			
1132mw	1131m	1129m	1130m	1137m	1136m
	1145				
1175vvw	1170vvw	1172w	1161w	1165s	1163m
1219sh	1216				
1227mw	1225mw		1228m	1222w	1221w
1238sh		1235m			1232w,sh

Table contd..

Table 4.2 contd..

λ_{exc}=5690Å		λ_{exc}=5640Å	λ_{exc}=5562Å	λ_{exc}=5145Å	
CuPP	CuMP	CoPP	CoMP	CuETP-IV in CS_2	CuETP-IV in KBr
1255		1250sh	1251vw		
	1268w		1267w	1266vw	
	1287				
1312mw,ap	1313wm,ap	1311wm,ap	1308mw	1316m	1313m
1320sh	1321				
1346sh,w	1334	1346wm,ap			
	1363w,ap		1363sh,ap	1368sh	
1371p	1377sh,p	1381w,p	1375wm,p	1380s	1377ms
1397w,p	1395sh,p				
	1409w,ap	1400vw	1407wm,dp	1411 m	1408m
1431w	1444	1436vw	1439vw		
1468w,dp	1467w,dp			1462w	
		1481w,dp	1474w,dp		
1504vw	1501			1509m	1505m
1550sh	1543	1555sh,dp			1559m,sh
1570sh,dp	1573s,dp	1575m,dp	1577s,dp	1577sh,s	1575sh,s
1581s,ap	1581sh,ap			1584s	1582s
		1599m,ap	1596wm,ap	1599sh,s	1597m,sh
1640s,dp	1640s,dp	1653s,dp	1649s,dp	1641s	1639s

Abbreviations: s=strong; m=medium; w=weak; v=very; sh=shoulder; p=polarized; dp=depolarized; ap=anomalously polarized.

TABLE 4.3 Summary of Raman and IR Bands.

RR frequencies(cm^{-1})			IR frequencies(cm^{-1})			Expected vinyl group modes as suggested by Choi et al[19]
HP	MP	PP	HP	MP	PP	
318			326 366 392	377 435	332 366	δ [$C_b C_\alpha C_\beta$(2)]
			466	460 482	466	
502	502	502				
514 606	606	605	625		625	
		658	670		670	
670	670	670	679 707	683 709	679 707	
				720		
			738	730 738	734	
741	741	741		760		
			770		775	
771	771	771		795		
			835	832	835	
843	843			854	850	
			879	888		
				898		
			913	905	910	$\gamma_s(=CH_2)$
				930		
929	924	933	950	959		
	954					
964	964	964 970				

Contd..

Table 4.3 contd..

RR frequencies(cm^{-1})			IR frequencies(cm^{-1})			Expected vinyl group modes as suggested by Choi **et al**[19]
HP	MP	PP	HP	MP	PP	
982	983	986		981		
996	996	996	990		989	γ(CH=)
1004						
1027			1035	1030		
1046	1044		1050		1050	
	1057			1056		
					1070	
	1084	1078	1072	1077	1076	$\delta_{as}(=CH_2)$
	1096					
1103	1102	1103		1101		
1113	1113	1113	1109	1115	1110	$\nu(C_b-C_a)(2)$
1128	1128	1128	1125		1125	
				1143		
1167	1167	1158	1166	1167		$\nu(C_b-C_a)(1)$
1181	1181	1170		1184	1168	
			1200	1195	1200	
	1214	1209				
1229	1229	1228	1230	1229	1228	
				1255		
1264		1260	1264	1264		
	1273			1275	1277	
1307	1295	1307	1300	1295	1302	δ(CH=)
				1311		
1315	1316	1321				
1328	1327	1332		1325		
	1353		1345		1345	
1356	1356	1356				$\delta_a(=CH_2)(2)$

Table contd..

Table 4.3 contd.

RR frequencies(cm^{-1})			IR frequencies(cm^{-1})			Expected vinyl group modes as suggested by Choi **et al**[19]
HP	MP	PP	HP	MP	PP	
1366	1366	1367		1374		
1387	1387	1386	1384		1384	
	1401		1405		1404	
1424	1419	1424		1414		$\delta_s(=CH_2)(1)$
	1438			1436		
			1446	1442	1440	
				1452		
	1464	1472		1462		
1479	1480	1481				
				1505		
1516		1514	1515		1510	
1542	1553	1541	1545		1545	
1545	1570	1563				
1588	1589	1586				
1599	1600					
1605		1605				$\nu(C=C)(2)$
				1610		
1617	1617	1612				$\nu(C=C)(1)$
			1630		1625	
	1660	1662				
1680	1682		1670		1670	
			1720	1732	1710	

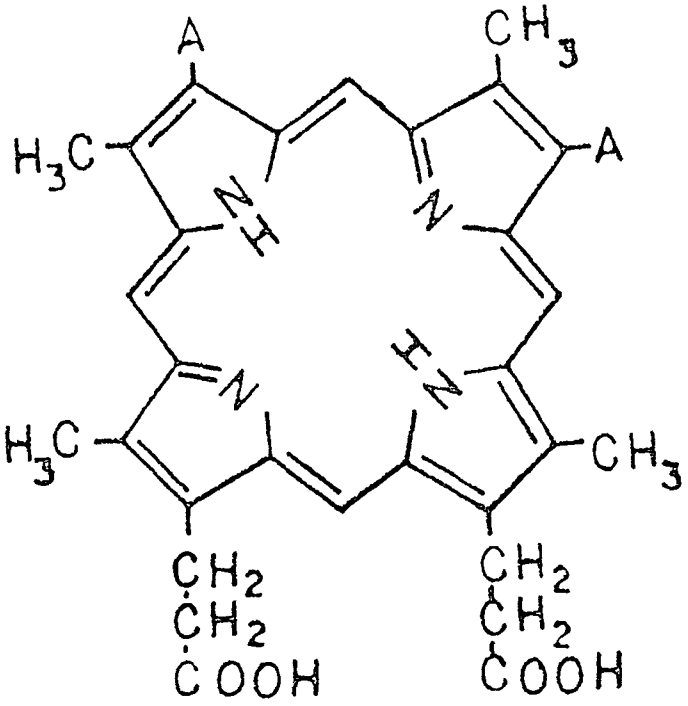

Fig.4.1 Structure of free base protoporphyrin-IX, mesoporphyrin-IX and haematoporphyrin-IX.

A = $-CH=CH_2$ for PP,
$-CH_2-CH_3$ for MP,
$CH_3-\underset{OH}{\underset{|}{C}}H-OH$ for HP.

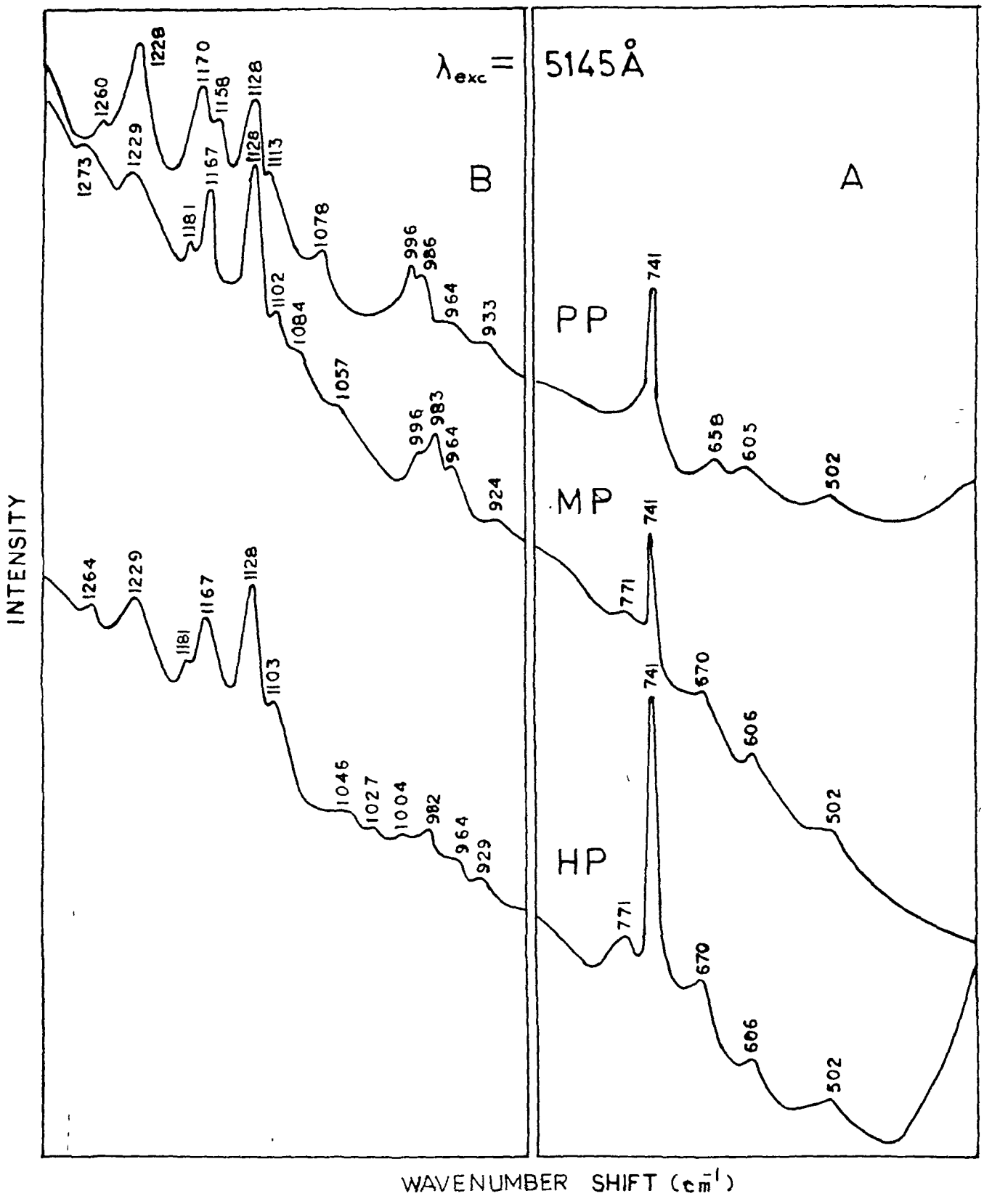

Fig.4.2a Resonance Raman spectra of free base porphyrins in KBr pellets with an excitation wavelength of 5145 Å. The vertical lines separate the two spectral regions as the full scale count rates were 2K for protoporphyrin-IX and mesoporphyrin-IX and 1.7K for haematoporphyrin-IX in A and 2K for protoporphyrin-IX and 2.2K for mesoporphyrin-IX and haematoporphyrin-IX in B.

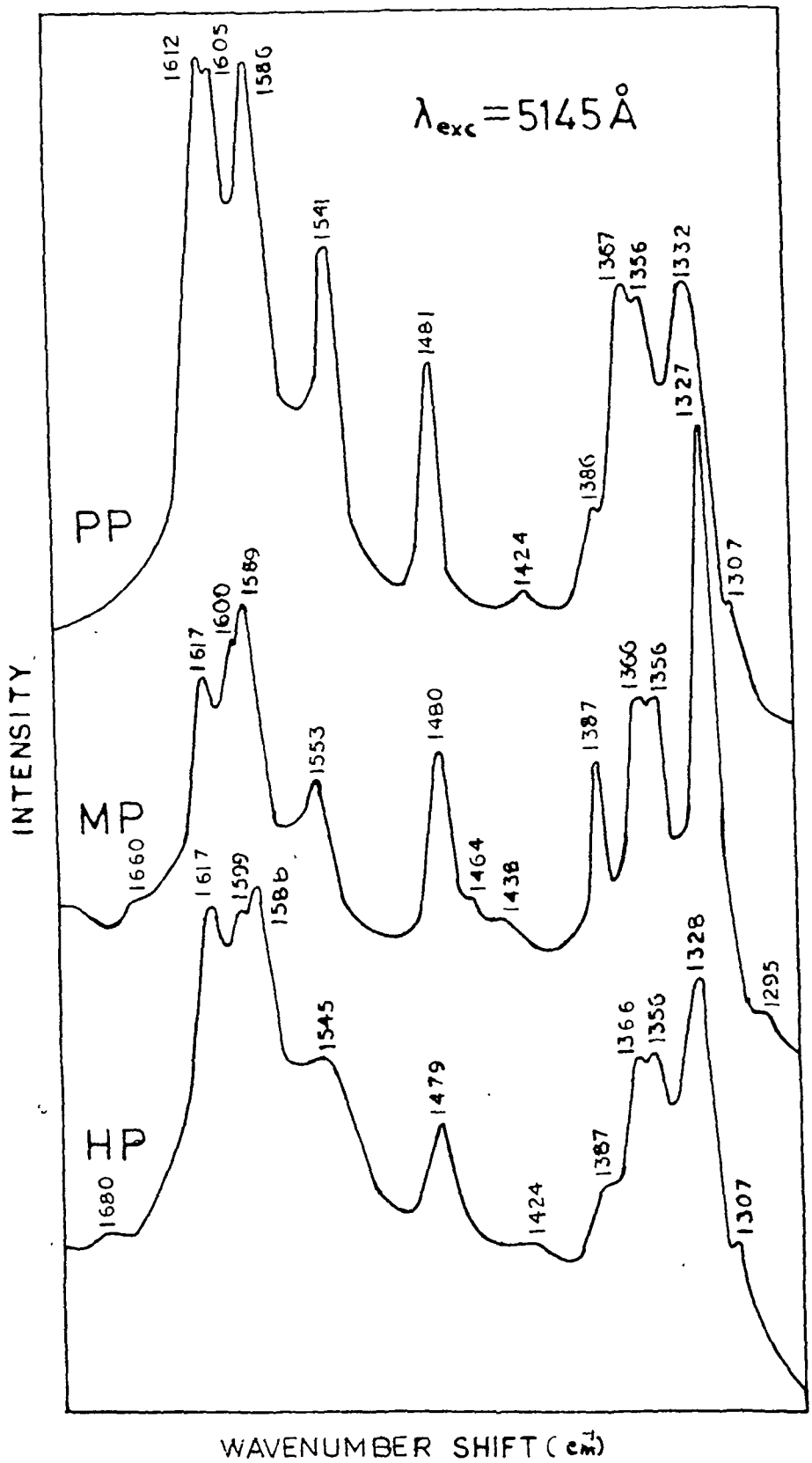

Fig.4.2b Resonance Raman spectra of free base porphyrins in KBr pellets with an excitation wavelength of 5145Å. The full scale count rates were 3.5K for protoporphyrin-IX, 2.5K for mesoporphyrin-IX and 3K for haematoporphyrin-IX.

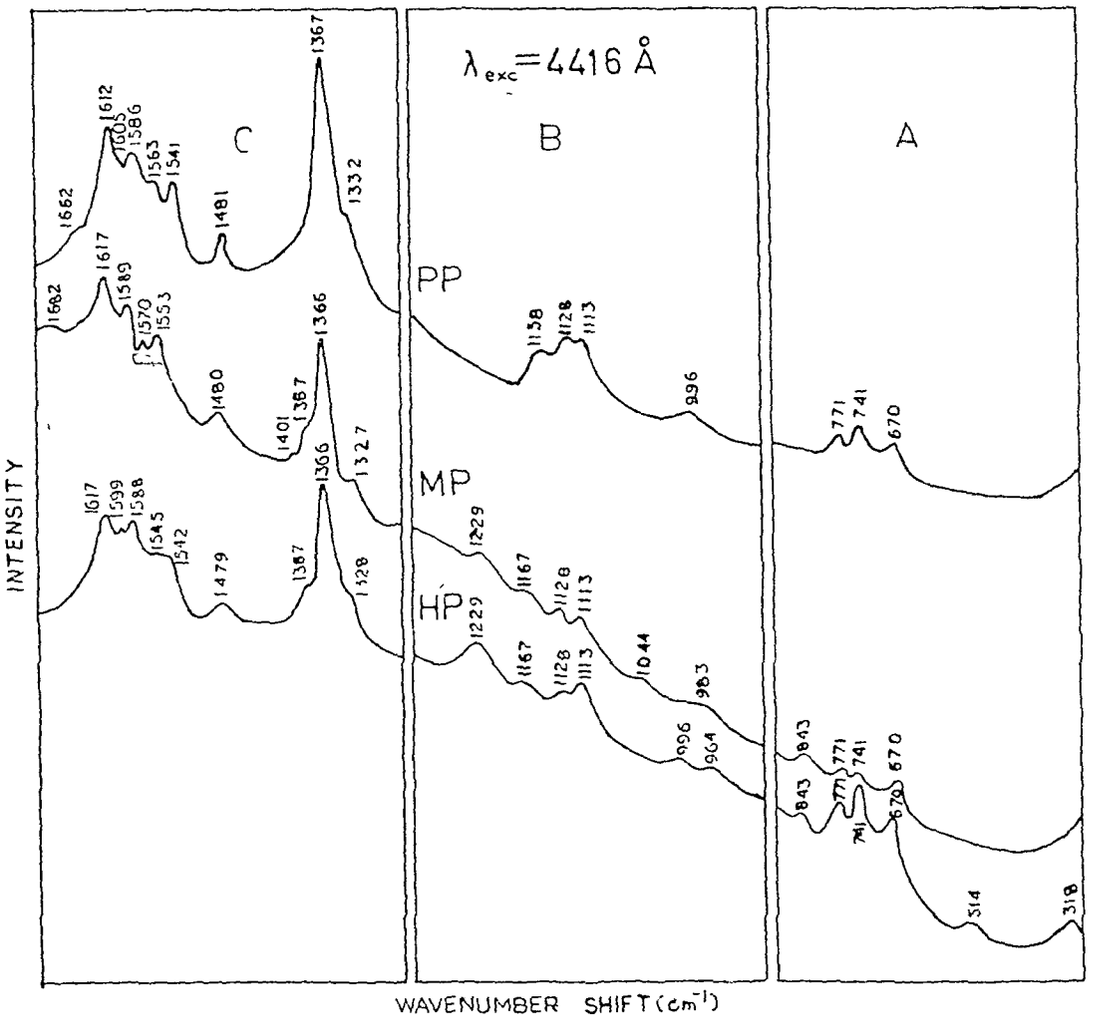

Fig.4.3 Resonance Raman spectra of free base porphyrins in KBr pellets with an excitation wavelength of 4416Å. The vertical lines separate the three spectral regions as the full scale count rates were 1K for protoporphyrin-IX, mesoporphyrin-IX and haematoporphyrin-IX in A, 2K for protoporphyrin-IX. mesoporphyrin-IX and haematoporphyrin-IX in B and 1K for protoporphyrin-IX, 1.4K for mesoporphyrin-IX and haematoporphyrin-IX in C.

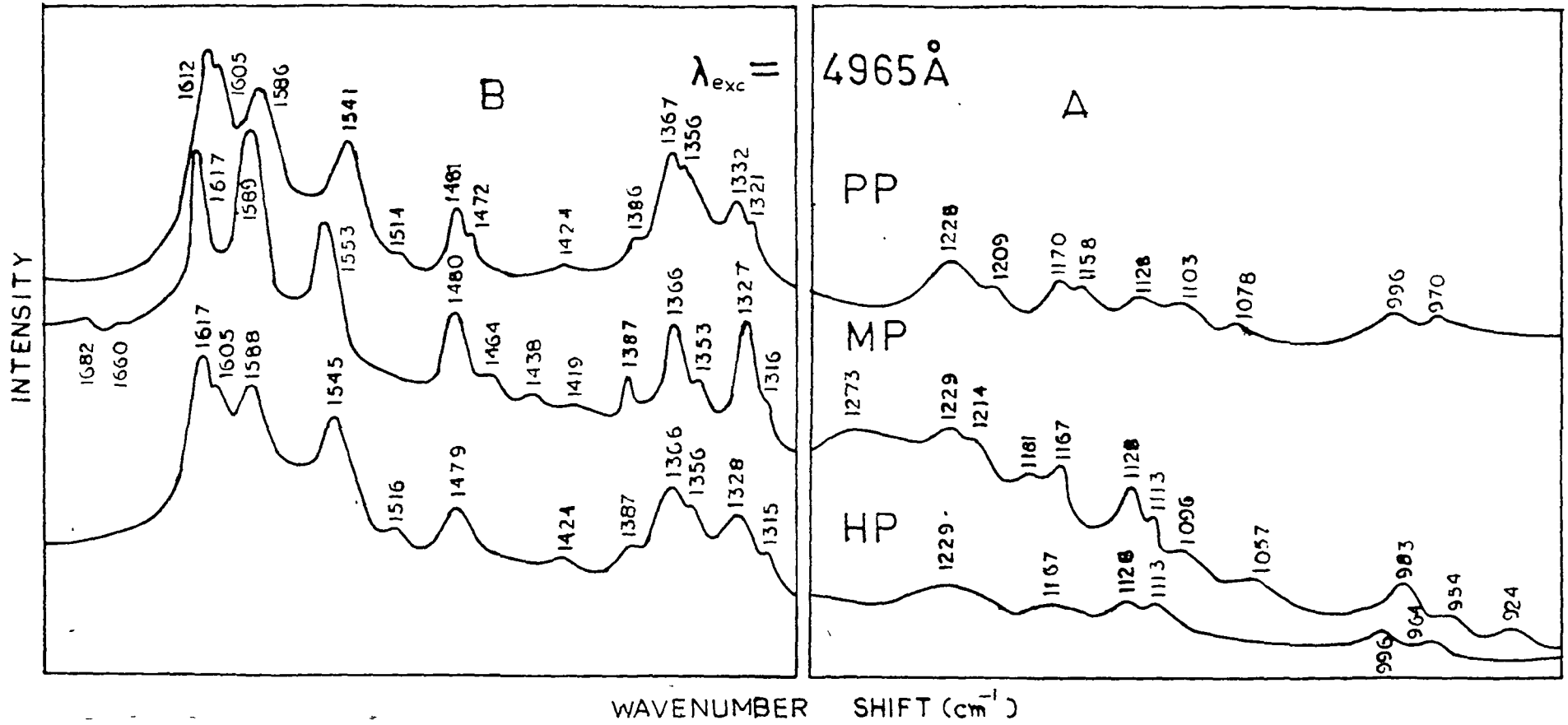

Fig.4.4 Resonance Raman spectra of free base porphyrins in KBr-pellets with an excitatation wavelength of 4965Å. The vertical lines separate the two spectral regions as the full scale count rates were 2K for protoporphyrin-IX, mesoporphyrin-IX and haematoporphyrin IX in A and 2.4K for all the porphyrins in B.

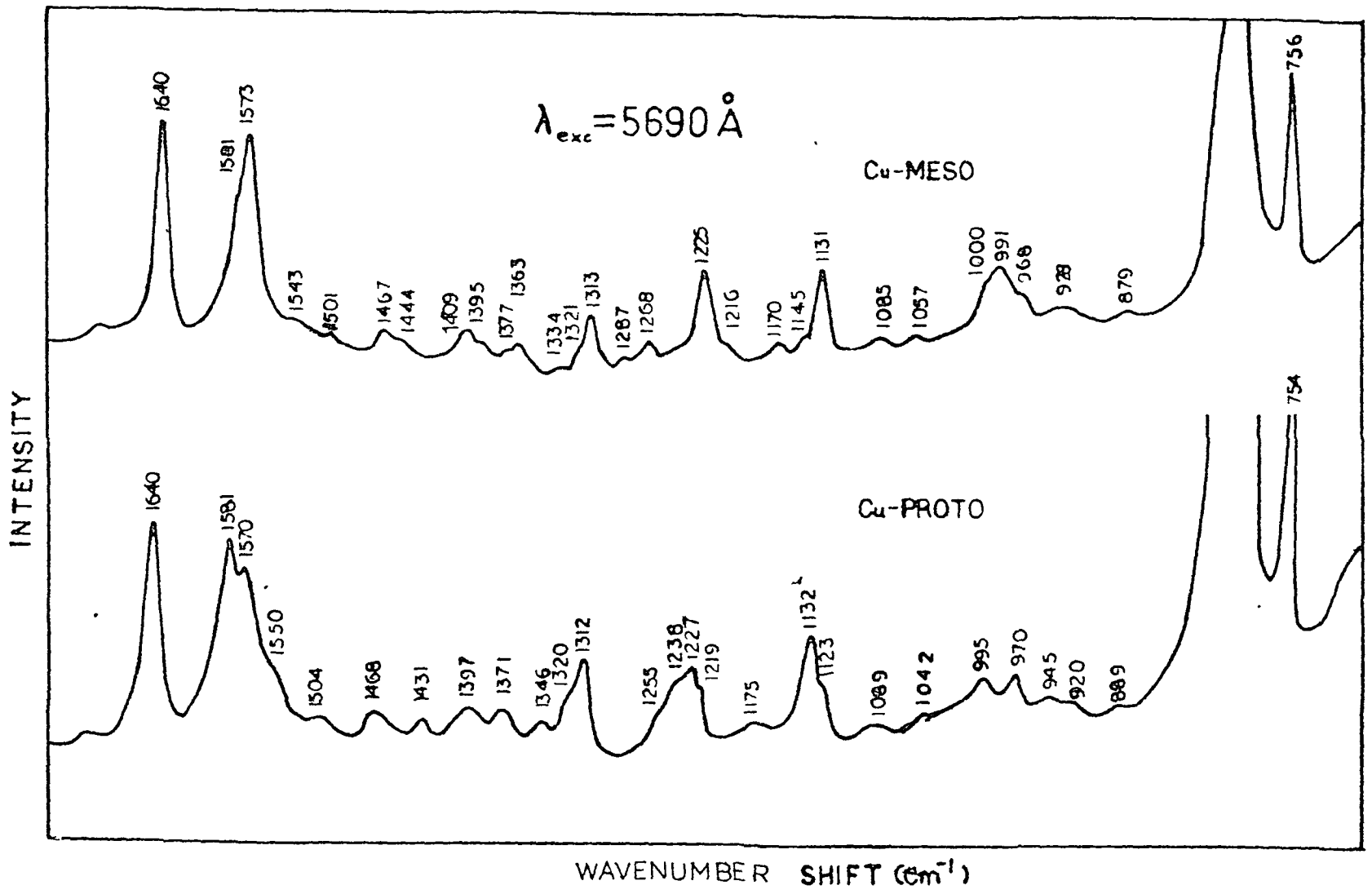

Fig.4.5 Resonance Raman spectra of CuPP and CuMP dimethyl esters with an excitation wavelength of 5690Å in CS_2 solution ($\sim 10^{-4}$M concentration).

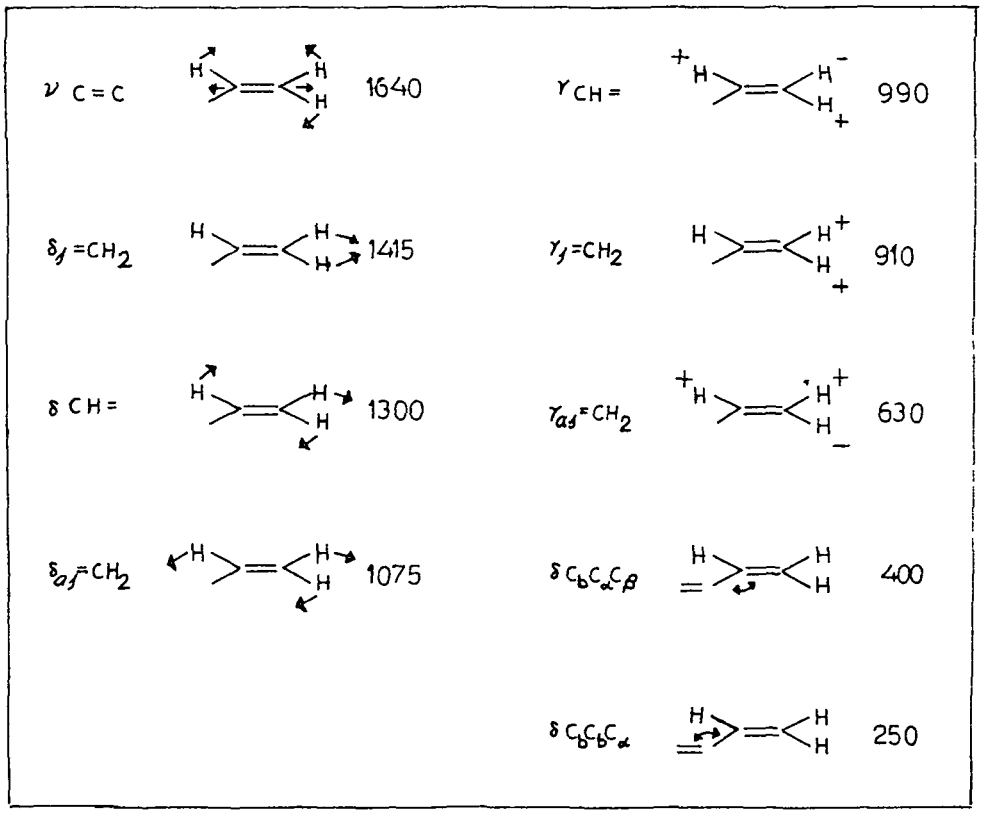

Fig.4.6 Schematic diagram of the vibrational modes of vinyl group and their expected frequencies.

RESONANCE RAMAN STUDIES OF TETRAPHENYLPORPHINATO MANGANESE(III) CHLORIDE (Mn(III)TPPCL)

ABSTRACT

Resonance Raman spectra of Mn(III)TPPCl in different solvents as well as in KBr pellet have been obtained with laser excitations in different regions of the atypical absorption spectrum of the system. The selective enhancement of vibrational modes arising from different parts of the molecule under excitation in different absorption regions has been used to assign the electronic transitions of the Mn(III)TPPCl. The strong absorption band at ~ 476 nm originates from a charge transfer transition between porphyrin and metal orbitals, while a weaker band at ~ 530 nm has been identified due to singlet-triplet (π , π^*) transitions. The present data do not provide distinct evidence for activation of the phenyl group modes under resonance Raman conditions indicating thereby that the phenyl groups may not be conjugatged with the porphyrin macrocycle. Depolarization ratios for some isolated bands show dispersion with excitation wavelengths due to reduction of the chromophore symmetry.

5.1 Introduction

The study of Mn(III)-porphyrin complexes has been an area of growing research activity during recent years.[1-6] These complexes exhibit an atypical electronic absorption spectrum which is diagnostic of their unusual electronic structure. The metal orbitals in these systems have much stronger influence on the ligand orbitals; the metal-porphyrin π mixing do not only alter the normal porphyrin $\pi \rightarrow \pi^*$ spectra, but also induce distinct new features to appear in the absorption spectra. Many studies have been concerned about the nature of these extra features, yet their origin is not fully understood and many controversial reports exist in literature. The intense band at $\sim$ 476 nm has been ascribed due to charge transfer transition,[1,2,4,6] charge transfer mixed with $\pi \rightarrow \pi^*$ transitions[3,7] etc. The near IR bands have been ascribed due to $d \rightarrow d$ transitions of the metal,[8,9] $d \rightarrow \pi$ charge transfer transitions,[6] triplet $\pi \rightarrow \pi^*$ transitions mixed with charge transfer character,[10] while the bands III and IV have been associated with the $\pi \rightarrow \pi^*$ transitions and/or charge transfer transitions.[1,3,6] However, to our knowledge, no attempt has yet been made to understand the origin of a band around 530nm in the absorption spectra of Mn(III)TPPCl. Thus, the characterization of the electronic spectra of these complexes is by no means certain and in view of the previous scattered and inclusive reports, it is highly desirable to probe the

electronic structure of the Mn(III)-porphyrin complexes in greater details. This may provide a clue about the nature of interactions between the metal and ligands and the electronic properties of these systems as well as sound theoretical base for understanding the metalloporphyrin absorption spectra, in general.

In addition to the spectroscopic properties, it is also necessary to probe the structural details of these systems responsible for their specific role in various biological processes. In this respect, it is necessary to elucidate the role of the external conjugating groups in perturbing the basic electronic structure of the chromophore.

Varieties of physical methods have been applied which have helped to achieve considerable deeper insight of these systems. More recently resonance Raman(RR) technique has been applied by several workers[2-4] to study these complexes. The appearance of resonance enhanced Raman features depends upon the particular excited electronic state(s) and thus can be used to elicit the electronic transitions in the absorption spectra. RR data can also be used to obtain information about the effect of the side chain substituents on the chromophore. There are some studies[11-14] which report the contribution of the peripheral substituents in the RR spectra of metalloporphyrins, while some other reports[15-17] do not support this view. Therefore it is necessary to study these complexes

in more details.

In this chapter, we report the RR studies of Mn(III)TPPCl with different excitation wavelengths. Selective enhancement of certain vibrational modes arising due to excitation in different parts of the optical spectra have been used to assign the electronic transitions. Secondly, the intensity dependence of some modes, which have been previously ascribed due to phenyl group modes, were monitored as a function of exciting frequency and the state of conjugation of the phenyl rings with the porphyrin macrocycle was explored. Finally, the depolarization ratios of some isolated bands with different excitation wavelengths have been measured to provide information about the symmetry of the system.

5.2 Experimental Results

The structure of Mn(III)TPPCl is shown in Fig. 5.1. Absorption spectra of MnTPPCl were reported in different solvents such as carbondisulphide(CS_2), dichloromethane(CH_2Cl_2), benzene(Bz) and pyridine(Py). Fig. 5.2 shows the absorption spectra of MnTPPCl in CS_2 and Py solutions and Table 5.1 lists the absorption maxima obtained in all the above solvents. Bands are labelled following Boucher.[1] The intensity pattern of the bands are rather similar in all the cases, although the intensity ratios differ. However, in Py solution, the relative intensities of the bands III and IV change and a new feature appears at ~ 425 nm. Although the absorption

maxima of different bands clearly vary in different solvents, there is no simple correlation by which they can be assigned to a particular type of transition based on expected solvent dependence.

RR spectra of MnTPPCl in KBr pellet with λ_{ex}=4765Å, 5309Å, 5831Å and 6116Å have been displayed in Figs.5.3a and 5.3b. Fig. 5.3c gives the RR spectra of MnTPPCl in KBr pellet with λ_{ex}=4416Å, while Figs. 5.4 (5.4a, 5.4b, 5.4c, 5.4d) give the Raman spectra of MnTPPCl in CS_2 and C_2Cl_4 solutions with λ_{ex}=4765Å, 5840Å and 6198Å. The locations of the laser lines for the pellet spectra have ben shown in Fig. 5.2. The corresponding Raman frequencies in KBr pellet as well as in CS_2 (and C_2Cl_4) solution have been given in Table 5.2 and Table 5.3 respectively. The depolarization ratios of most of the bands have been measured.Almost all the bands have analogous in the RR spectra of FeTPP systems[11,13,14] and have been assigned correspondingly with other known assignments. It is interesting to note that the lower frequency vibrations (i.e. < 500 cm^{-1}) are enhanced mainly with the 4765Å and 4416Å excitations. This is the region where metal-ligand vibrations are expected to occur. Excitation in all other regions enhance the higher frequency vibrations, i.e., the vibrations related to the TPP macrocycle. For further confirmation that the lower frequency vibrations are related to metal, Raman spectra of MnTPPCl in Py solution have been

obtained. Figs. 5.4a, 5.4b and 5.5 and Table 5.4 give a comparison of the Raman data obtained in the two solvents. It is known, that in Py solutions, the axial positions of Mn in the MnTPPCl are occupied by the Py molecules resulting in a shift of Mn ion with respect to the porphyrin plane. This should obviously affect the metal related vibrations. As can be seen from Figs. 5.4a, 5.4b and 5.5, the Raman spectra obtained in pyridine solution differ markedly compared to the spectra obtained in CS_2 solution. A medium intensity band at 262 cm^{-1} observed in CS_2 solution disappears in the spectra with pyridine solution. The features appearing at 221 cm^{-1} and 301 cm^{-1} in CS_2 solution shift to 227 and 293 cm^{-1} respectively in pyridine solution. The relative intensities of the bands also change drastically.

The absence of the band at 262 cm^{-1} in Py solution suggests it to be associated with the Mn-Cl stretching vibration. This assignment is consistent with previous work on related systems.[4,6] From the observed shift in the 221 and 301 cm^{-1} bands (CS_2) to 227 and 293 cm^{-1} (Py), these features may be associated with Mn-nitrogen stretching and deformation modes respectively. The higher frequency spectra (500-1700)cm^{-1} show somewhat similar features in the two solvents.

Excitation in the 530 nm absorption enhances mainly higher frequency vibrations, Figs. (5.3a, 5.3b; Table 5.2).

One peculiar observation in this regard was that the sample seemed to be decomposed after a certain interval of time, in spite of the low power of the exciting radiation (~ 50mW) and high speed of the spinning cell. Such degradation effects were not observed by excitation in any other absorption regions. Resonance Raman spectra of MnTPPCl in Py solution with excitation wavelength at 5309Å have also been obtained and shown in Fig. 5.6 which has mainly the polarized bands.

The RR spectra obtained by exciting in Bands III and IV also show enhancement of mostly higher frequency modes. Several depolarized and anomalously polarized features also appear in addition to the polarized modes. On the other hand, RR spectra obtained by 4416Å excitation show enhancement of both lower frequency as well as higher frequency vibrations. The general experimental details and methods of preparation of samples have been given in Chapter III.

5.3 Discussion

The optical absorption spectra of normal metalloporphyrins can be interpreted nicely by the four-orbital model proposed by Gouterman.[18,19] However, the complexity of the Mn(III)-porphyrin system require much deeper understanding. As stated earlier, the disruption of the normal metalloporphyrin $\pi \rightarrow \pi^*$ spectra arises because of strong metal porphyrin π interactions. Theoretical calculations predict[20] that the

metal $d\pi$ orbitals for the Manganese and Iron match in energy with the porphyrin π orbitals. Therefore strong mixing between the metal $e_g(d_\pi)$ levels and porphyrin π levels can occur when they are energitically close. As a consequence, a number of additional bands become allowed and appear in the absorption. These bands were variously ascribed to porphyrin $\pi \rightarrow \pi^*$, charge transfer or metal $d \rightarrow d$ transitions and so on. In principle, each individual band is expected to show different solvent dependence, depending on its origin. For example, the bands arising due to metal d-d transition and charge transfer transitions should be more sensitive to different solvents as compared to those arising from $\pi \rightarrow \pi^*$ transitions. However, experimentally this was not observed by us. The lack of observation of the expected solvent effects is also indicative of the complex electronic structure of the system. It is quite probable that the absorption peaks in the spectra do not arise due to a pure transition and may be an admixture of two or more transitions, and therefore the positions and intensities of the bands will depend on a complicated manner in different solvents. In view of this, electronic absorption spectroscopy cannot provide a proper interpretation of the complicated absorption spectra of such systems. Resonance Raman studies can provide more useful information in such situations and we have been able to assign some of these bands using RR data in different spectral regions. In order

to correlate RR data with electronic absorption, we first discuss the pertinent theoretical aspects of RR scattering applicable to such situations. Although some of these details have been given in Chapter II, some important aspects are repeated here for self consistency.

The intensity enhancement of specific vibrfational modes under resonance excitation can take place either through a mechanism involving A-type term or through a B-type term of the scattering tensor $(\alpha_{\rho\sigma})_{gi,gj}$.[21]

The A-type term of the scattering tensor is of the form,

$$A_{\rho\sigma} = \frac{1}{h} \sum_{v} \left[\frac{(m_\rho)^o_{g,e} (m_\sigma)^o_{g,e} \langle gi|ev\rangle\langle ev|gj\rangle}{\nu_{ev,gi} - \nu_o + i\Gamma_{ev}} \right]$$

and B-type term of the scattering tensor is of the form,

$$B_{\rho\sigma} = -\frac{1}{h} \sum_{v} \sum_{s} \sum_{a} h^a_{es} \left[\frac{(m_\rho)^o_{g,e} (m_\sigma)^o_{g,s} \langle gj|ev\rangle\langle ev|Q_a|gi\rangle + (m_\sigma)^o_{g,e} (m_\rho)^o_{g,s} \langle gi|ev\rangle\langle ev|Qa|gj\rangle}{(\nu_{ev,gi} - \nu_o + i\Gamma_{ev})(\nu_s - \nu_e)} \right]$$

The A-type term connects the ground electronic state to the excited state involved in resonance through Franck-Condon overlap and relates to Raman scattering from totally symmetric modes, while the B-term is responsible for connecting the resonant electronic state with another one of higher energy via vibrational perturbation and can enhance those vibrations which are contained in the direct product of the two electronic transition representations. This theoretical

treatment can be applied to understand the absorption and RR spectra of Mn(III)-porphyrin complexes. The ground state of Mn(III)TPPCl can be written as follows:

$$|g\rangle = \Psi_p \Psi_m$$

$$= NA \prod_i^m \Phi_{p_i}^2 \Phi_p^{*0} d_{xy}^1 d_{xz}^1 d_{yz}^1 d_{z^2}^1 d_{x^2-y^2}^0.$$

The excited states of the system may be written as:

$$|e\rangle = N_e A \prod_i^{m-1} \Phi_{p_i}^2 \Phi_{p_m}^1 \Phi_p^{*1} d_{xy}^1 d_{xz}^1 d_{yz}^1 d_{z^2}^1 d_{x^2-y^2}^0 ,$$

$$|s\rangle = N_s A \prod_i^{m-2} \Phi_{p_i}^2 \Phi_{p_{m-1}}^1 \Phi_{p_m}^2 \Phi_p^{*1} d_{xy}^1 d_{xz}^1 d_{yz}^1 d_{z^2}^1 d_{x^2-y^2}^0 ,$$

$$|d\rangle = N_d A \prod_i^m \Phi_{p_i}^2 \Phi_p^{*0} d_{xy}^1 d_{xz}^0 d_{yz}^1 d_{z^2}^1 d_{x^2-y^2}^1,$$

and

$$|c\rangle = N_c A \prod_i^{m-1} \Phi_{p_i}^2 \Phi_{p_m}^1 \Phi_p^{*0} d_{xy}^1 d_{xz}^1 d_{yz}^2 d_{z^2}^1 d_{x^2-y^2}^0.$$

where $|e\rangle, |s\rangle$ denote excited states reached by $\pi \rightarrow \pi^*$ transition, $|d\rangle$ excited state reached by $d \rightarrow d$ transition and $|c\rangle$ excited state reached by charge transfer transition respectively.

Here Ψ_p, Ψ_m represent the wavefunctions of TPP and metal respectively; N is the normalization factor, A is the antisymmetrizer. Φ_{p_i} are the occupied molecular orbitals in the ground state configuration of TPP, Φ_p^* is the lowest unoccupied TPP molecular orbital, d_{xy} etc. represent the atomic orbitals of Manganese. The superscripts indicate the electron occupancy of the orbitals.

The enhancement of resonance Raman features by the A-term will depend upon the factors $\langle gi|ev\rangle\langle ev|gj\rangle$. Within Born-Openheimer approximation a molecular state can be separated into an electronic and vibrational components so that, the wavefunction of molecule in a state $|e\rangle$ becomes, $\Psi_e=\Phi(q,Q)\kappa(Q)$ where Φ and κ are electronic and vibrational wavefunctions respectively. To proceed further, it is necessary to break $\kappa(Q)$ in terms of modes mainly associated with the macrocycle and metal such that, $\kappa(Q)=\kappa_p(Q)\kappa_m(Q)$. Thus,

$$|gi\rangle = \Phi_p \Phi_m \kappa_p^i \kappa_m^i,$$
$$|gj\rangle = \Phi_p \Phi_m \kappa_p^j \kappa_m^j,$$
$$|ev\rangle = \Phi_p^e \Phi_m \kappa_p^{ev} \kappa_m^v,$$
$$|cu\rangle = \Phi_p^{*+} \Phi_m^{*-} \kappa_p^{u*+} \kappa_m^{u*-}$$

As has already been shown in Chapter II, for resonance with a state $|e\rangle$, reached by a $\pi\rightarrow\pi^*$ transition, the Franck-Condon factor is of the form,

$$\sum_v [\langle\kappa_p^j|\kappa_p^{ev}\rangle\langle\kappa_p^{ev}|\kappa_p^i\rangle][\langle\kappa_m^j|\kappa_m^v\rangle\langle\kappa_m^v|\kappa_m^i\rangle]$$

Since the $\pi\rightarrow\pi^*$ transition involves charge redistribution in the porphyrin macrocycle, the distortion of the excited electronic state occurs within the macrocycle as opposed to the metal. Therefore, maximum change of the equilibrium nuclear configuration occurs within the macrocycle. This results in different potentials within the Hamiltonian for the excited state compared to the ground state. This implies,

$\langle \kappa_p^j | \kappa_p^{ev} \rangle \langle \kappa_p^{ev} | \kappa_p^i \rangle \not\cong \delta_{ij}$ and intensity of Raman bands by the A-terms will occur for j=i+1. However, the change in potential about the metal is small and $\langle \kappa_m^j | \kappa_m^v \rangle \langle \kappa_m^v | \kappa_m^i \rangle \cong \delta_{ij}$ and hence the metal modes will not be enhanced. Similarly, it can be shown that the change of excited configuration occurs within both the macrocycle and metal when the excitation occurs within a charge transfer band and as a result both metal and macrocycle modes will be enhanced.

To obtain the nature of vibrations, which should be expected to gain intensity via B-term, examination of the transition density matrix elements is necessary. The type of transition density matrix elements that must be considered are between states reached by $\pi \rightarrow \pi^*$ transitions, charge transfer transitions and d→d transitions. Although no d→d transitions are allowed under D_{4h} symmetry, a d→d transition from one of the degenerate d orbitals to the $d_{x^2 - y^2}$ orbital is allowed under C_{4v} symmetry. The change from D_{4h} to C_{4v} symmetry in a metalloporphyrin can occur by axial ligation and out of planarity of the metal ion.

Suppose, the two states $|e\rangle$ and $|s\rangle$ that are coupled are both reached by $\pi \rightarrow \pi^*$ transition. Then we should have, $\langle e | \Phi'(r) | s \rangle = -e' \int \Phi^1_{p_{m-1}} \delta(r - r_j) \Phi^1_{p_m} dr_j$ where $\Phi_{p_{m-1}}$ and Φ_{p_m}

are the highest occupied molecular orbitals. These orbitals are localized in the porphyrin macrocycle and occupy similar regions of space. Therefore the vibrations which will show intensity enhancement via this term are those of the macrocycle.

If a charge transfer band in which an electron goes to a d_{yz} or d_{xz} orbitals of metal is coupled with a state reached by $\pi \rightarrow \pi^*$ transition from the same occupied molecular orbital, then we have,

$$\langle c | \Phi'(r) | e \rangle = -e' \int d^1_{yz}\, \delta(r - r_j) \Phi_p^{*1}\, dr_j.$$

This integral represents the spatial overlap of a d orbital of the metal and a π orbital of porphyrin. Since the region of maximum overlap will occur around the metal and pyrrole nitrogens, vibrations around the central metal will be enhanced by excitation in this region of absorption.

If the two charge transfer states involved in the coupling originate from the same porphyrin ground state occupied molecular orbitals but end in different metal d orbitals, we have, $\langle c_1 | \Phi'(r) | c_2 \rangle = -e' \int d_1^1\, \delta(r - r_j)\, d_2^1\, dr_j$

Here d_1 and d_2 are the two different d orbitals that are occupied by the promoted electrons. This term is usually small, since the two different d orbitals occupy different regions of space unless axial ligand vibrations and the constraints imposed by the pyrrole nitrogens mix the d orbitals.

In that case vibrations of the axial ligands are expected to be enhanced.

If the two charge transfer states which terminate in the same d orbitals but originate from different porphyrin π orbitals are coupled, we have, $\langle c_1|\Phi'(r)|C_3\rangle = -e'\int\Phi^1_{p_m}\,\delta(r-r_j)\Phi^1_{p_{m-1}}\,dr_j$ vibrations related to the macrocycle will be enhanced.

States differing by the occupancy of more than one electron cannot couple under the vibrational perturbation so that charge transfer transitions differing in occupancy of both porphyrin and d orbitals cannot couple.

One final point is to be noted here. In porphyrins, the initial $\pi\rightarrow\pi^*$ states are mixed by configuration interaction so that, $|Q\rangle = M|Q^\circ\rangle + N|B^\circ\rangle$ and $|B = P|B^\circ\rangle + T|Q^\circ\rangle$, where M,N,P and T are the coupling coefficients and $|Q^\circ\rangle$ and $|B^\circ\rangle$ are the zero order $|Q\rangle$ and $|B\rangle$ states. The transition density matrix elements will be,

$\langle Q|\Phi'(r)|B\rangle = MT\langle Q^\circ|\Phi'(r)|Q^\circ\rangle + NP\langle B^\circ|\Phi'(r)|B^\circ\rangle + (MP+NT)\langle B^\circ|\Phi'(r)Q^\circ\rangle$

The overlap of the $|Q\rangle$ and $|B\rangle$ states with themselves equals unity and thus $\langle Q|\Phi'(r)|B\rangle$ will dominate and the vibrations related to macrocycle will be enhanced by excitation in this region.

5.4 Assignment of the Electronic Absorption Bands

The vibrations mostly enhanced by excitation in the absorption region of band V are related to the metal and therefore this band can be assigned to a charge transfer transition. Excitations in absorption regions of the band III and IV enhance many non-totally symmetric modes which are related to porphyrin macrocyclic vibrations. Similar features are observed in the Q band excited RR spectra of metalloporphyrins with typical absorption spectra.[22,23] Therefore bands III and IV can be correlated to α and β absorption bands respectively. It is important to mention here that in addition to the metal related vibrations, band V excitation does reveal the presence of some macrocyclic modes and similarly in addition to the macrocyclic vibrations, band III excitation shows some metal related modes. Although the enhancement of some macrocyclic vibrations in the charge transfer excitation may occur via A-term, both the A and B terms should contribute to the enhancement of mecrocyclic vibrations when the excitation occurs in a $\pi \rightarrow \pi^*$ absorption. Therefore the enhancement of few low frequency vibrations, especially the Mn-Cl stretching mode vibrations, with α band excitation indicates some charge transfer character in the band III. It was proposed[7,24] that the charge transfer bands arising from electronic excitations $a_{1u}(\pi)$, $a_{2u}(\pi) \rightarrow e_g(d_{\pi})$ of E_u symmetry mix with normal $\pi \rightarrow \pi^*$ transition of E_u symmetry, depending upon their relative energies. Our data is consistent with

this model. We propose that the four electronic configurations of E_u symmetry obtained in this way mix via configuration interactions and give rise to the absorptions corresponding to bands III, V, V_a and VI. The relative intensities of all the bands will depend in a complicated way on the transitions dipoles of the pure configurations and on the extent of mixing. However, band V has predominantly charge transfer character and band III has mainly $\pi \rightarrow \pi^*$ character. We could not obtain RR data by exciting in the absorption regions of the bands V_a and VI which could be useful in further confirmation of the above assignment scheme. The enhancement of both the lower and higher frequency vibrations with λ_{ex}=4416Å can be understood in the following way. The absorption in this region will have contributions from bands V, V_a and VI and since these bands have mixed character of charge transfer and $\pi \rightarrow \pi^*$ transitions, this may be responsible for enhancement of Raman lines corresponding to both the metal related modes as well as the macrocyclic modes.

The number of Raman bands observed in the KBr pellet is generally large compared to the spectra obtained in solution. It is known that the molecules occupy lower sites and are distorted in the solid form. Therefore many bands will be expected in the RR spectra with KBr pellet than in solution due to site and correlation field splittings and Raman activity of the forbidden IR modes.

The reversal of intensity of bands III and IV and Py solution probably is related to the change in porphyrin π levels. The axial ligands are occupied by the Py molecules in Py solution which indicates that the out of plane distance of the metal with respect to the porphyrin plane should be different in Py solution compared to that in MnTPPCl. RR data obtained with 4765Å supports this view. The change in the metal-nitrogen ligand strength should affect the $a_{2u}(\pi)$ level of the molecule, since it has electron density through the pyrrole nitrogens. As the intensity of the α band depends considerably on the relative energy gap between the a_{1u} and a_{2u} orbitals, it is expected that this will influence the intensity of the α band considerably. Finally, the absorption at ~ 425 nm in Py solution which disappears in other solvents can be tentetively correlated to metal-pyridine charge transfer transition. Similar features were observed in (TPP)Fe(II)Py_2[25] as well as in (OEP)M$(Py)_2$[26] systems where M=Fe(II), RU(II), OS(II). However, further work will obviously be helpful in confirming this assignment.

The most interesting results were obtained by exciting in the 530 nm absorption region. The RR bands observed correspond mainly to macrocyclic vibrations. The appearance of mainly the macrocyclic vibrations via A-term can occur provided this absorption originates from a $\pi \rightarrow \pi^*$ transition. Enhancement of mainly macrocyclic vibrations can also occur via B-term

in the case where the two coupled states both originate from $\pi \rightarrow \pi^*$ transition or when the two states that are coupled are reached by two charge transfer transitions which originate from different porphyrin π levels but end in the same metal d level. However, the modes which should be expected to be enhanced mainly via B-term are non-totally symmetric. On the other hand, polarization data in Py solution indicates that mainly the totally symmetric vibrations are enhanced by excitation with 5309Å laser line. Even the Raman bands obtained in pellet spectra correspond mainly to the totally symmetric modes as observed in solution. This implies that the enhancement of vibrations with excitation in the 530nm absorption occurs via the A-term and hence the absorption should be of $\pi \rightarrow \pi^*$ origin. In view of the present evidence, one of the plausible assignment for this absorption band may be singlet $\rightarrow$ triplet (π, π^*) transition. This transition is spin forbidden and not observed in the normal absorption spectra. The mixing of $e_g(\pi^*)$ and $e_g(d\pi)$ levels can cause extra features in the absorption and also can introduce large spin-orbit coupling providing a relaxation pathway for the singlet $\rightarrow$ triplet transition to occur. Kobayashi **et al**[10] have shown that in Mn(III) and Fe(III) porphyrin systems, the charge transfer states do not only mix with the singlet (π, π^*) states, but they also mix with the triplet (π, π^*) states, making singlet $\rightarrow$ triplet (π, π^*) transition mixed with some

charge transfer character, partly allowed. However, the bands in the near IR region have been mainly attributed to of singlet → triplet (π ,π *) origin. It was shown previously[7] that the porphyrin lowest triplet transition are of (π , π *) origin and should be represented as a pure single configuration arising from either $(a_{1u} \rightarrow e_g)^T$ or $(a_{2u} \rightarrow e_g)^T$ transitions because the coupling integral which causes mixing of the singlet transitions, vanishes for the triplet states if the molecule has D_{4h} symmetry. However, in Mn(III)-porphyrin systems the interactions between the central metal and porphyrin ligand cause large perturbation to the electronic structure and as a result, the above formulation may breakdown resulting in similar configuration interaction, even in the excited triplet states. We propose that the band at ~530 nm and one of the bands in the near IR region arise due to singlet-triplet (π , π*) transitions. The decomposition of the samples by excitation with the 5309Å laser line may be understood qualitatively in terms of the longer lifetime of the triplet state. The molecules in the excited triplet state may undergo photodecomposition before they return to the ground state. Therefore, the present observation also supports the assignment of this band of singlet → triplet (π, π*) origin. Thus, although a reasonable explanation for the band around 530 nm can be offered, a proper understanding will require detailed theoretical study.

5.5 Activation Of The Phenyl Modes

Earlier workers[11,13,14] have reported the presence of some phenyl modes in the RR spectra of FeTPP systems. This implies that phenyl groups are conjugated with the whole macrocycle and also the internal modes of the phenyl groups must be coupled to the electronic transitions of the whole macrocycle. In the ground state, the phenyl rings are twisted almost perpendicularly with the macrocycle and therefore conjugation between the phenyl rings and macrocycle cannot occur. The conjugation of the phenyl rings and observation of the phenyl modes in the RR spectra were attributed to an excited state interaction.[11] It was suggested that during the Q state excitation the electron density moves towards the meso-carbon atoms which provide a driving force for rotation of the phenyl groups in the porphyrin plane resulting in electron delocalization through the phenyl groups. The bands at 995 cm^{-1}(p), 1030 cm^{-1}(p), and at 1599 cm^{-1}(p) were associated with the phenyl vibrations based on the meso carbon deuteriation shift.[11] Following the argument of Burke **et al**,[11] the phenyl modes are expected to be more strongly enhanced by excitation in band III as well as with excitation at ~530 nm absorption. In the RR spectra of Mn(III)TPPCl, the feature at 997 cm^{-1} is more strongly enhanced with λ_{ex}=4416Å, 4765Å, 5309Å, less strongly with λ_{ex}=5831Å and not observed with λ_{ex}=6116Å in the KBr pellet spectra. The observation

of the band with λ_{ex}=5309Å is in agreement with the previous suggestion, while non-observation of this band with excitation in the α band region does not support this contention. On the other hand, the band at 1598 cm^{-1} was not detectable with 5309Å excitation, but was observed with 4416Å and 6282Å excitations. Although the appearance of this band during α band excitation does support the assignment of this band to phenyl group vibration, its absence with the 5309Å excitation contradicts this proposal. Another band at 1030 cm^{-1} has also been assigned to a phenyl mode. In MnTPPCl, two bands are seen in this region in the pellet spectra. Owing to very small frequency difference, these two features mostly overlap and one of them may be hidden under the envelop of the other in the solution spectra. However, our observation of only one medium intense and depolarized band with visible band excitation in the solution spectra in this region does not support its assignment to a phenyl group mode. Bands at similar position were also observed in RR spectra of non-phenyl metalloporphyrins. RR bands were observed at 998 cm^{-1} and 1004 cm^{-1} for Cu-porphin,[27] at 984 cm^{-1}, 1001 cm^{-1} and at 1598 cm^{-1} for Cu-aetioporphyrin-I[23] and at 991 cm^{-1}, 998cm^{-1} and 1599 cm^{-1} for Cu-aetioporphyrin-IV[23] and at 988 cm^{-1}, 1003 cm^{-1} and 1028 cm^{-1} for Mn(III)-aetioporphyrin-I,[4] which may be correlated to the corresponding bands in TPP. Thus our study does not provide distinct evidence of conjugation

of the phenyl groups with the macrocycle either in the ground or in the excited electronic states of the system. Even the RR study of meso-formyl and meso-nitro substituted Ni(II)-octaethylporphin[16] does not support the idea of conjugation between the meso-substituents and porphyrinπ systems. Therefore the features at 997, 1029 and 1598 cm^{-1} in MnTPPCl may be related to porphyrin macrocyclic modes. It is also to be mentioned that since the various skeletal modes in these systems are strongly coupled, deuterium shifts of certain modes cannot be taken as a sole criterion for assignment. The deuterium substitution of four meso-hydrogens in Cu-porphin shifts many bands. For example, the 732, 802, 1059, 1065, 1322, 1562 and 1587 cm^{-1} bands in the RR spectra of Cu-porphin shift to 710, 780, 1023, 1078, 1261, 1556 and 1574 cm^{-1} in the RR spectra of Cu-porphin-d_4[28] which strongly indicates the highly coupled nature of various skeletal modes.

5.6 Dispersion Of Depolarization Ratio (ρ_1)

In normal Raman scattering the polarizability tensor is generally assumed to be symmetric ($\alpha_{\rho\sigma} = \alpha_{\sigma\rho}$). However, Placzek[29] showed that as resonance is approached the tensor may become asymmetric and must be described by three invariants:

$$\bar{\alpha}^2 = \tfrac{1}{9}\left(\Sigma\alpha_{\rho\rho}\right)^2,$$

$$\gamma_s^2 = \tfrac{1}{2}\sum_{\rho,\sigma}\left(\alpha_{\rho\rho} - \alpha_{\sigma\sigma}\right)^2 + \tfrac{3}{4}\sum_{\rho\neq\sigma}\left(\alpha_{\rho\sigma} + \alpha_{\sigma\rho}\right)^2,$$

and

$$\gamma_{as}^2 = \tfrac{3}{4}\sum_{\rho\neq\sigma}\left(\alpha_{\rho\sigma} - \alpha_{\sigma\rho}\right)^2$$

where $\bar{\alpha}$, γ_s, γ_{as} represent the isotropic, symmetric anisotropic and antisymmetric anisotropic tensor invariants. The modified expression for the linear depolarization ratio is then obtained as

$$\rho_l = \frac{I_\perp}{I_{||}} = \frac{3\gamma_s^2 + 5\gamma_{as}^2}{45\bar{\alpha}^2 + 4\gamma_s^2}$$

The possible range of ρ_l values for the vibration of different symmetry species under various point groups can be used to determine the symmetry of the system.[30] Since the Manganese atom is out of the porphyrin plane, the symmetry of the system is expected to be C_{4v} for symmetric placement of the phenyl groups. As has been shown by McClain[30] that under the point group D_{4h} or (C_{4v}), the range of ρ_l values expected for the A_{1g} (A_1 in C_{4v}), A_{2g} (A_2 in C_{4v}), B_{1g} (B_1 in C_{4v}) or B_{2g} (B_2 in C_{4v}) type of vibrations are $\frac{1}{8} - \frac{3}{4}$, $\propto$ and $\frac{3}{4}$ respectively. The depolarized and anomalously polarized modes should not show any dispersion. Similar results are expected for the D_{2d} and D_4 point group symmetries. However, two well resolved bands at 850 cm^{-1} (dp) and at 1012 cm^{-1}(ap) show slight dispersion. ρ_l varies between 0.6 to 0.75 for the 850 cm^{-1} band and between 2 to 3 for the 1012 cm^{-1} band with different excitations. This indicates that the structure of the chromophore is distorted from C_{4v} symmetry. One of the plausible explanations for such distortion may be given in terms of the possible orientations of the phenyl groups. X-ray structural

data[31] of bis-(imidazole)-α, β, γ, δ - tetraphenylporphinato Fe(III)Cl indicates that in these systems, the dihedral angle made by the phenyl rings with the porphyrin plans in the adjacent I and IV position (Fig. 5.1) is 88° and between the phenyl rings of the other two adjacent positions with the molecular plane is 76°. In that case the molecular symmetry of MnTPPCl is C_s. It is probable that even in solution the molecular symmetry of MnTPPCl molecule as a whole is C_s because of similar orientation of the phenyl groups. This lowering of symmetry can give rise to enhancement of additional bands as compared to the C_{4v} structure.

5.7 Conclusions

We can summarize the findings as follows: The intense band V can be interpreted as arising due to charge transfer transitions while bands III and IV are of $\pi \rightarrow \pi^*$ origin mainly. The absorption at ~530 nm may be due to singlet-triplet (π, π^*) transitions. No direct evidence for the enhancement of the phenyl modes was found; therefore conjugation of the phenyl rings with the porphyrin macrocycle is less likely although the system is highly complicated and more studies may be required to decide about this point. Moreover, the variation of depolarization ratio for some bands with exciting frequency indicates that the effective molecular symmetry of the chromophore is lowered from C_{4v} and the rigorous molecular symmetry may be only C_s.

REFERENCES

1. L.J. Boucher, Coord. Chem. Rev. **7**, 289(1972).

2. R.R. Gaughan, D.F. Shriver and L.J.Boucher, Proc. Natl. Acad.Sci. USA, **72** 433(1975).

3. J.A. Shelnutt, D.C. O'shea, N.-T. Yu, L.D. Cheung and R.H.Felton, J. Chem. Phys. **64**, 1156(1976).

4. S. Asher and K. Sauer, J. Chem. Phys. **64**, 4115(1976).

5. L.O. Spreer, A.C. Maliyackel, S. Holbrook, J.W. Otvas and M. Calvin, J. Am. Chem. Soc. **108**, 1949(1986).

6. L.J. Boucher, J. Am. Chem. Soc. **92**, 2725(1970).

7. M. Gouterman, in "The Porphyrin" ed. D. Dolphin, Academic Press: New York, vol. **III**, 1(1978).

8. E.W. Baker and J.R. Perumareddi, Z.Naturforsch **25b**, 911(1970).

9. R.E. Linder and J.R.Rowlands, Spectry. Letts. **4**, 227(1971).

10. H. Kobayashi, Y. Yanagawa, H. Osada, S. Minami and M.Shimizu, Bull. Chem. Soc. Jpn. **46**, 1471(1973).

11. J.M. Burke, J.R. Kincaid and T.G. Spiro, J. Am. Chem. Soc. **100**, 6077(1978).

12. S. Choi, T.G. Spiro, K.C. Langry and K.M. Smith, J. Am. Chem. Soc. **104**, 4337(1982).

13. G.A. Schick and D.F. Bocian, J. Am. Chem. Soc. **105**, 1830(1983).

14. J.A. Hofmann and D.F. Bocian, Inorg. Chem. **23**, 1177(1984).

15. H. Brunner and H. Sussner, Biochim, Biophys. Acta **310**, 20(1973).

16. T.M. Ivanova and V.V. Berdyugin, J. Mol. Struct. **117**,287(1984).

17. M. Sarkar and A.L. Verma, J. Raman Spectrosc. **17**, 407(1986).

18. M. Gouterman, J. Mol. Spectrosc. **6**, 138(1961).

19. M. Gouterman, in 'Excited States of Matter' ed. C.W. Shoppee, Grad.Stud. Texas Tech Univ. Lubbock, TX, vol. II, 63(1973).

20. M. Zerner and M.Gouterman, Theoret. Chim. Acta **4**, 44(1966).

21. A.C. Albrecht,J. Chem. Phys. **34**, 1476(1961).

22. A.L. Verma, R. Mendelsohn and H.J. Bernstein, J. Chem. Phys. **61**, 383(1974).

23. R. Mendelsohn, S. Sunder, A.L. Verma and H.J. Bernstein, J. Chem. Phys. **62**, 37(1975).

24. M. Gouterman, L.K. Hanson, G.-E. Khalil and W.R. Leenstra, J. Chem. Phys. **62**, 2343(1975).

25. H. Kobayashi and Y. Yanagawa, Bull. Chem. Soc. Jpn. **45**, 450(1972).

26. G.A. Schick and D.F. Bocian, J. Am. Chem. Soc. **106**, 1682(1984).

27. A.L. Verma and H.J. Bernstein, J. Chem. Phys. **61**, 2560(1974).

28. A. L. Verma, M. Asselin, S. Sunder and H.J. Bernstein, J. Raman Spectrosc. **4**, 295(1976).

29. G. Placzek, in 'Rayleigh and Raman Scattering', UCR L Transl.No. 526(L) for 'Handbuch der Radiologie' ed. E. Marx, Akademische Verlagsgesellschaft VI: Leipzig, vol. **2**, 209(1934).

30. W.M. McClain, J. Chem. Phys. **55**, 2789(1971).

31. D.M. Collins, R. Countryman and J.L. Hoard, J. Am. Chem. Soc. **94**, 2066(1972).

TABLE 5.1 Absorption Maxima (nm) for Mn(III)TPPCl in Different Solvents ($\sim 10^{-5}$M Concentration).

CS_2	CH_2Cl_2	Benzene	Pyridine
755	758	753	783
698	700	700	713
675	675		685
620	614	616	605
583	578	578	570
530	525	530	523
476	468	472	470
			425
400	400	395	403
380	370	368	378

TABLE 5.2 Resonance Raman Frequencies (cm^{-1}) of Mn(III)TPPCl in KBr pellet with different excitation wavelengths.

4416Å	4765Å	5309Å	5831Å	6116Å
199m	199wm			
	217w			
238w,vbr	238wm			238wm
	260wm			
	278wm			
	298vw			
313vw	313w			
334w	334wm			
			358vw,br	
381s				
392s	392vs	392vw	392w	392wm
406w,sh			406w	
436w				
450vw	450vw,br			
564w				
637m	637wm			
659w				
673w				
703vw				
724vw				
746vw				
762vw				
787w	787wm			
800vw,sh				
830vw			830wm	830wm
850w	850w	850w	850wm	850wm
869vw,sh				869vw
887m	887w			887w
997m	997wm	997wm	997vw	
1007m	1007s	1007m	1007w	1007w
1024w	1024w	1024m		
1029w	1029w		1029wm	1029m
1045vw		1045vw		1045w
		1070w		
1080wm	1080w	1080wm		
		1084w	1084w,br	1084w
		1132w		
		1188m		1188w

Contd....

Table 5.2 contd..

4416Å	4765Å	5309Å	5831Å	6116Å
1233m	1233wm	1233wm,br	1233ms,br	1233ms,br
		1246vm		
		1265wm		1265w
	1278w,br	1278w	1278w	1278w
			1292w	
			1314w	
1343m			1343ms	1343m
1354vw				
1367m		1367s	1367s	1367s
1373wm,br	1373wm	1373m,sh		1373sh
	1397vw			
1452sh		1452vw,br		
1458wm				
1486w,sh				
1500m	1500m	1500m	1500m	1500ms
		1526vw		
1530wm		1530vw	1530s	1530ms
1537w	1537vw		1537s	1537ms
		1551vw		
1558s	1558w,vbr			
1564sh		1564w	1564w	1564w
		1574m,sh	1574w,sh	
1583m	1583m	1583s	1583m	1583s
1598w				
1628vw				

Abbreviations: s=strong; m=medium; w=weak; v=very; br=broad; sh=shoulder.

TABLE 5.3 Resonance Raman Spectra of Mn(III)TPPCl in CS_2 Solution ($\sim 10^{-4}$M Concentration)

4416Å	4765Å+	5840Å	6198Å	Assignment
	202p			
	221p			$\nu(Mn-N_4)$
	239p		239p	
	262p	262p	262p	$\nu(Mn-Cl)$
301p	301p			$\delta(Mn-N_4)$
334p	334p			
*396	*396	*396	*396	
	453			
	596			
	620			
	703			
	*787			
801				
809		809	809	
			830ap	
		850dp	850dp	
887p				
			922	
	1000p			
	1008p	1008p		$\nu(C_\alpha-C_m)$
	1028p	1028dp	1028dp	
			1049	
	1082p			$\delta(C_\beta-H)$
		1088dp	1088dp	$\delta(C_\beta-H)$
			1190dp	
		1234ap	1234ap	$\nu(C_\alpha-N)+\delta(C_\beta-H)$
	1237p			$\nu(C_m-Ph)$
	1251			
	1270			
	1286			
		1343ap	1343ap	$\nu(C_\alpha-C_\beta)+\delta(C_\beta-H)$
1368p	1368p	1368p	1368p	$\nu(C_\alpha-N)+\delta(C_\beta-H)$
1374dp	1374			
1452				$\nu(C_\alpha-C_\beta)+\delta(C_\beta-H)$
1458				
1497	1497			

Contd...

Table 5.3 contd.

4416Å	4765Å +	5840Å	6198Å	Assignment
	202p			
1502	1502	1502dp	1502dp	$\nu(C_\beta - C_\beta)$
		1531ap	1531ap	
		1537ap	1537ap	$\nu(C_\alpha - C_m)$
		1550sh	1550sh	
1561				
	1564	1564	1564	
	1573			
1585	1585	1585	1585	

Abbreviations: p=polarized; dp=depolarized; ap=anomalously polarized; sh=shoulder;

The bands which are interferred by the solvent peaks are indicated by *, +, The frequencies quoted from (1300-1700) cm^{-1} region are in C_2Cl_4 solution.

TALE 5.4 Comparison of the RR bands (cm^{-1}) of Mn(III)TPPCl in CS_2 and Pyridine Solutions with Band V Excitation; λ_{ex}=4765Å.

CS_2+	Py
202p	202p
221p	227p
239p	240
262p	
	274
301p	293p
	318
334p	334p
*396	396p
453	453
	557
595	592
620	620
	638
	651
703	
	733p
*787	787p
	834
	850dp
	887p
	908p
	934p
	*978
1000p	*1000
1008p	1008p
1028p	*1028
1082p	
	1146
	1179
	1189
	*1227
1237p	1237
1251	
1270	
1286	

Table contd..

Table 5.4 contd..

CS_2^+	Py
	1341
1368p	1368
1374	1374
	1384
1497	
1502	1500
	1551sh
	1559sh
1564	
1573	*1573
1585	*1580
	1598p

Abbrebiations: p=polarized; dp=depolarized; sh=shoulder.

The bands which are interferred by the solvent peaks are indicated by *, +, The frequencies quoted from (1300-1700)cm^{-1} region are in C_2Cl_4 solution.

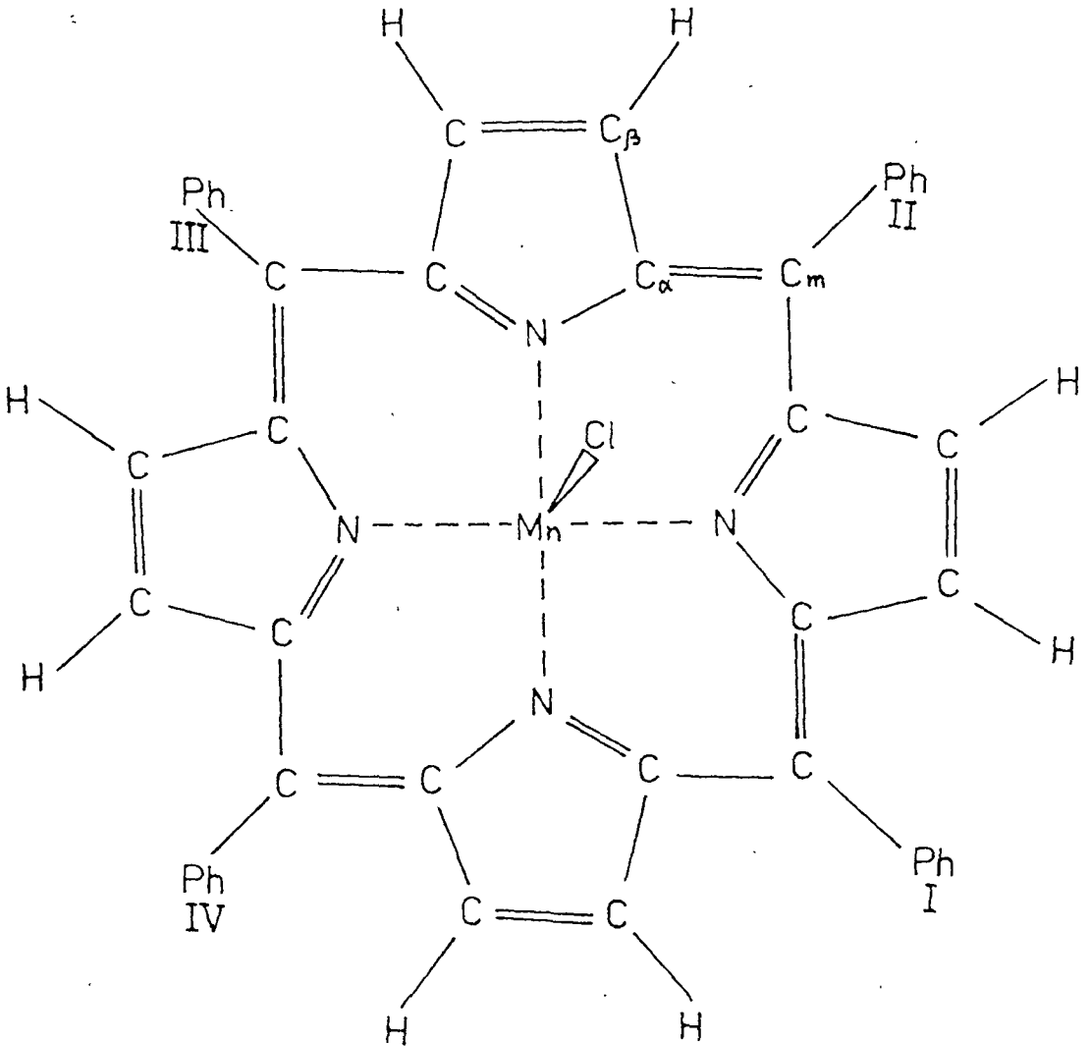

Fig.5.1 Structure of tetraphenylporphinato Manganese(III) Chloride. Ph denotes phenyl group.

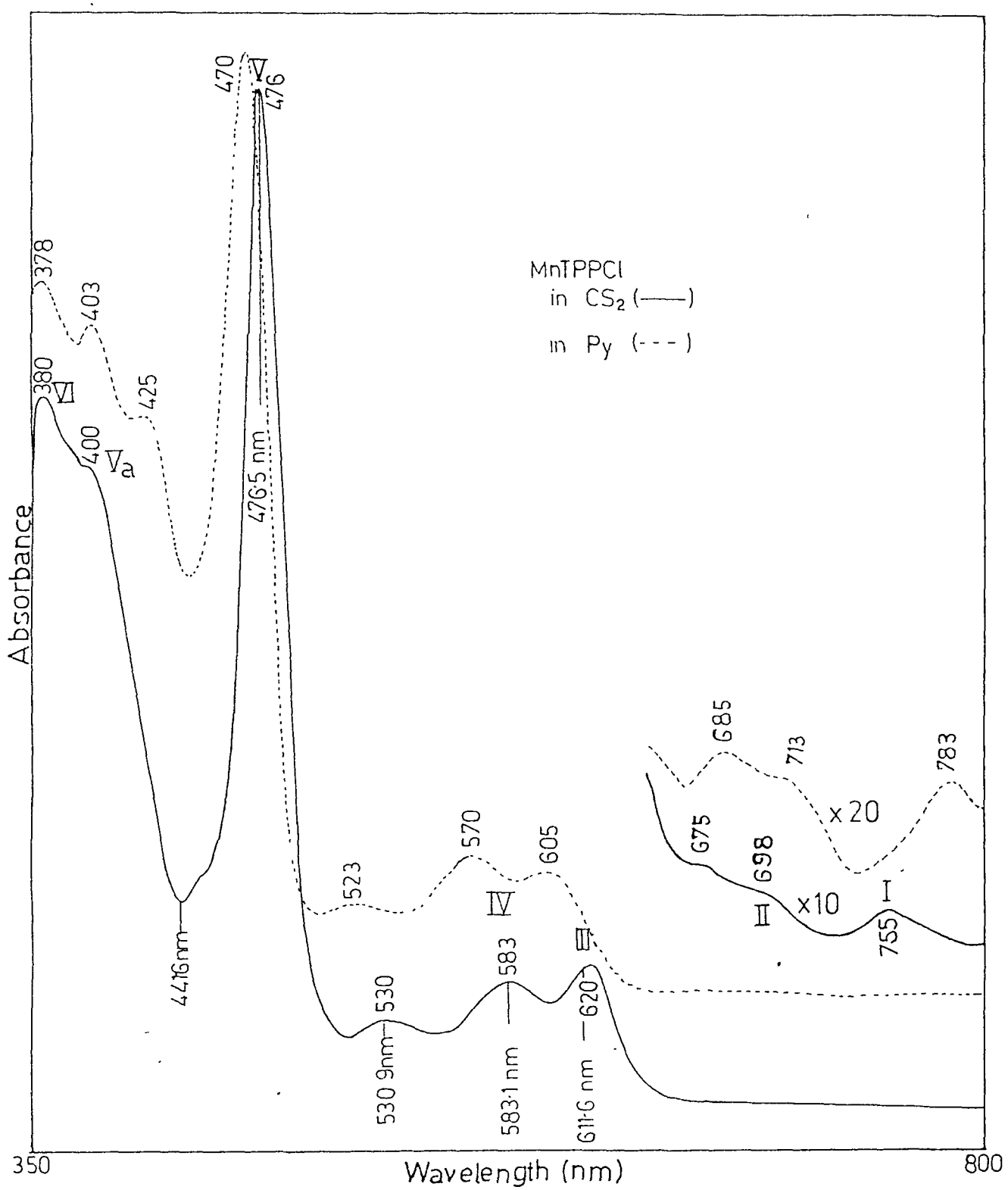

Fig.5.2 Absorption spectra of Mn(III)TPPCl ($\sim 10^{-5}$M) in CS_2 (——) and in pyridine (- - - - - - -) solutions.

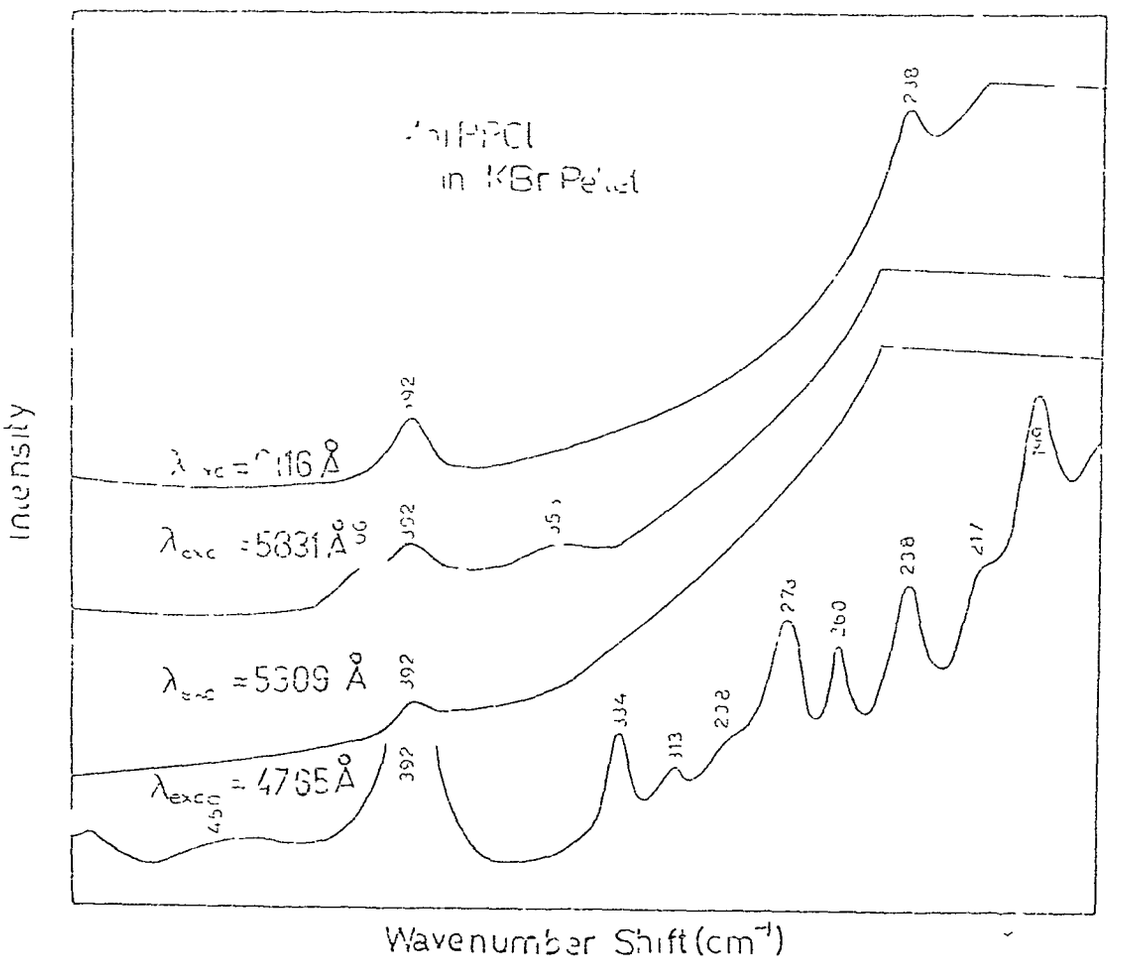

Fig 5.3a Low frequency Resonance Raman spectra of Mn(III)TPPCl in KBr pellet with different excitation wavelengths

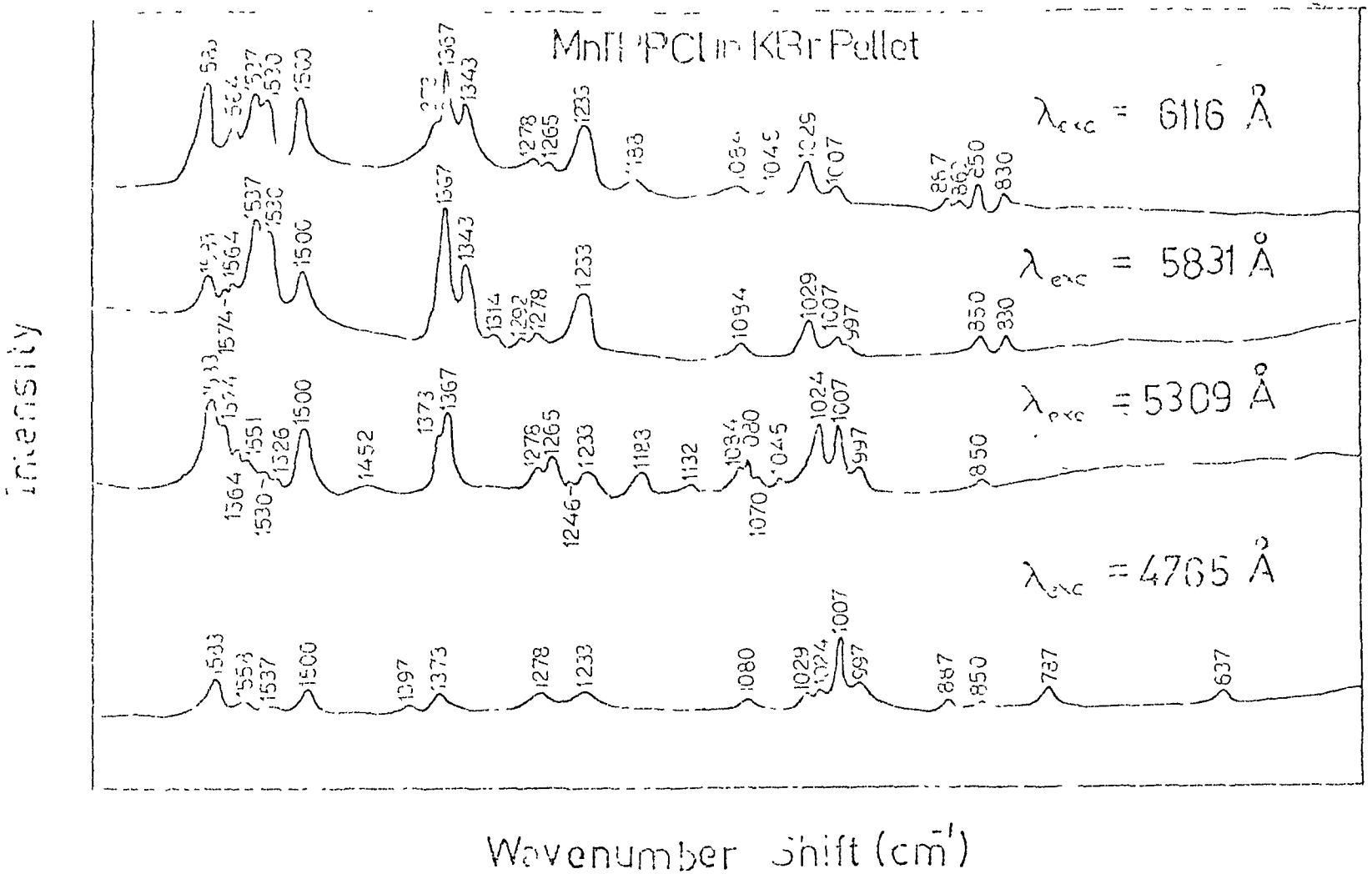

Fig.5.3b Resonance Raman spectra of Mn(III)TPPCl in KBr pellet with different excitation wavelengths in the higher frequency region.

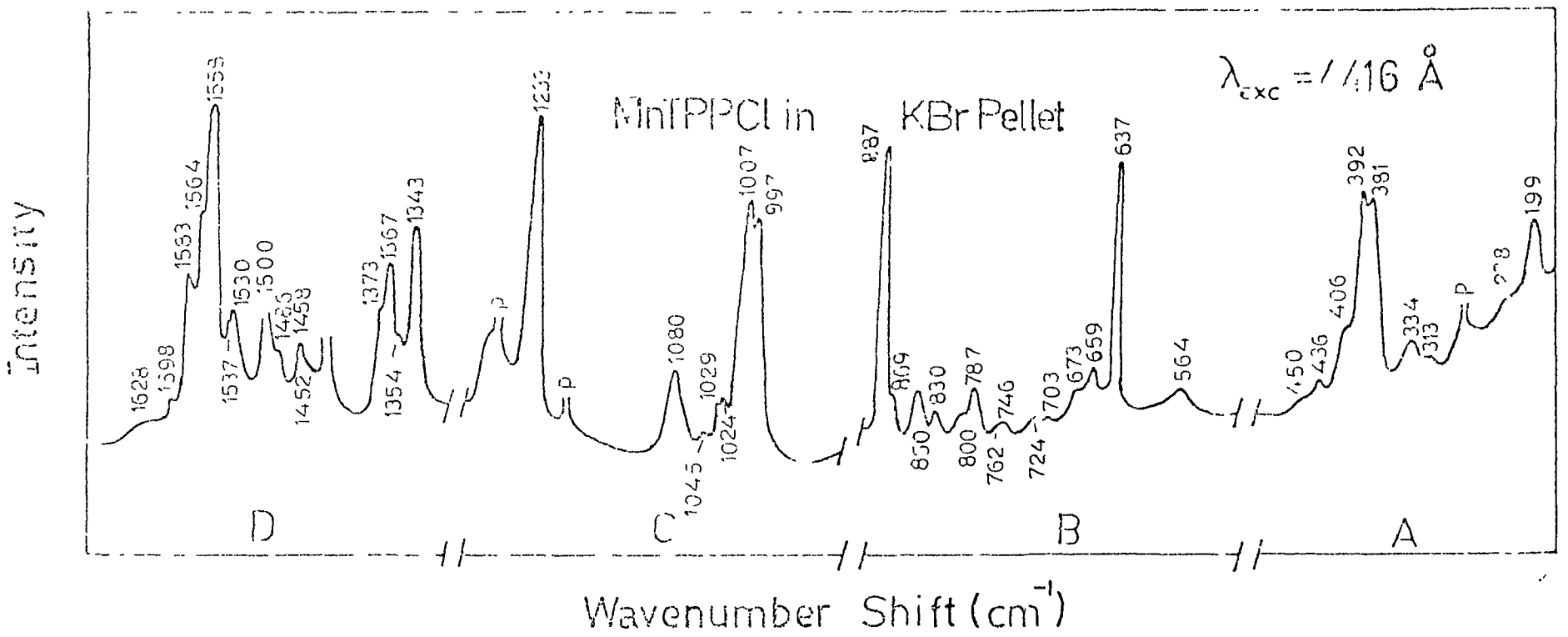

Fig.5.3c Resonance Raman spectrum of Mn(III)TPPCl in KBr pellet with λ_{ex}=4416Å. The breaks between different regions indicate difference in scales. The full scale count rates are 2.5 K for part A, 0.8 K for part B, 1.5 K for part C and 2.2 K for part D. Plasma lines are indicated by 'p'.

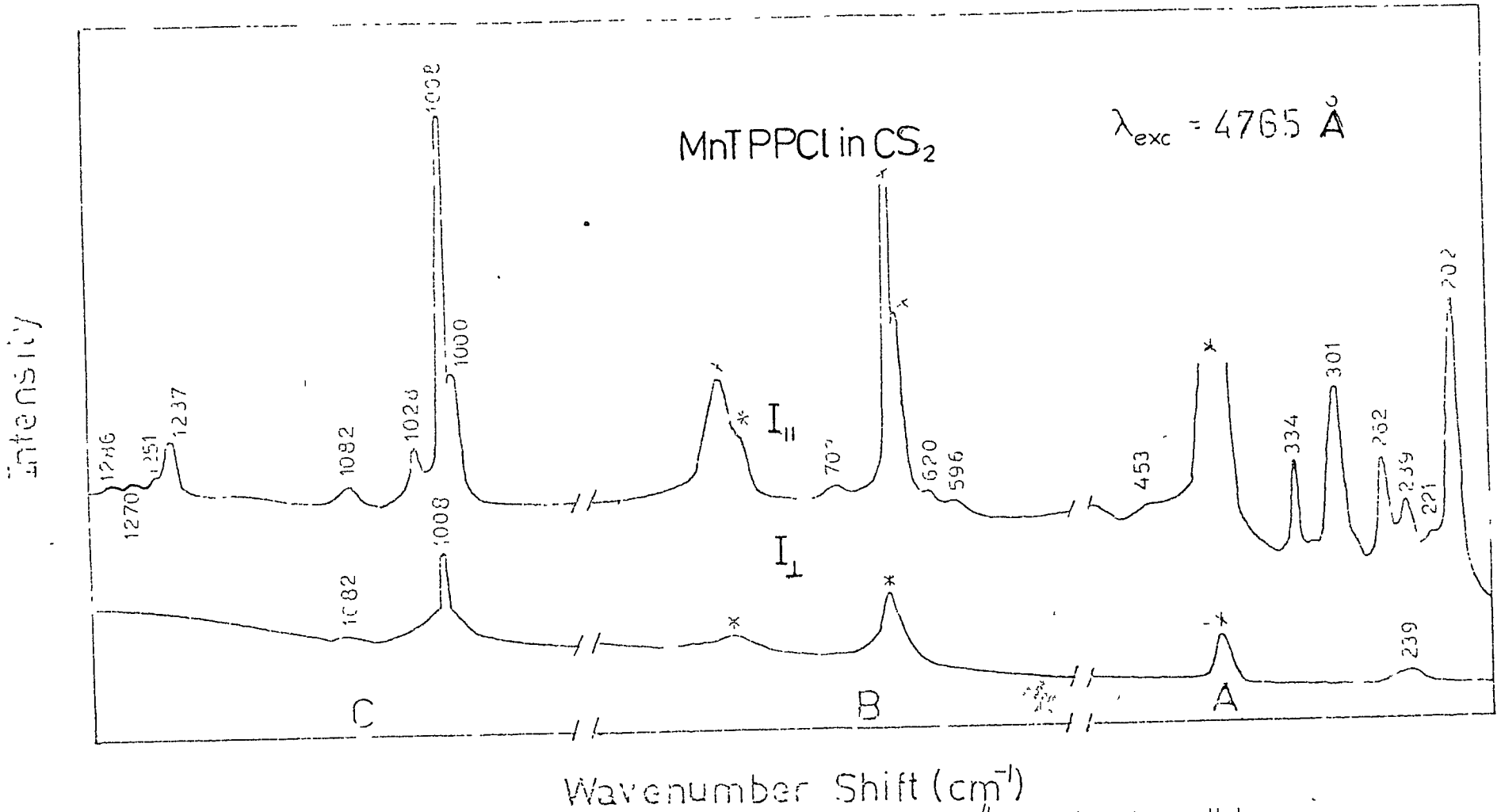

Fig.5.4a Resonance Raman spectra of Mn(III)TPPCl in CS_2 ($\sim 10^{-4}$M conc) with parallel (upper trace) and perpendicular (lower trace) components for λ_{ex}=4765Å. The breaks between different regions indicate difference in sclaes. The full scale count rates for part A for $I_{\parallel}$ and $I_{\perp}$ are 1.2K, 1.1 K respectively. Similarly, for part B, and C, they are 0.8K, 0.7K and 1.75K, 1 K respectively. Solvent peaks or bands which are interferred by solvents are indicated by '*'.

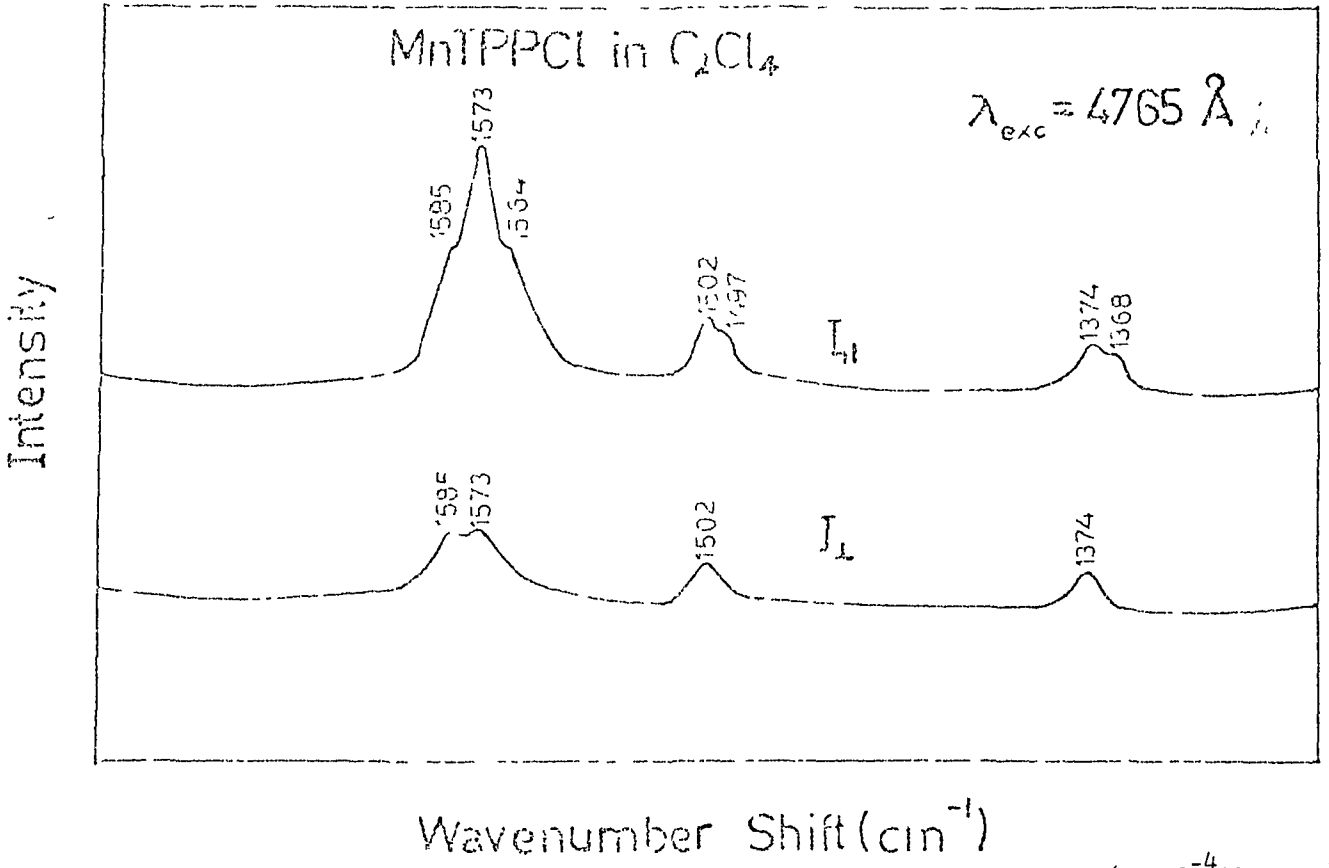

Fig.5.4b Resonance Raman spectra of Mn(III)TPPCl in C_2Cl_4 solution ($\sim 10^{-4}$M conc), with parallel and perpendicular components for λ_{ex}=4765Å.

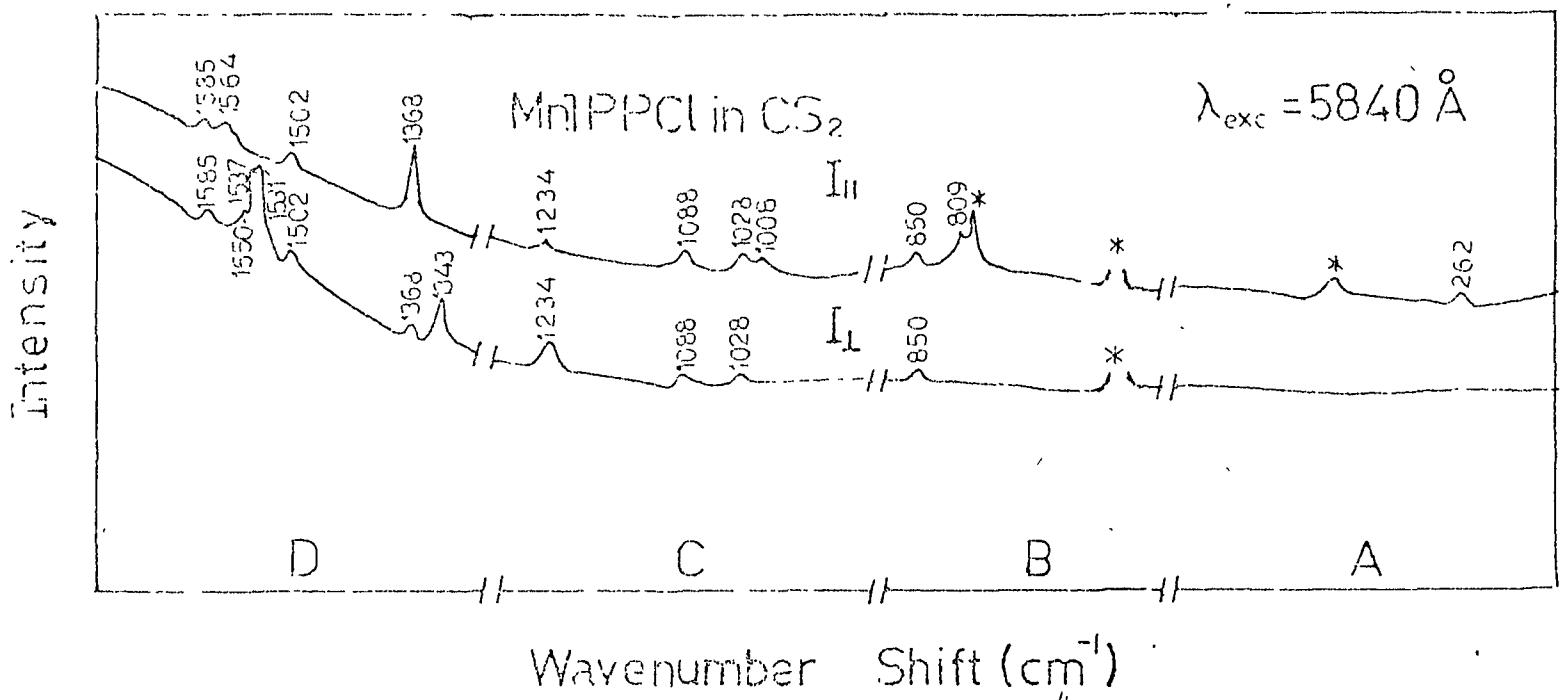

Fig.5.4c Resonance Raman spectra of Mn(III)TPPCl in CS_2 ($\sim 10^{-4}$M conc) with parallel (upper trace) and perpendicular (lower trace) components for λ_{ex}=5840Å. The breaks between different regions indicate difference in scales. The full scale count rates for part A for $I_{\parallel}$ and $I_{\perp}$ are 4.1 K and 4 K respectively. Similarly for part B, C and D they are 4.2K, 4K; 4.1K, 4K and 5.5K, 3K respectively. The solvent peaks and bands which are interferred by solvents are indicated by '*'.

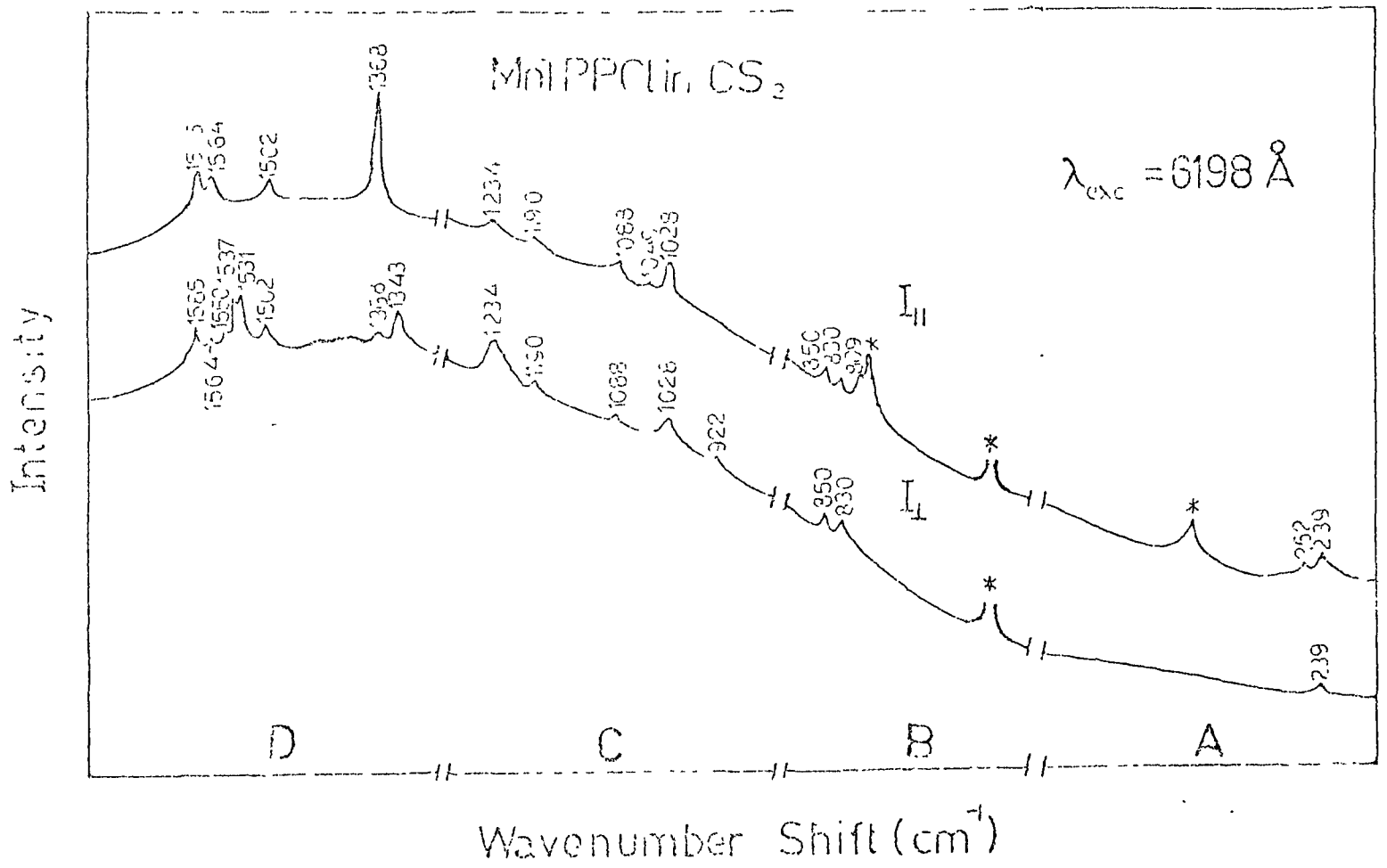

Fig.5.4d Resonance Raman spectra of Mn(III)TPPCl in CS_2 ($\sim 10^{-4}$M conc) with parallel (upper trace) and perpendicular components for λ_{exc}=6198Å. The breaks between different regions indicate difference in scales. The full scale count rates for part A, for $I_{\parallel}$ and $I_{\perp}$ are 3.1K and 3K respectively. Similarly for Part B, C and D they are 6K, 5.9K, 7K, 6K and 6.1K, 6K respectively. The solvent peaks and bands which are interferred by solvents are indicated by '*'.

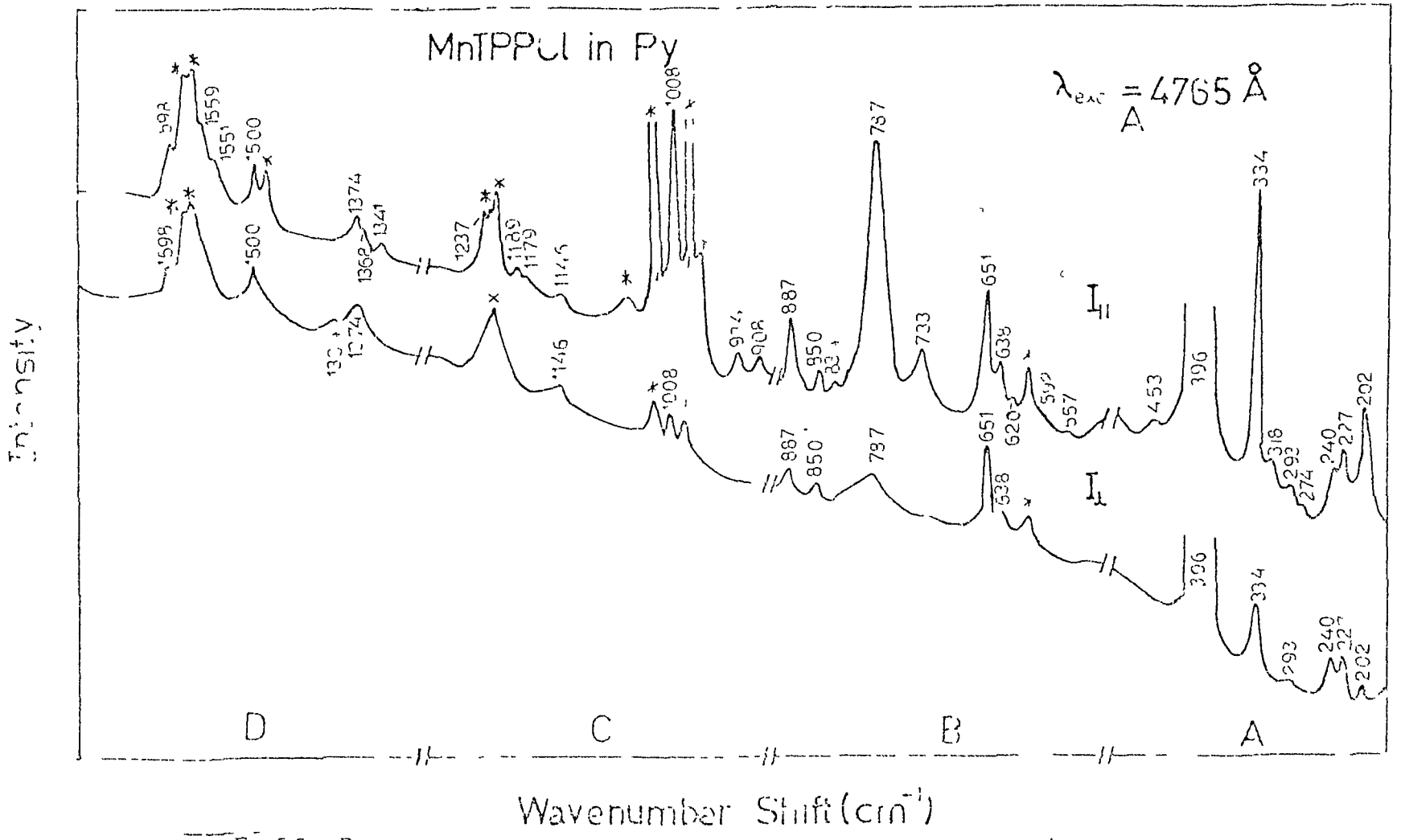

Fig.5.5 Resonance Raman spectra of Mn(III)TPPCl in Pyridine ($\sim 10^{-4}$M conc) with parallel (upper trace) and perpendicular (lower trace) components for λ_{exc} =4765Å The breaks between different regions indicate difference in scales. The full scale count rates for part A for $I_{\parallel}$ and $I_{\perp}$ are 4.5K and 2.5K respectively. Similarly for part B, C and D they are 2.2K, 2K, 4K, 3K and 4K and 3.1K respectively. The solvent peaks and bands which are interferred by solvents are indicated by '*'.

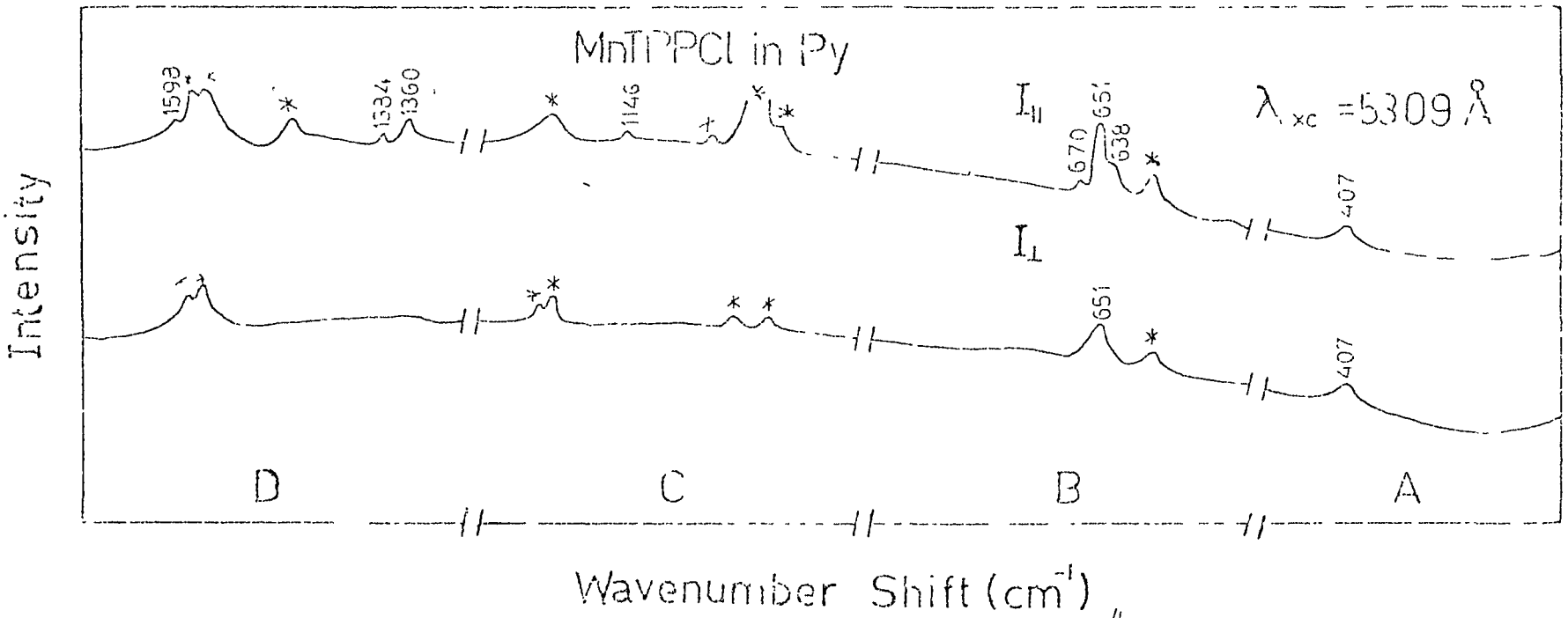

Fig.5.6 Resonance Raman spectra of Mn(III)TPPCl in Pyridine ($\sim 10^{-4}$M conc) with parallel (upper trace) and perpendicular (lower trace) components for λ_{ex}=5309Å. The breaks between different regions indicate difference in scales. The full scale count rates for part A for $I_{\parallel}$ and $I_{\perp}$ are 2.55K and 2.5K respectively. Similarly for part B, C and D they are 3.1K, 3K; 5K, 3.5K and 6K, 5K respectively. The solvent peaks and bands which are interferred by solvents are indicated by '*'.

RESONANCE RAMAN STUDIES OF MANGANESE(III) TETRAPHENYL-PORPHIN AND ITS OXYGEN-BRIDGED DIMER

ABSTRACT

Resonance Raman(RR) spectra are reported for Manganese (III) tetraphenylporphin chloride as well as for the oxygen-bridged dimer of Manganese(III) tetraphenylporphin using different excitation wavelengths encompassing the electronic absorption region. RR bands due to in plane porphyrin ring vibrations are assigned by analogy to those observed for the oxygen- and nitrogen-bridged Iron tetraphenylporphin dimers. As in the case for $(TPPFe)_2X[X=O,N,C]$ complexes, no evidence is found for dimer vibrational splittings, indicating thereby that the interaction between the two units is non-significant. The modes due to Mn-Cl stretching vibrations, Mn-O-Mn symmetric stretching vibrations(RR) and Mn-O-Mn asymmetric stretching vibrations(IR) have been assigned. From the observed RR data, we could not attribute any bands to phenyl group modes directly. A detailed and comparative study of the monomer and dimer is presented in this chapter.

6.1 Introduction

Manganese(III) porphyrin complexes have received much attention[1-3] because of their unique absorption spectra, indicative of an unusual electronic structure. As has been stated earlier in Chapter V, the atypical absorption spectra arises because of strong metal ligand interactions, thereby inducing distinct new features in the absorption spectra alongwith modification of the normal $\pi \rightarrow \pi^*$ spectra. However, the characterization of these bands are somewhat uncertain and needs further investigations. Resonance Raman spectroscopy has been shown to be a very sensitive probe for these systems and can yield information about the structure and conformations of the molecules.

In this chapter, we report the resonance Raman(RR) spectra of MnTPPCl and of oxygen-bridged Manganese tetraphenylporphin dimer ($O-(H_2OMnTPP)_2$). The significance of the structural and electronic properties of the aggregates of the metalloporphyrin molecule is obvious in elucidating the energy transduction mechanisms in various biological processes. Out of the many oligomeric metalloporphyrins known, axially bridged dimeric species are particuarly important as model systems for monitoring the interchromophore induced perturbations as they are generally very stable and rigid. The characterization of the dimers is therefore essential to clarify several aspects of biological chemistry. However, despite

the utility of RR spectroscopy for characterizing metalloporphyrin complexes, only few applications have been made to dimeric species.[4-7] RR studies of oxygen-,[4] nitrogen-,[5] and carbon-[6] bridged FeTPP dimer and of oxygen- and nitrogen-[7] bridged FeOEP dimer did not show any evidence for dimer vibrational splittings. In order to further investigate the question of intradimer coupling in axially bridged metalloporphyrin complexex, we have examined the RR spectra of oxygen-bridged Manganese tetraphenylporphin dimer. Resonance Raman spectra of monomer and dimer in KBr pellet as well as in different solvents have been obtained over a wide range of excitation wavelengths. We first present the results of RR data obtained with band V excitation and confirm its assignment. Next we consider the evidence for intradimer coupling between the two units of the molecule. We then consider the possibility of resonance enhancement of the phenyl modes. Finally, we discuss about the spin and oxidation states of the metal centre in the dimeric complex.

6.2 Experimental Results

The absorption spectra of MnTPPCl monomer and μ-oxo-bis tetraphenylporphinato MnTPP dimer in CS_2 solution have been shown in Fig. 6.1. The bands are labelled following Boucher.[1] Table 6.1 lists the corresponding absorption maxima. Although the two spectra are qualitatively similar, certain

differences are clearly evident. As can be seen from Fig. 6.1, the relative intensities of some bands differ for the dimeric complex as compared to the monomer; especially the relative intensities of bands III and IV change. Also, some bands shift to the higher energy side of the spectra. It is to be noted that similar spectral trend is observed in the absorption spectra of MnTPPCl in pyridine solution.

The Raman spectra of monomer and dimer in KBr pellet with the λ_{ex}=4416Å, 4765Å, 4880Å, 5145Å and 6116Å are shown in Figs. 6.2, 6.3, 6.4, 6.5 and 6.6 respectively. The corresponding Raman data is presented in Table 6.2. Raman spectra of both monomer and dimer in CS_2 and C_2Cl_4 solution with λ_{ex}=4765Å have also been obtained and shown in Fig. 6.7 (6.7a, 6.7b and 6.7c) respectively. As can be seen from Figs. 6.2 to 6.6 and 6.7 that the enhanced low frequency Raman spectra is obtained mainly with band V excitation, although λ_{ex}=4416Å also enhances these modes with relatively weaker intensities. Previous study has revealed that the low frequency spectra contain mainly metal related modes. Comparisons of the monomer and dimer spectra also provides convincing support to this assignment. Considering the phenyl rings as point masses, MnTPPCl has C_{4v} molecular symmetry, the metal being out of the porphyrin mean plane, along the axial chloride ion. On the formation of dimer, the axially bound chloride ion is replaced; Manganese is attached to oxygen of the oxygen-bridged

dimeric species. The other axial coordination is filled by water molecules. This should shift the position of the Mn ion with respect to the mean porphyrin plane which in turn should affect the metal related vibrations, mainly. Excitation at ~ 476.5 nm absorption indeed shows many distinct changes in the low frequency RR spectra of dimer. A medium intensity band at 260 cm^{-1} (in pellet), which is observed in the spectra of monomer, disappears completely in the spectra of dimer. This together with the fact that similar effect was observed when the spectra were obained in pyridine solution led us to conclude definitely, that this corresponds to Mn-Cl stretching vibration. The assignment of the bands related to metal-axial ligand vibration is of special interest because the bonds to the central metal ion are directly affected by the chemical changes at the haeme group. The intensity pattern of the bands also changes drastically in the low frequency region. However, the intensity pattern of the bands in the higher frequency region show similar pattern. This is qualitatively in accord with the RR data of MnTPPCl in pyridine solution.

Excitation in the visible region absorption enhances mainly the higher frequency vibrations including many non-totally symmetric modes. RR data obtained with λ_{ex}=5309Å also show enhancement of mainly the macrocyclic vibrational modes, which are totally symmetric.

Comparison of the RR spectra of both the complexes do not reveal any substantial shift in the relative band positions but distinct changes in the relative intensity pattern is observed. Moreover, a new feature at 325 cm^{-1} appears in the RR spectra of dimer with λ_{ex}=4416Å, which does not appear in the RR spectra of monomer. The IR spectra of both the samples have also been recorded and shows a distinct new feature at 879 cm^{-1} for the dimer molecule (Fig. 6.8). The genral experimental details and methods of preparation of samples have been given in Chapter III.

6.3 Discussion

For metalloporphyrins with typical electronic spectra, the visible and near ultraviolet absorption spectra derive from two $\pi \rightarrow \pi^*$ porphyrin electronic transitions. Under D_{4h} symmetry, these transitions are both of E_u symmetry and undergo strong configuration interactions. The transition dipoles add for the higher energy transition, i.e., Soret band, and nearly cancel for the lower energy transition giving rise to the Q band. The latter is split into two vibronic components which are designated as α and β. As is known, the absorption spectra of Mn(III)porphyrin complex display a complex electronic absorption spectrum which is atypical of the metalloporphyrins. Our study on Mn(III)TPPCl reported in previous chapter indicates that the strong absorption band V is of predominantly charge

transfer character, while bands III and IV are of $\pi \rightarrow \pi^*$ origin. The weak absorption at ~ 530 nm has been identified to arise from singlet-triplet(π, π^*) transition.

The enhancement of resonance Raman intensity occur either via A-type term or by B-type term of Albrecht[8] (c.f. chapter II).The A-type term should contribute the macrocyclic modes to the Raman spectra, when excitation occurs in a $\pi \rightarrow \pi^*$ transition region, while excitation in a charge transfer region should contribute both the metal related modes as well as macrocyclic modes, via A-type term. The B-type term results from the vibrationally induced mixing of different electronic states produced by perturbation by the vibrational modes. The vibrtional mode which is most active in mixing the states will show the greatest Raman activity. Thus it can be shown that, when two excited states both obtained by $\pi \rightarrow \pi^*$ transitions are mixed, vibrations active in the macrocycle will show maximum enhancement. Similarly, when vibrational coupling occurs between an excited charge transfer state in which an electron goes to a d_{yz} or d_{xz} metal orbital with an excited state reached by a $\pi \rightarrow \pi^*$ transitions from the same occupied molecular orbital, then the vibrational modes which will be enhanced will be those around the central metal. On the other hand, when two different charge transfer states which arise from the same porphyrin ground state molecular orbital but ends in different metal d orbital are coupled,

the vibrations corresponding to metal-axial ligand and some metal related vibrations should be picked out. It is to be noted that as itself, this term is small since the two different d orbidals occupy different regions of space, unless axial ligand vibrations and the constraints imposed by the pyrrole nitrogens mix the d orbitals. Similarly when coupling occurs between two charge transfer states which are initiated from different porphyrin orbitals but ends in same d orbitals, the vibrations active in the macrocycle will show intensity enhancement.

It has been observed that excitation within band V absorption mainly enhances the metal related modes. This is to be expected for charge transfer character of band V and hence band V is assigned to a charge transfer band. Also, enhancement of totally and non-totally symmetric modes with band III and IV excitations supports the idea that they correspond to α and β bands of normal porphyrins. We could not obtain RR data in solution at ~ 530 nm absorption, may be because the absorption is too weak in this region. However, the spectrum obtained in KBr pellet, shows the presence of some macrocycle vibrations only and hence adds further confirmation to its assignment of (π,π*) origin. The absorption spectra of dimer, although varies from monomer, there is no direct evidence for which these differences have to be correlated to intradimer interactions. For example, the absorption bands did not show

any splittings, nor their widths differ from the corresponding bands of the monomer. This, together with the fact that similar spectral trend was observed in the absorption spectra of MnTPPCl in pyridine solution suggests that the changes can be associated to axial-ligation effect. The change in relative intensities of bands III and IV can then be correlated in the following way. The replacement of chloride by other axial ligands in dimer, should alter the metal-nitrogen ligand strength. This should then affect the $a_{2u}(\pi)$ orbitals since it has electron density through the pyrrole nitrogens. Since the intensity of the α band depends considerably on the energy gap between the $a_{1u}(\pi)$ and $a_{2u}(\pi)$ orbitals, it is expected that this will influence considerably the intensity of the α band.

6.4 Mn-O-Mn Stretch

The additional band at 325 cm^{-1} observed in the RR spectra of dimer has been assigned to symmetric Mn-O-Mn stretching mode, while the extra band observed in the IR spectra at 879 cm^{-1} has been assigned to asymmetric Mn-O-Mn stretching mode. In this regard, the symmetric and asymmetric Fe-X-Fe stretching vibrations for $(TPPFe)_2O$, $(TPPFe)_2N$ and $(TPPFe)_2C$ complexes are observed at 363 cm^{-1}(RR), 885 cm^{-1}(IR)[4]; 424(RR), 910 cm^{-1}(IR)[5] and at 443 cm^{-1}(RR), 939 cm^{-1}(IR)[6] respectively. Unfortunately, the confirmation of the bands via isotopic

shift could not be done because of unavailability of Manganese isotope. The absence of the antisymmetric stretching vibration in the Raman spectra and absence of symmetric stretching vibration in the IR spectra, suggests that the molecule has centre of symmetry. This indicates that the molecule is linear along the Mn-O-Mn axis which is in agreement with the theoretical prediction.[9]

6.5 Intradimer Coupling

As long as the two monomeric units of the dimer do not interact significantly, the pair of vibrational modes originating from the two monomeric modes will remain degenerate. However, if the interaction energy between the monomeric units is comparable to the vibrational energy, then the degenerate modes should show a splitting into an in-phase and out-of-phase combination. For a centrosymmetric molecule, the in-phase combination should be active in Raman while the out-of-phase combination should be active in IR spectra. However, the present observation is not consistent with this situation outlined here. Comparison of RR spectra of monomer and dimer shows that the frequencies of the bands of dimer lie very close to the frequencies of the corresponding bands in monomer and no splitting is observed. This strongly suggests that intradimer coupling between the two units is extremely weak or non-existent, a result similar to that found for

the other similar systems.[4-7] Since the strength of interactions depend upon $1/R^3$, where R is the distance between the two monomeric units, it is possible that the absence of intradimer coupling is due to large separation of the two TPP units. One final point can be made with the data at hand. It must be remembered that in RR spectra while the frequencies are determined by the ground electronic properties, intensities are mainly determined by the properties of the excited electronic states. Since the corresponding Raman frequencies are essentially coincident in both complexes, it is implied that the ground electronic state is minimally perturbed while the change in relative intensities of different bands indicate that the excited electronic states are perturbed on aggregation. The shift in some absorption maxima must also be a property of excited states.

6.6 Other Modes Observed

Certain Raman bands in the FeTPP systems have been previously implicated as arising from phenyl group vibrational modes. Phenyl groups are known to be oriented out of the mean porphyrin plane in the ground electronic state. As discussed in chapter V, the conjugation of phenyl groups with the macrocycle and enhancement of phenyl modes in the RR spectra has been attributed to an excited state interactions. The bands at 995 cm^{-1}(p), 1030 cm^{-1}(p) and 1599 cm^{-1}(p) were attributed to phenyl vibrational modes in the RR spectra

of $(FeTPP)_2O$.Bands at similar positions at 997 cm^{-1}, 1029cm^{-1} and 1598 cm^{-1} have also been observed in MnTPP systems. Following the previous arguments, the maximum enhancement for these bands are expected during the Q state excitation. On the other hand, for both monomer and dimer, the band at 997 cm^{-1} is hardly detectable with visible region excitation, while it becomes more stronger with higher energy excitations. This is in contrast with the previous suggestion. The band around 1029 cm^{-1}(p) has also been attributed to a phenyl group mode, these bands are indeed resonance enhanced with visible region excitation. Depolarization ratio measurement for this band with visible region excitation reveals it to be a depolarized mode. Although there are two close by features present in this region and it may be difficult to resolve them from the measured value of depolarization ratio (for monomer) it seems highly unlikely to correlate this band to a phenyl ring vibrational mode. Similarly, the band at 1598 cm^{-1} is observed with both λ_{ex}=4416Å and 6282Å excitations in monomer. However, this band is seen with 4416Å, 4880Å and 5145Å excitations in dimer and is not observed with the visible region excitation and therefore do not support the assignment. We suggest those bands are also characteristic macrocycle vibrational modes and vary in intensity depending on the exciting frequency used. Further, it has also been seen that bands at similar positions are observed in the

resonance Raman spectra of non-phenyl metalloporphyrins.[2,10,11] Therefore our data do not agree with the idea of conjugation of the phenyl rings either in the ground or in the excited state and this contention is supported by the similar sutides[12] on meso-formyl and meso-nitro substituted Ni(II)-octaethyl-porphin[12] which also do not indicate any π conjugation between the meso-substituents and porphyrin π system.

6.7 Spin and Oxidation States Of The Metal Centre

RR bands sensitive to the spin and oxidation states of the Fe ion in $(TPPFe)_2N$ are observed[5] at 1567 cm^{-1}(p), 1538 cm^{-1}(ap), 1367 cm^{-1}(p) and 1374 cm^{-1}(dp) which are shifted to 1553 cm^{-1}, 1511 cm^{-1}, 1359 cm^{-1} and at 1368 cm^{-1} in the RR spectrum of high spin $O-(TPPFe)_2$ complex. This data clearly reflect low spin character for Fe ion in $(TPPFe)_2N$. The analogous bands corresponding to those at 1567 cm^{-1}, 1538 cm^{-1}, 1367 cm^{-1} and 1374 cm^{-1} are observed at 1564 cm^{-1} for monomer and 1562 cm^{-1} for dimer, 1530/1537 cm^{-1} for monomer and dimer 1367 cm^{-1} for monomer and 1365 cm^{-1} for dimer and 1373 cm^{-1} for monomer and dimer in the RR spectra of monomer and dimer. It is quite reasonable to assume that if the spin and oxidation states of the metal change these bands should show a shift. An examination of the RR spectra of MnTPPCl in pyridine and of $O-(H_2OMnTPP)_2$ dimer do not show any substantial shift of these bands. This indicate that even in dimer, Manganese

remains as high spin d^4 system.

6.8 Conclusions

The RR data obtained with band V excitation is indicative of charge transfer character of this band. Comparison of RR spectra of MnTPPCl and O-$(H_2OMnTPP)_2$ shows that perturbations induced in the porphyrin π electronic structure by dimer formation are negligible. There is no evidence of phenyl ring conjugation either in the ground or excited electronic state. Also, the spin and oxidation states of the metal do not change upon the formation of dimer.

REFERENCES

1. L.J. Boucher, Coord. Chem. Rev. **7**, 289(1972).

2. S.Asher and K. Sauer, J. Chem. Phys. **64**, 4115(1976).

3. J.A. Shelnutt, D.C. O'shea, N.-T. Yu, L.D. Cheung and R.H. Felton, J. Chem. Phys. **64**, 1156(1976).

4. J.M. Burke, J.R. Kincaid and T.G. Spiro, J. Am. Chem. Soc. **100**, 6077(1978).

5. G.A. Schick and D.F. Bocian, J. Am. Chem. Soc. **105**, 1830(1983).

6. J.A. Hofmann and D.F. Bocian, Inorg. Chem. **23**, 1177(1984).

7. J.A. Hofmann and D.F. Bocian, J. Phys. Chem. **88**, 1472(1984).

8. A.C. Albrecht, J. Chem. Phys. **34**, 1476(1961).

9. K. Tatsumi and R. Hoffmann, J. Am. Chem. Soc. **103**, 3328(1981).

10. R. Mendelsohn, S. Sunder, A.L. Verma and H.J. Bernstein, J. Chem. Phys. **62**, 37(1975).

11. A.L. Verma and H.J. Bernstein, J. Chem. Phys. **61**, 2560(1974).

12. T.M. Ivanova and V.V. Berdyugin, J. Mol. Struct. **117**, 287(1984).

TABLE 6.1 Absorption Maxima (nm) of Manganese Tetraphenylporphin Chloride and of Oxygen-Bridged Manganese Tetraphenylporphin Dimer in CS_2 ($\sim 10^{-5}$M Concentration).

MnTPPCl	O-$(H_2OMnTPP)_2$
755	
698	700
675	665
620	613
583	578
530	525
476	473
400	400
380	375

TABLE 6.2 Resonance Raman Bands (cm^{-1}) of MnTPPCl and O-$(H_2OMnTPP)_2$ in KBr Pellet with Different Excitation Wavelengths.

MnTPPCl							O-$(H_2OMnTPP)_2$							
4416Å	4765Å	4880Å	5145Å	5309Å	5831Å	6116Å	4416Å	4765Å	4880Å	5145Å	5309Å	5831Å	6116Å	Assignment
199m	199wm	199wm	199w				201wm	201m	201wm					
	217w	217wm	217w					218m	218wm					$\delta(Mn-N_4)$
							232w,br							
238w,vbr	238wm	238m	238vw,br			238wm		238m	238wm					
	260wm	260w												$\nu(Mn-Cl)$
	278wm	278ms	278vw					278m	278ms					
	298vw	298vw						295vw	295vw					$\delta(Mn-N_4)$
313vw	313w	313vw						317 vw						
							325sh							$\nu(Mn-O-Mn)$
334w	334wm	334wm	334w				334w	334ms	334m	334w				
					358vw,br									
381s							380m							
392s	392vs	392vs	392m	392vw	392w	392wm	392m	392vs	392vs	392w			392wm	
406w,sh		406sh	406w		406w		406sh			406sh				
436w							436 w							
450vw	450vw,br								456					
		517vw					517vw	517vw						
		552vw						550vw	550w,br					
564w		564sh												
							572w,br							
		594sh												
		607vw							607w					
637m	637wm	637w	637vw				637m	637wm	637wm					
659w							659vw							
673w		673w					671vw	671w	671w,br					
703vw		703vw					703vw							

Table contd..

Table 6.2 contd..

MnTPPCl							O-(H_2OMnTPP)$_2$							
4416Å	4765Å	4880Å	5145Å	5309Å	5831Å	6116Å	4416Å	4765Å	4880Å	5145Å	5309Å	5831Å	6116Å	Assignment
		715vw						714w						
724vw							726vw	726w,br	726w,br					
		736w							736sh					
746vw							746vw							
762vw							762vw							
787w	787wm	787wm					790w	790ms	790m					
800vw,sh		800sh					800sh	800sh	800sh					
830vw		830vw			830wm	830wm	830vw	830vw	830vw	830w		830w	830w	
850w	850w	850wm	850w	850w	850wm	850wm	850w	850w	850wm	850w		850vw	850w	
869vw,sh		869vw	869vw			869vw								
887m	887w	887w				887w	885m	885wm	885wm					
997m	997wm	997m	997vw	997wm	997vw		997m	997m	997wm					
1007m	1007s	1007vs	1007m	1007m	1007w	1007w	1005ms	1005vs	1005s	1005m		1005w		ν(C$_\alpha$-C$_m$)
										1014sh			1014w	
1024w	1024w	1024wm	1024wm	1024m					1024wm					
1029w	1029w	1029wm			1029m	1029m	1029vw	1029m	1029wm			1029w	1029w	
1045vw			1045vw	1045vw		1045w								
									1063w	1063w		1063vw		
				1070w										
1080wm	1080w	1080w	1080w	1080wm			1077w			1077vw				δ(C$_\beta$-H)
		1084w	1084w	1084w	1084w,br	1084w,br		1086w	1086vw	1086vw		1086vw	1086w,br	δ(C$_\beta$-H)
		1120vw												
				1132w										
											1151wm			
										1175vw				
		1188vw	1188w	1188m		1188w				1188w				
										1214w				
1233m	1233wm	1233wm	1233m,br	1233wm,br	1233ms,br	1233 ms,br	1235s	1235wm	1235wm	1235w		1235vw	1235w,br	ν(C$_\alpha$-N)+ δ(C$_\beta^\alpha$-H)/ ν(C$_m^\beta$-Ph)

Table contd..

Table 6.2 contd..

MnTPPCl							O-(H_2OMnTPP)$_2$							
4416Å	4765Å	4880Å	5145Å	5309Å	5831Å	6116Å	4416Å	4765Å	4880Å	5145Å	5309Å	5831Å	6116Å	Assignment
				1246vw										
		1265w	1265wm	1265wm		1265w				1265wm,br				
	1278w,br	1278w	1278sh	1278w	1278w	1278w		1278vw	1278vw,br					
					1292w							1286wm		
					1314w					1317w		1317w		
1343m		1343vw	1343w		1343ms	1343m	1341m		1341vw	1341w			1341w	$\nu(C_\alpha-C_\beta)+\delta(C_\beta-H)$
1354vw							1354sh							
1367m		1367sh	1367sh	1367s	1367s	1367s	1365w	1365sh			1365m		1365m	$\nu(C_\alpha-N)+\delta(C_\beta-H)$
1373wm,br	1373wm	1373m	1373ms	1373m,sh		1373sh		1373wm	1373wm	1373w				
	1397vw									1393vw				
							1404vw		1404vw					
										1441vw				$\nu(C_\alpha - C_\beta)$
1452sh				1452vw,br										$+\delta(C_\beta-H)$
1458wm							1458m,br	1458vw	1458w	1458w			1458m,br	
1486w,sh							1486w							
										1494w				
1500m	1500m	1500m	1500s	1500m	1500m	1500ms	1500w	1500wm	1500wm	1500w	1500wm		1500w	$\nu(C_\beta-C_\beta)$
				1526vw										
1530wm				1530vw	1530s	1530ms	1530w							$\nu(C_\alpha-C_m)$
1537w	1537vw		1537vw		1537s	1537ms			1537vw				1537w	
				1551vw										
1558s	1558w,vbr						1556s							
1564sh		1564sh	1564m	1564w	1564w	1564w		1562wm	1562sh	1562m			1562wm	
		1574sh	1574sh	1574m,sh	1574w,sh				1572w		1572sh			
1583m	1583m	1583s	1583vs	1583s	1583m	1583s		1583m	1583m	1583m	1583m		1583m	
1598w							1598w		1598w	1598w				
1628vw							1628vw,br							

Abbreviations: s=strong; m=medium; w=weak; v=very; br=broad; sh=shoulder.

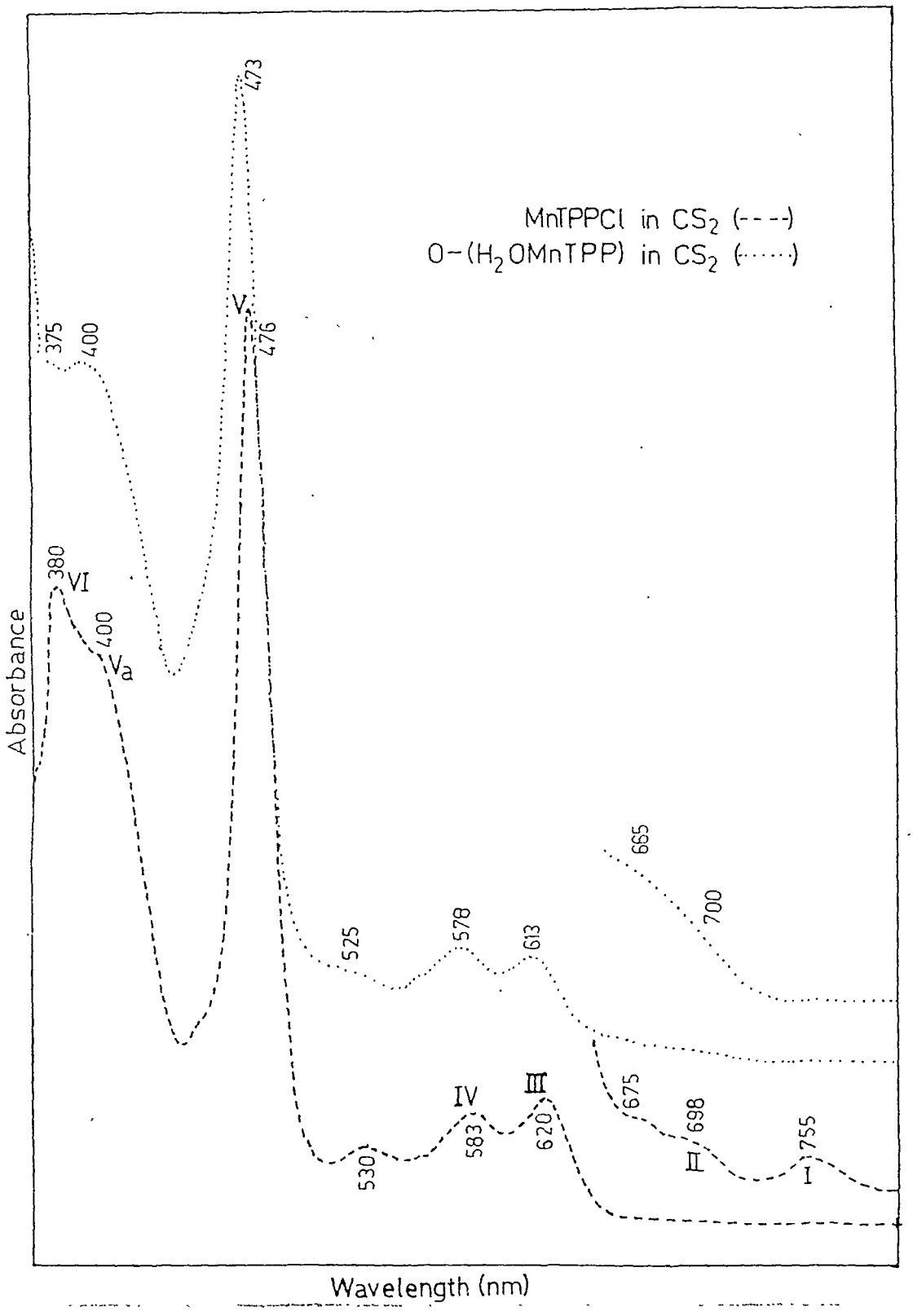

Fig.6.1 Absorption spectra of MnTPPCl and O-(H_2OMnTPP)$_2$ in CS_2 solution ($\sim 10^{-5}$ M concentration).

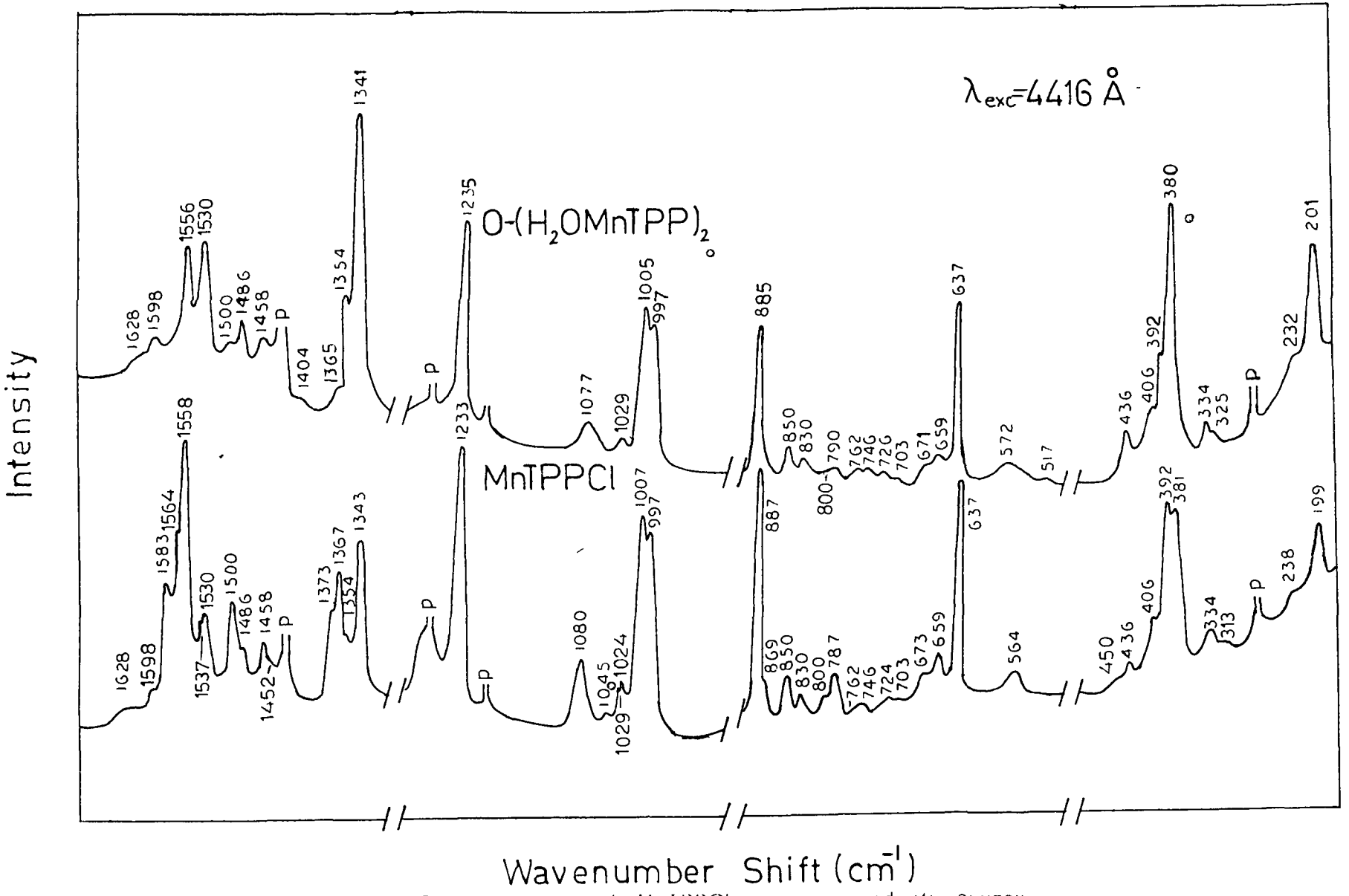

Fig.6.2 Resonance Raman spectra of MnTPPCl monomer and its oxygen bridged dimer in KBr pellet with λ_{ex}=4416Å. The breaks between different indicate difference in scales.

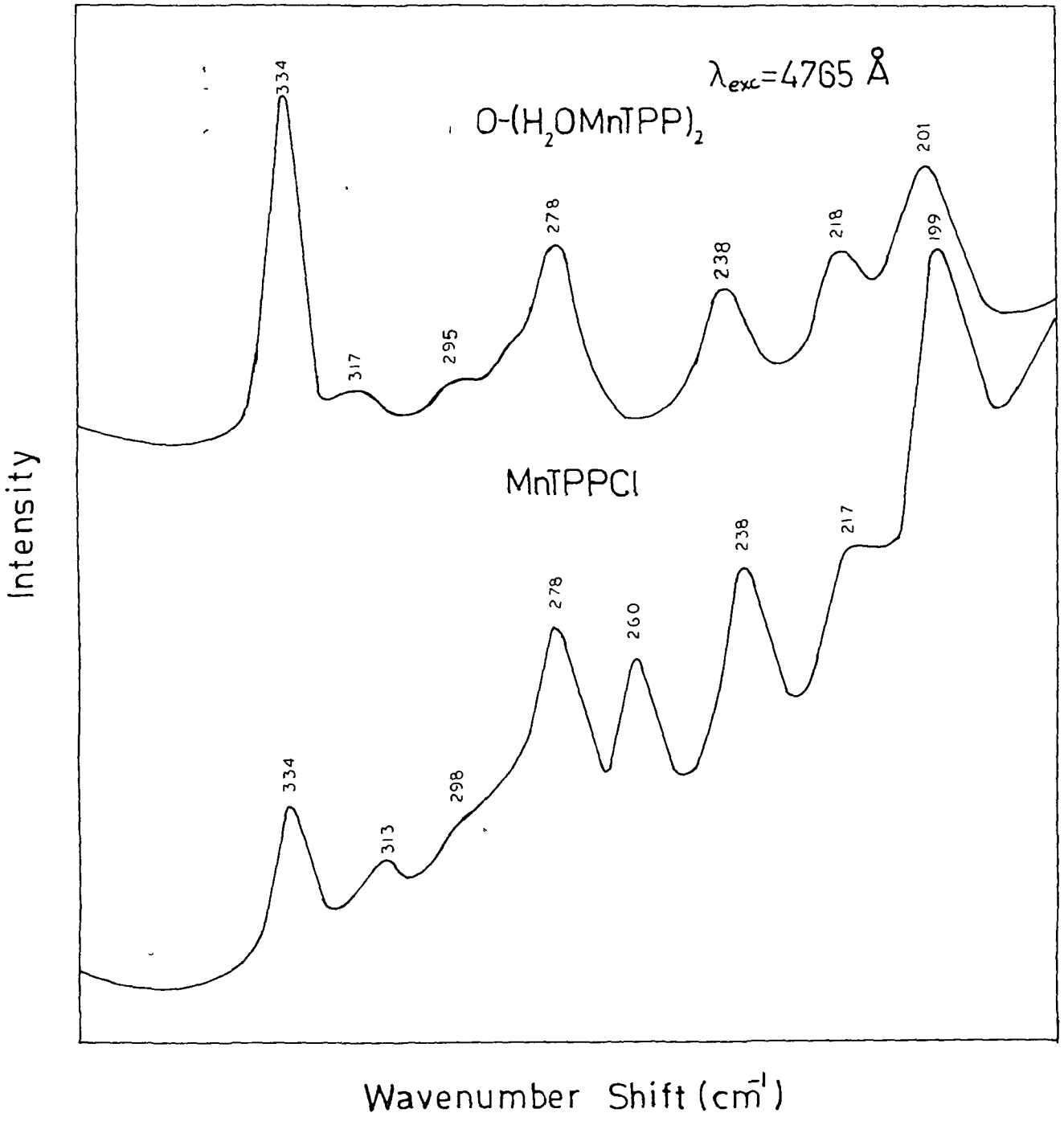

Fig.6.3 Resonance Raman spectra of $MnTPPCl_2$ monomer and its oxygen bridged dimer in KBr pellet with λ_{ex}=4765Å.

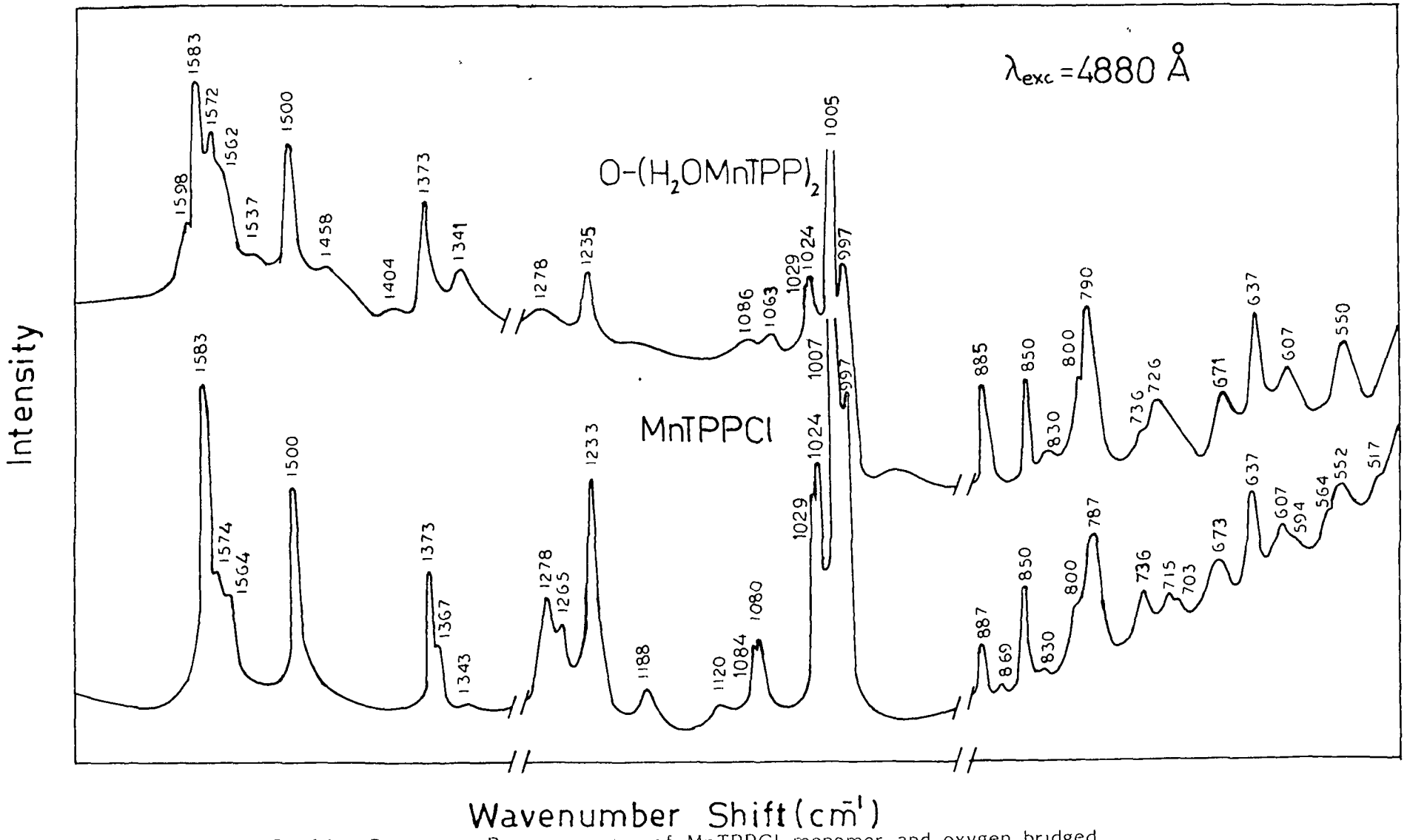

Fig.6.4 Resonance Raman spectra of MnTPPCl monomer and oxygen bridged dimer in KBr pellet with λ_{ex}=4880Å. The breaks between different regions indicate difference in scales .

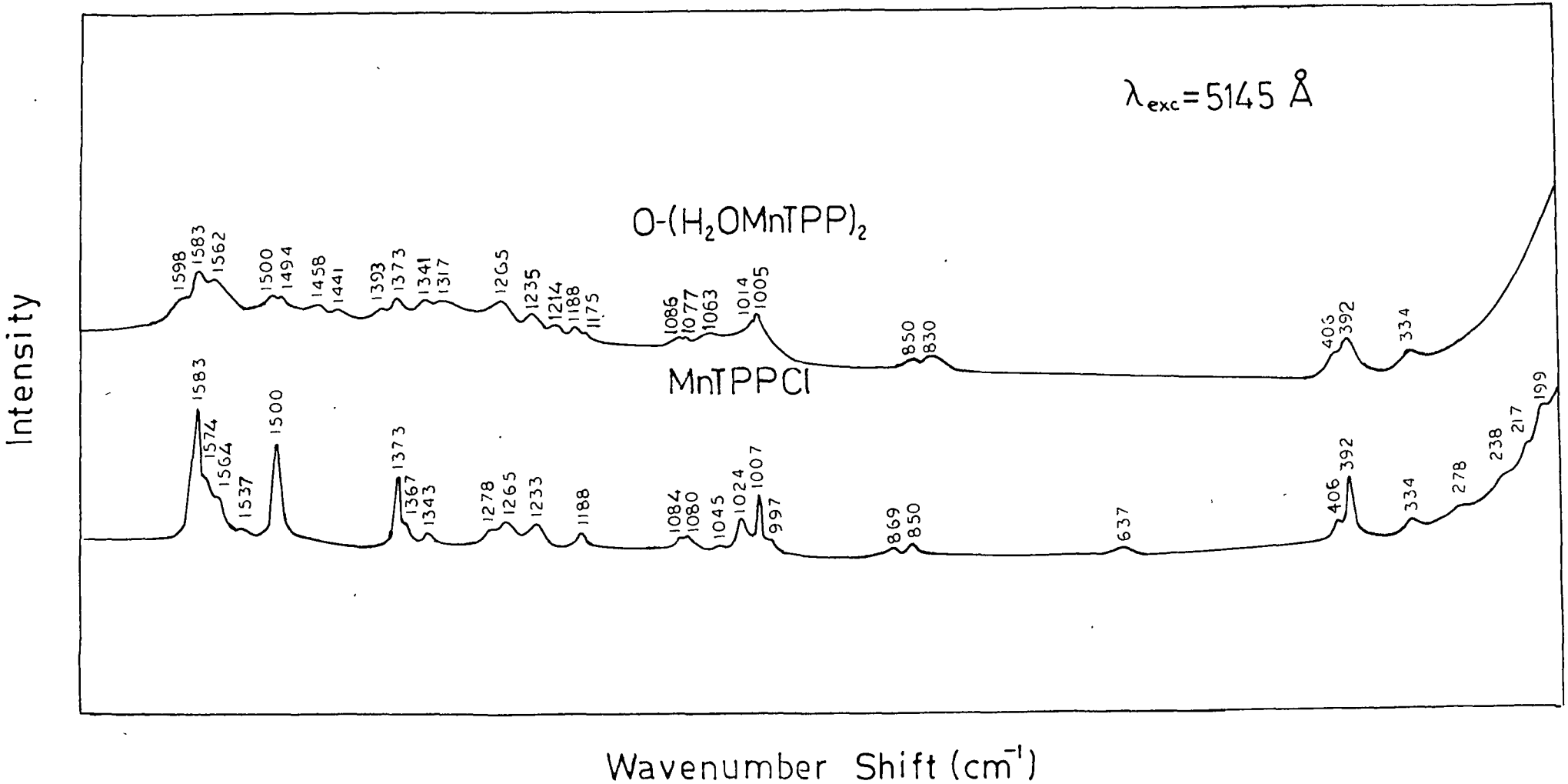

Fig.6.5 Resonance Raman spectra of MnTPPCl monomer and its oxygen bridged dimer in KBr pellet with λ_{ex}=5145Å.

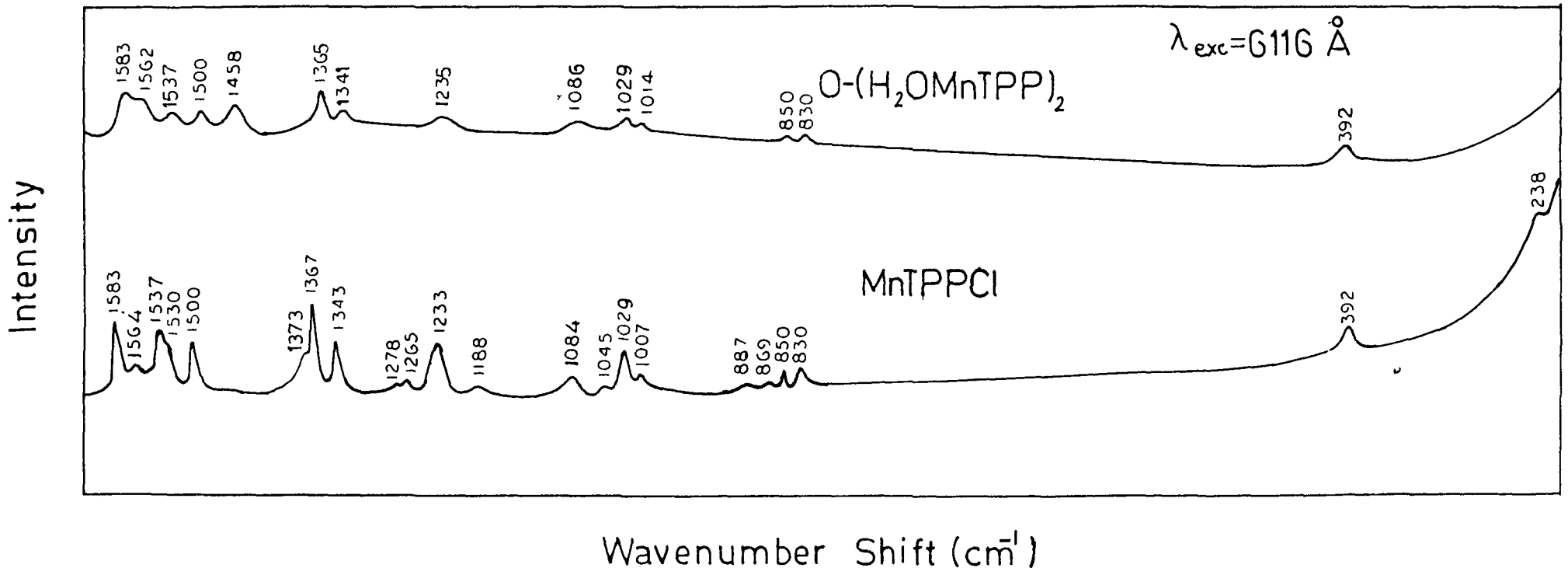

Fig.6.6 Resonance Raman spectra of MnTPPCl monomer and its oxygen-bridged dimer in KBr pellet with λ_{ex}=6116Å.

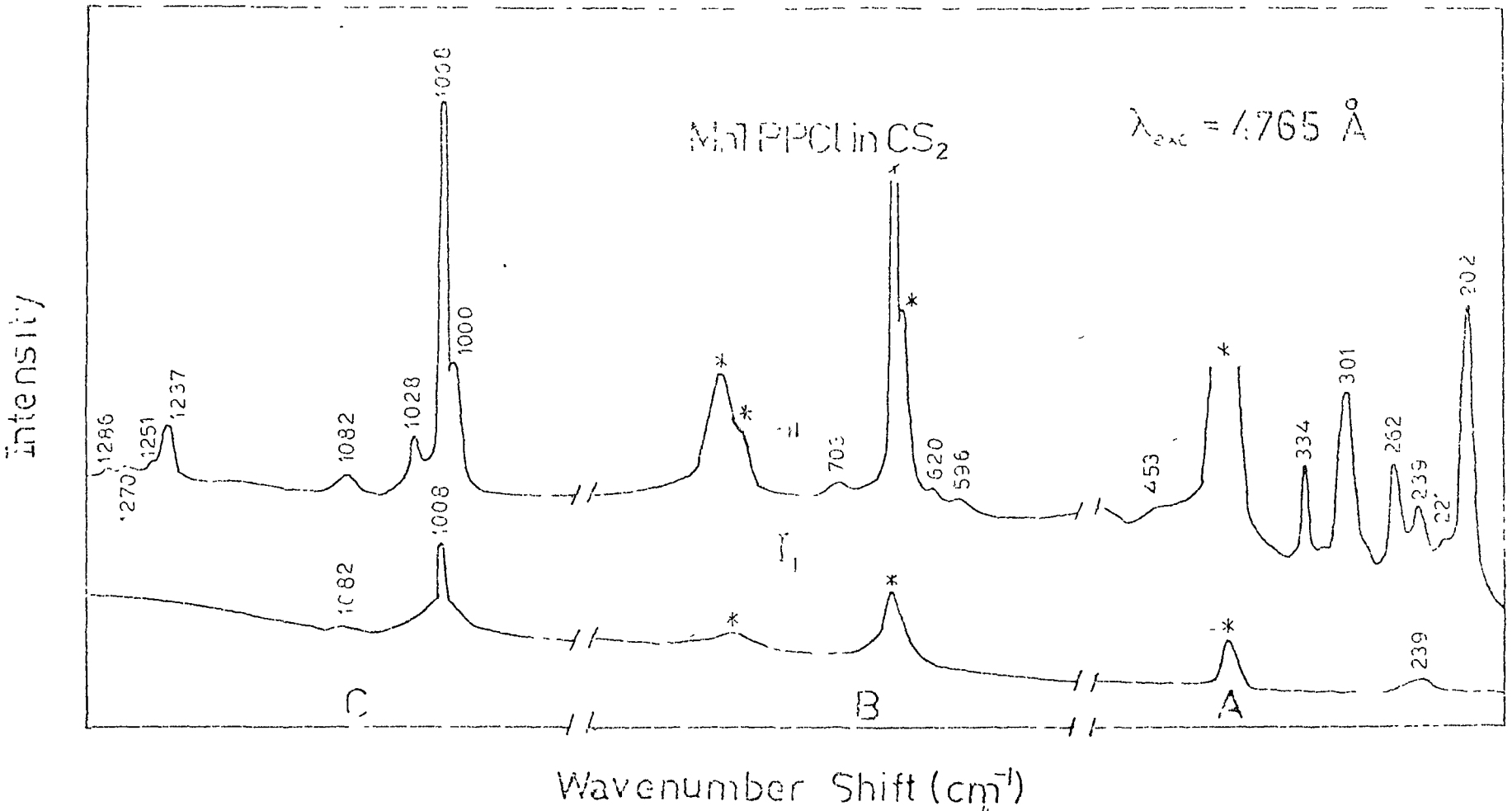

Fig.6.7a Resonance Raman spectra of Mn(III)TPPCl in CS_2 ($\sim 10^{-4}$M conc) with parallel (upper trace) and perpendicular (lower trace) components for λ_{ex}=4765Å. The breaks between different regions indicate difference in sclaes. The full scale count rates for part A for $I_\parallel$ and $I_\perp$ are 1.2K, 1.1 K respectively. Similarly, for part B, and C, they are 0.8K, 0.7K and 1.75K, 1 K respectively. Solvent peaks or bands which are interferred by solvents are indicated by '*'.

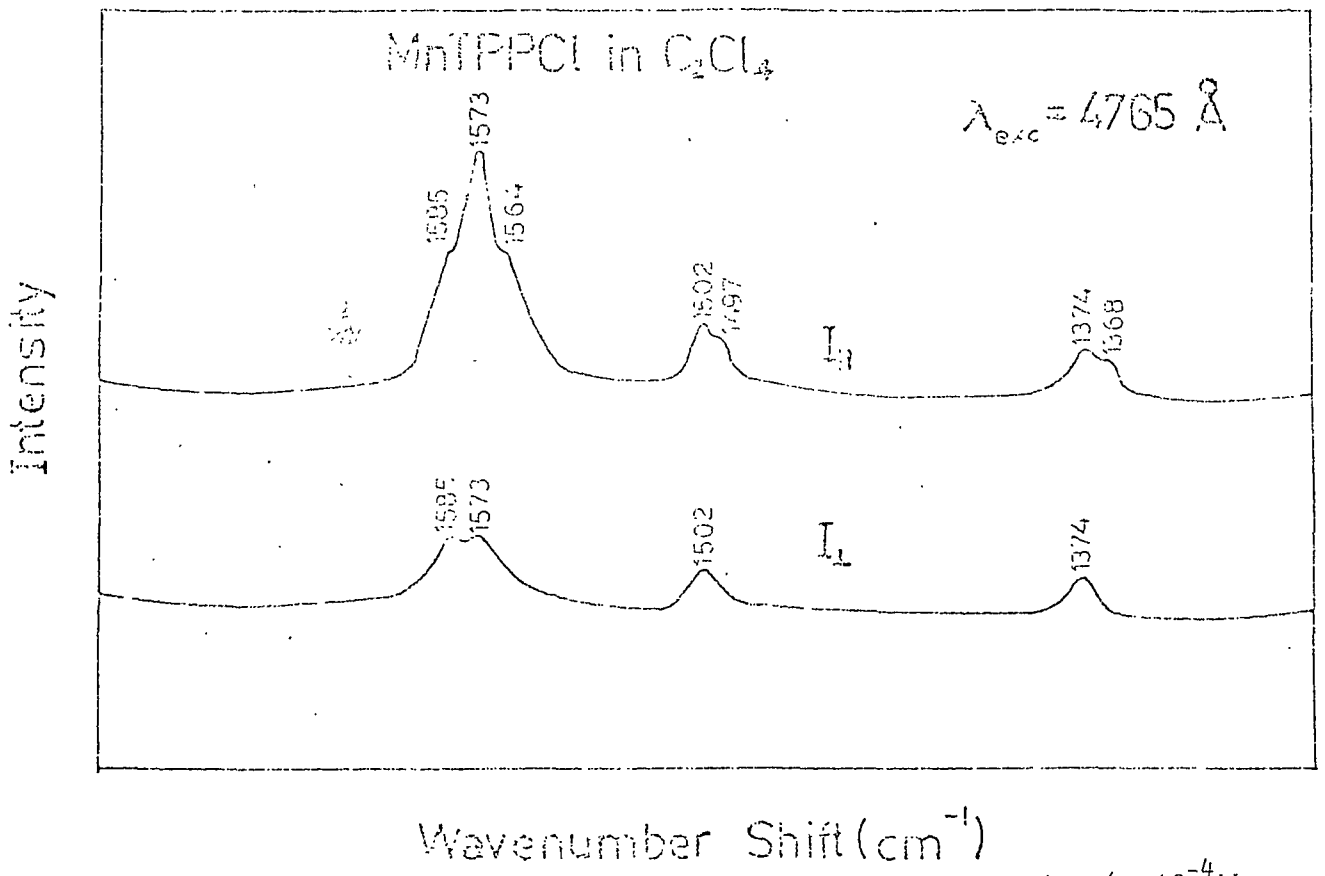

Fig.6.7b Resonance Raman spectra of Mn(III)TPPCl in C_2Cl_4 solution ($\sim 10^{-4}$M conc), with parallel and perpendicular components for λ_{ex}=4765Å.

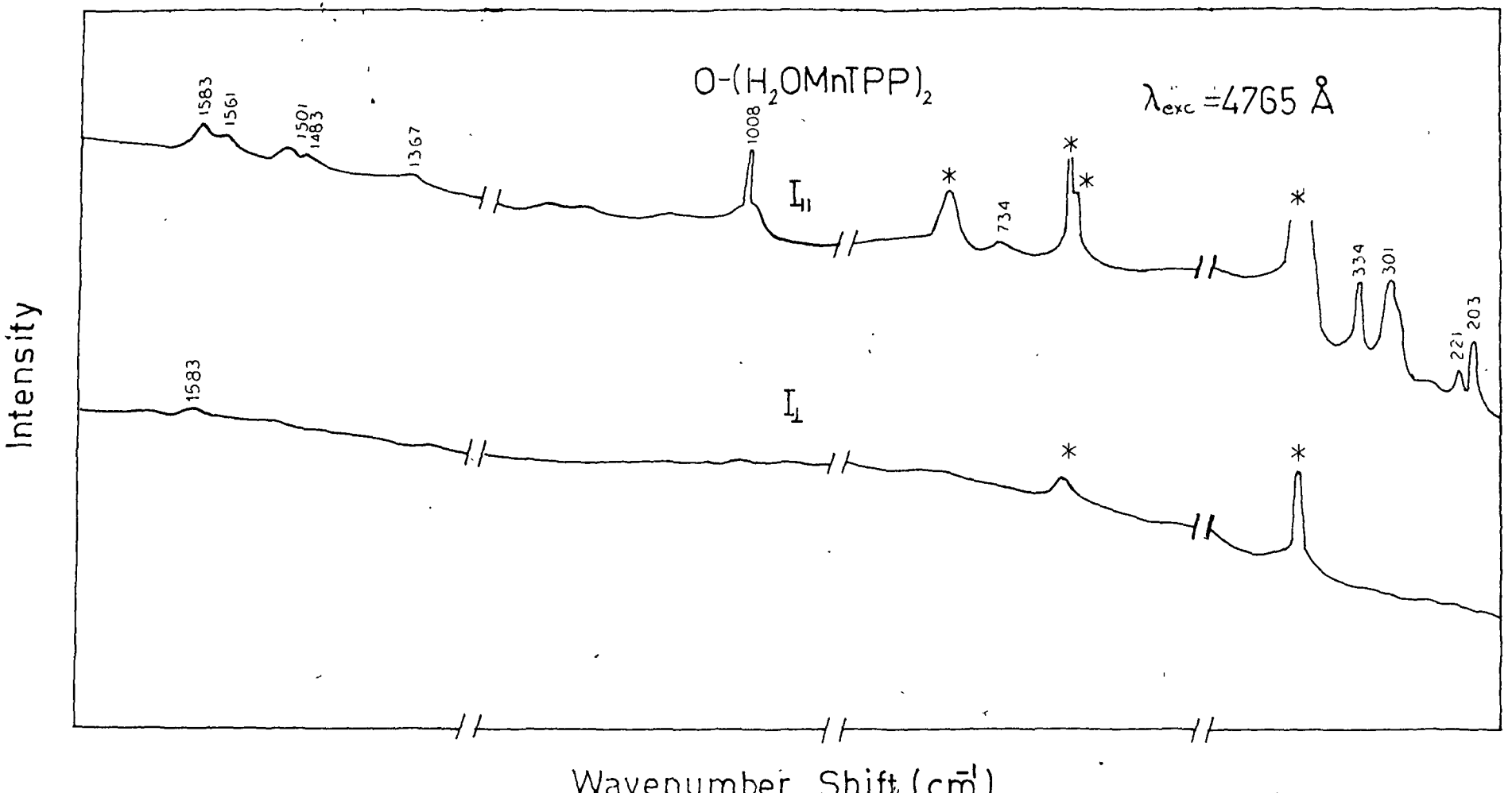

Fig.6.7c Resonance Raman spectra of O-$(H_2OMnTPP)_2$ in CS_2 ($\sim 10^{-}$ M conc) with parallel (upper trace) and perpendicular (lower trce) components for λ_{ex}=4765Å. The breaks between different regions indicate difference in full scales. The full scale count rates for part A for $I_{\parallel}$ and $I_{\perp}$ are 1K and 0.8K respectively. Similarly for part B, C and D they are 1.5K, 0.5K; 1K, 0.9K and 1.5K, 1.3K respectively. The solvent peaks and bonds which are interferred by solvents are indicated by (*).

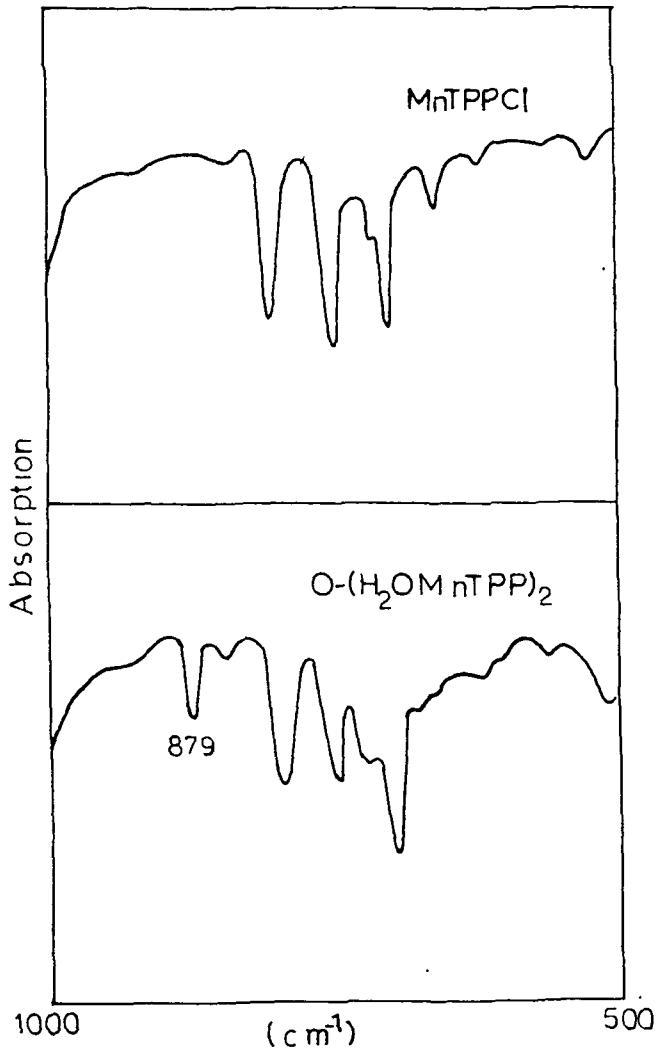

Fig.6.8 Infrared spectra of MnTPPCl and O-$(H_2OMnTPP)_2$ in KBr pellet

SUMMARY AND CONCLUSIONS

The scope of the thesis is to provide an understanding of the electronic and geometrical structures of some porphyrins and metalloporphyrins by the resonance Raman technique. The systems under consideration were free base protoporphyrin-IX, mesoporphyrin-IX, haematoporphyrin-IX alongwith Copper and Cobalt chelates of protoporphyrin-IX and mesoporphyrin-IX dimethyl esters; tetraphenylporphinato Manganese(III) chloride and oxygen - bridged Manganese(III) tetraphenylporphin dimer. We have reviewed the available informations, interpretations, controversies and ambiguities on these systems given by earlier workers using different experimental and theoretical techniques. Because of their relevance with immensely important biological systems, several books, monograms and periodic series of edited books are being published even currently on metalloporphyrins.

The complexity of biological systems render a detailed study of their mechanism, very difficult either in vivo or vitro. In spite of several studies, the specific role of vinyl groups in the cooperative binding of oxygen in haeme proteins is not well understood and even if some suggestions seem interesting, further work has to be performed to confirm them.

A great deal of interest has also been stimulated on the study of Mn(III)-porphyrin complexes during recent years. They display an absorption spectrum which is atypical of normal metalloporphyrin spectra. The highly complex absorption spectra of these systems are not yet properly understood and many controversial reports exist in literature.

Another aspect which has drawn much current attention is the characterization of the aggregates of metalloporphyrin molecules. However, most of the RR studies are directed towards the monomeric complexes and little emphasis has been laid on the dimeric complexes. The present investigation was undertaken to study some of these systems more thoroughly. We have been able to understand few important aspects of these systems quite satisfactorily and our findings are discussed in this thesis.

We have presented general theoretical background in Chapter II in order to understand the absorption and resonance Raman spectra of porphyrins and metalloporphyrins. The experimental results have been analyzed in light of theories discussed in this chapter. Because of the high sensitivity and selectivity offered by RR spectroscopy, this technique offers the potential to resolve several of the outstanding questions in this field.

Chapter III deals with the methods of sample preparation,

the details of experimental technique used for the study, etc. In the course of the work, we found that a very careful preparation of the sample and use of proper experimental conditions is extremely necessary to obtain good quality RR spectra before any meaningful conclusions can be drawn from the data.

In Chapter IV, we consider the RR studies of protoporphyrin-IX(PP) and its analogues, in order to delineate the contributions of vinyl groups in the RR spectra of PP-IX. From the present study, it is evident that the vinyl group vibrational modes are not resonance enhanced in the RR spectra of PP with any of the excitation wavelength used in this study. In other words, it implies that the vinyl side chains are not coplanar with the porphyrin ring and therefore vinyl π electrons cannot exert considerable influence on the porphyrin π electrons due to decrease in conjugation. It may also possible that vinyl group vibrational modes are not vibronically coupled to the $\pi\rightarrow\pi^*$ electronic transitions of the molecule. RR data indicate that the vinyl side chains perturb the basic chromophore in a similar manner as the other saturated substituents in MP and HP, resulting in C_s symmetry for all the systems. We have also attempted to correlate our data with those for different haeme proteins and have given a systematic and consistent interpretation for understanding the scattered data on these systems.

In Chapter V, we have given detailed RR study of

tetraphenylporphinato Manganese(III) chloride(Mn(III)TPPCl). A number of important aspects have emerged out from this study. One of the most intigruing questions concerning these systems is the complex nature of their electronic absorption spectra. Although there are some earlier experimental and theoretical studies, the absorption spectra of these systems were not fully and properly understood. By proper choice of excitation wavelengths, we have obtained RR spectra by excitation in different regions of absorption bands of MnTPPCl. The results of the RR study have provided a better understanding of the electronic spectra of these systems. It was observed that the vibrational modes, primarily enhanced at band V excitation, are metal related. On the other hand, excitations in the abssorption regions of bands III and IV enhance mainly the macrocycle modes, which also include many non-totally symmetric modes. We conclude that band V is of charge transfer origin, while bands III and IV are of $\pi \rightarrow \pi^*$ origin and correspond to α and β bands of normal metalloporphyrins. A further observation was the presence of some metal related modes in the RR spectra at band III and IV excitations and some macrocyclic modes at band V excitation. From detailed theoretical considerations of RR scattering process, this implies the presence of some charge transfer character in bands III and IV and similarly some $\pi \rightarrow \pi^*$ character in band V. We have interpreted our results in the following way. The configurations resulting

from electronic excitations from $a_{1u}(\pi)$, $a_{2u}(\pi)$ — $e_g(\pi^*)$ porphyrin orbitals and $a_{1u}(\pi)$, $a_{2u}(\pi)$ — $e_g(d_\pi)$ metal orbitals are both of E_u symmetry and undergo configuration interactions to yield four excited electronic states. Transitions from these states to the ground electronic state give rise to absorption bands numbered III, V, V_a and VI. However, band V has predominantly charge transfer character and bands III and IV have $\pi - \pi^*$ character mainly. The assignments for bands V_a and VI could not be verified quantitatively because of non availability of excitation lines in that range.

The most interesting results were obtained by excitation at $\sim$530 nm absorption, where enhancement of mainly totally symmetric macrocyclic modes was observed. This implies that this band must be of $\pi - \pi^*$ origin. We suggest this band to be of singlet-triplet (π, π^*) origin. Singlet-triplet transition is spin forbidden and therefore not observed in absorption spectra normally. However, the presence of large spin orbit coupling may provide a relaxation pathway for this transition to occur. A peculiar observation in this regard was that by excitation with 5309 Å, the sample decomposed after a certain interval of time, in spite of low power of the exciting radiation and high speed of the rotating cell. We have correlated this observation to the longer lifetime of the triplet states. A molecule in an excited triplet state can accumulate sufficient heat to decompose the sample before it comes back to the ground

state. Thus RR data have yielded significant insight into the absorption spectra of Mn(III)TPPCl and to the best of our knowledge, the absorption at $\sim$ 530 nm in MnTPPCl, has been explained for the first time in our study.

There has also been considerable interest in the possibility of the conjugation of the phenyl groups with the porphyrin macrocycle in TPP systems. A direct consequence of the phenyl ring conjugation with the macrocycle would be the appearance of phenyl group modes in the RR spectra. However, we could not attribute any bands in our RR data to phenyl group modes directly and therefore conclude that the possibility of conjugation of the phenyl rings with the porphyrin macrocycle is unlikely.

The third aspect of our study on Mn(III)TPPCl was to probe the symmetry of the chromophore. A close examination of the value of depolarization ratios (ρ_1) for some isolated bands showed dispersion with excitation frequency. This implies that the molecule does not retain its expected C_{4v} symmetry. X-ray crystallographic studies on bis-(imidazole)-$\alpha, \beta, \gamma, \delta$ — tetraphenylporphinato Iron(III) chloride show that the dihedral angles between the phenyl rings and the macrocycle are not equal for all the cases. This then provides a basis for understanding the dispersion of ρ_1 in terms of lowering of molecular symmetry. We believe that the phenyl rings of MnTPPCl are

oriented in a similar manner in solution also and thus effectively reducing the molecular symmetry to C_s.

Chapter VI presents the results of RR study on oxygen-bridged MnTPP dimer. Here we have attempted to probe the intradimercoupling between the two units. The coupling between the two TPP units should be reflected in the RR spectra by shifting and splitting of certain bands and appearance of new bands. However, our data do not provide any evidence for the dimer vibrational splittings, i.e. for intradimer coupling and we conclude that the two monomeric units retain their identity even on aggregation. It is likely that large separation between the two units is responsible for the lack of intradimer coupling. From our study, we could assign the bands corresponding to the Mn-Cl stretching, Mn-O-Mn symmetric stretching(RR) and Mn-O-Mn asymmetric stretching(IR) modes. In this system also we did not observe any evidence of phenyl ring conjugation with the macro ring and these conclusions are similar to those in MnTPPCl.